Design and Analysis of a Switched Reluctance Machine for Traction in a Hybrid Automotive Application

by

Ahmad Talha

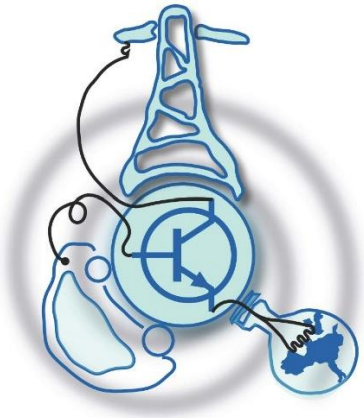

Submitted to the Department of Electrical Engineering, Electronics, Computers and Systems in partial fulfilment of the requirements for the degree of Erasmus Mundus Masters Course in Sustainable Transportation and Electrical Power Systems at the

UNIVERSIDAD DE OVIEDO

September 2017

Author…….

Certified by…….

Dr. Tom Cox

University of Nottingham

Certified by…….

Dr. Gaurang Vakil

University of Nottingham

Design and Analysis of a Switched Reluctance Machine for Traction in a Hybrid Automotive Application

by

Ahmad Talha

Submitted to the Department of Electrical Engineering, Electronics, Computers and Systems on September 15, 2017, in partial fulfilment of the requirements for the degree of Erasmus Mundus Master Course in Sustainable Transportation and Electrical Power Systems

Abstract

A switched reluctance machine (SRM) is very robust and capable to perform well under harsh conditions. It is simple in construction and avoids the use of magnets so it is cheap to manufacture. The powertrain of a hybrid vehicle presents challenging conditions for an electric machine. A SRM is a potentially strong contender for such applications. In this project, a 43 kW SRM is designed for a hybrid traction application. Three topologies: three-phase 6/4, three-phase 12/8 and 4-phase 8/6 machines are considered as possible design choices. The main design objectives are to satisfy the torque and efficiency requirements and a secondary objective is to minimise the torque ripple. A base design is developed for each topology under consideration. The base designs are improved by carefully focusing on the impact of all important machine geometrical parameters such as rotor diameter, pole arcs and stator back-iron thickness on torque and efficiency. One design topology is selected as the final design of choice for the application based on the simulated performance. Results show that SRM can meet torque and efficiency requirements. The efficiency increases with the speed so SRM is better suited to high speed traction application. The area of concern is the torque ripple as it increases with the speed and needs to be controlled both at the design and control stages.

Thesis Supervisor: Dr. Tom Cox

Title: Assistant Professor, University of Nottingham

Thesis Co-Supervisor: Dr. Gaurang Vakil

Title: Assistant Professor, University of Nottingham

ACKNOWLEDGEMENTS

This thesis has been carried out at University of Nottingham as a part of Erasmus Mundus Masters Course (EMMC) in Sustainable Transportation and Electrical Power Systems (STEPS).

Firstly, I would like to give special thanks to my thesis supervisors Prof. Tom Cox and Prof. Gaurang Vakil for their continuous support and guidance during this project. Their help and encouragement meant a lot during the whole process.

I would also like to thank Prof. Giulio De Donato and Prof. Fabio Giulii Capponi of University of Sapienza, Rome. Their lectures, during the first semester of EMMC STEPS programme, helped me a lot in developing better understanding of electrical machines and their control.

I would also like to acknowledge the support of STEPS programme coordinators and all the support staff. In particular, I want to thank Ms. Jodie Clifford at University of Nottingham, Ms. Susana Menendez at University of Oviedo and Ms. Martina Vizzani at University of Sapienza for their administrative help.

I also owe thanks to my fellow students and friends of EMMC STEPS especially of Sustainable Transportation track. Our discussions post-lectures and during our preparation for the exams were always thought provoking. I feel honoured to have studied alongside such a talented bunch of people.

Finally, I would like to thank my family and friends for their support and prayers throughout this programme.

Contents

List of Figures

List of Tables

List of Abbreviations

AC	Alternating current
DC	Direct current
EMF	Electromotive force
EV	Electric vehicle
FEM	Finite element method
HEV	Hybrid electric vehicle
IM	Induction machine
PM	Permanent magnet
PWM	Pulse width modulation
SRM	Switched reluctance machine

Keywords

Finite Element Analysis, Hybrid Electric Vehicle, Reluctance Torque, Switched Reluctance Machine, Torque Ripple.

List of Symbols

β_r	Rotor pole angle
β_s	Stator pole angle
B_s	Peak flux density
D_r	Rotor outer diameter
D_s	Stator outer diameter
D_{sh}	Shaft diameter
n_c	Number of coils per phase
Np	Number of turns per phase
R_r	Rotor radius
t_r	Rotor pole width
t_s	Stator pole width

Chapter 1

Introduction

1.1 BACKGROUND

The electric vehicle (EV) was invented before the internal combustion engine. It provided comfort and ease of use but also suffered because of heavy batteries and long charging times. The arrival of the internal combustion engine caused a paradigm shift in transportation. Gasoline was cheap and readily available and so the EV gradually ran out of competition.

With increasing awareness about the impact of burning of fossil fuels on our environment, a greener solution was required. This requirement coupled with advancements in power electronics, electric machines and batteries, electric vehicles became relevant again. The electric vehicle is now seen as sustainable and a greener replacement of the gasoline vehicle.

It is important to note that to maximise the benefit of electric vehicles, electricity generation should be made emission free as much as possible. The rate of penetration of electric vehicles in the transportation sector must be matched by the rate of renewable sources replacing the conventional fossil-fuel based sources. Otherwise we would not be able to maximise the benefits of electric vehicles.

An electric vehicle has some specific requirements that an electric machine should satisfy. These requirements as summarised in [1, 2] are:

- High torque density
- High power density
- Wide constant power speed range with high efficiency
- Large starting torque
- Large peak power at high speeds
- Capability to operate under taxing conditions e.g. exceeding temperatures.
- High reliability
- Low vibration and noise
- High performance and cost effective
- Safely operable
- Requiring less frequent maintenance
- Capability to tolerate a fault
- Tough and robust
- Space and weight constraints [3]

All these requirements make the design of an electric machine a challenging task. *Fig. 1-1* depicts the torque-speed characteristics required of an electric machine for application in vehicles. It is divided into two regions: constant torque and constant power. In the low speed (speed below nominal/rated speed ω_n) constant torque region, flux in the machine is kept constant and supply voltage is gradually increased to compensate for the increasing back-EMF. At speeds above ω_n supply voltage is kept constant to its rated value V_{an} and flux is reduced using the magnetizing/field current to reduce the back-EMF. Therefore, constant power is also called the flux weakening region. Power remains constant in this region as the magnitude of the supply current and voltage is kept constant whereas shaft speed increases with decreasing torque.

Various types of machines have been tried for EV or hybrid electric vehicle (HEV) [4, 5, 6, 7, 8, 9, 10, 11, 12, 13]. *Fig. 1-2* shows the classification of the machines. An overview can now be provided for the important types of machines considered for traction applications over the years.

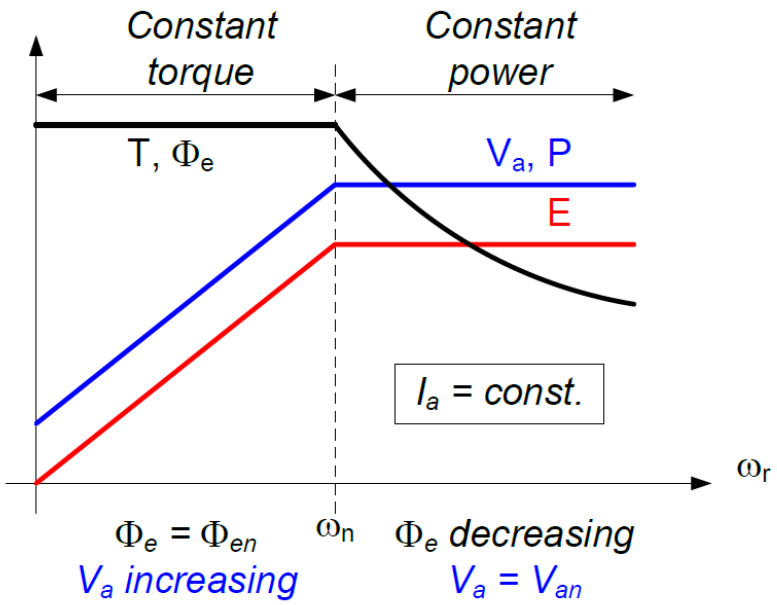

Fig. 1-1. Required Torque-speed characteristics of a machine in EV *[14]*

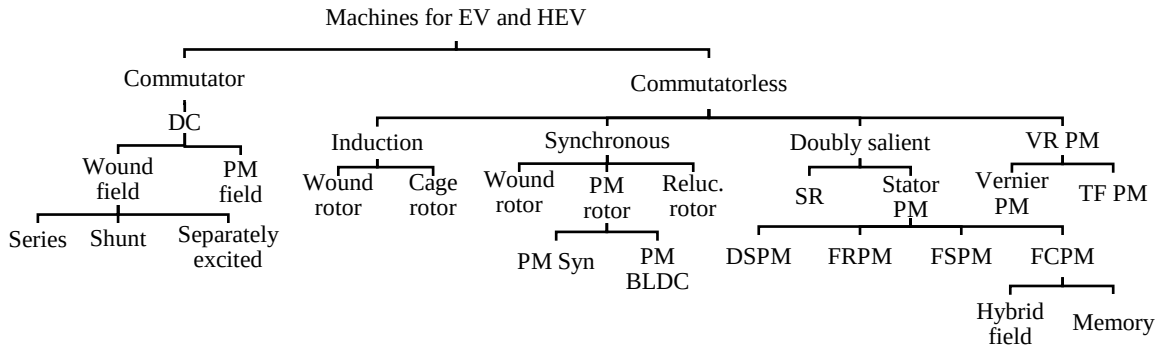

Fig. 1-2 Classification of electrical machines for EVs and HEVs *[2]*

1.1.1 DC MACHINE

A DC machine is arguably the simplest electric machine. There are basic types of a DC machine namely series, shunt and compound. Each of these types have torque-speed characteristics which vary according to the load conditions [15]. From the point of view of field excitation, DC motors can be divided into separately excited and self-excited motors. Further classification can be done based on the excitation method i.e. wound field DC (which use a field winding) and permanent magnet DC (which use magnets as source of field excitation instead of a wound coil supplied by DC current) motors [2].

The control of a DC machine is simple. Armature current provides the control of torque and field current controls the flux for flux weakening region of torque-speed characteristics. A DC machine may be easy to control but it requires frequent maintenance due to commutator and carbon brushes. Most losses in a DC machine occur in the rotor so for high power applications, a complex cooling system would be required. These factors make the brushed DC machine unsuitable for modern traction applications.

1.1.2 INDUCTION MACHINE

Induction machines (IM) are most widely used electric machines in industry for a variety of applications because of their ruggedness, low cost and high reliability. These characteristics combined with wide field weakening region make induction machines an appropriate choice for electric vehicles [16]. Induction machines have two rotor types: squirrel cage and wound [15]. For traction applications, squirrel cage type is generally used. The control of IM is quite complex as compared to DC machine. However, the field-oriented control approach, which employs the coordinate transformation method, provides an efficient way to control IM.

The disadvantages of induction machines are the restricted overload capability because of rotor losses, limited torque capability at low speeds, lower torque density and lower efficiency [3, 16]. Also core losses increase with increase in frequency at higher speeds and additional losses due to harmonics in the inverter applied voltage can also be limiting factors. All these factors should be considered while designing the IM for a specific traction application [16].

1.1.3 PERMANENT MAGNET MACHINE

A permanent magnet (PM) machine is a very attractive choice for electric vehicles owing to high efficiency, compactness, high torque at low speeds and ease of control for regenerative braking [16]. PM machines can be made for both AC and DC but only PM synchronous and PM brushless DC machines are used for electric vehicles [16]. *Fig. 1-3* shows categorisation of PM machines.

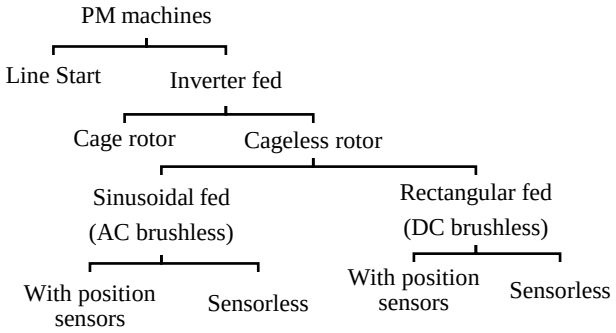

Fig. 1-3. Classification of PM machines

Brushless DC PM machine has higher power density than PM synchronous machine [2]. Based on the placement of the magnets on the rotor, PM machines can be surface-mounted PM (SPM) machines or interior PM (IPM) machine. *Fig. 1-3* shows the two rotor configurations for PM machines.

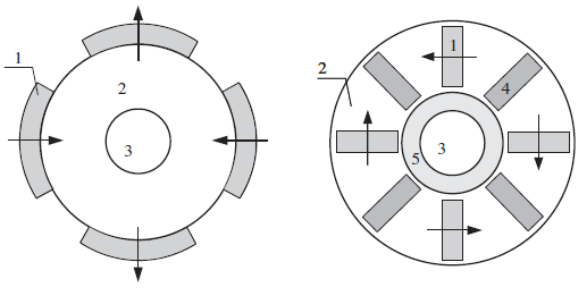

Fig. 1-4. SPM (left) and IPM (right) configurations
(1 – magnet; 2 – iron core; 3 – shaft; 4 – non-magnetic material; 5 – non- magnetic material) *[16]*

In SPM machines magnets are attached to the rotor using an adhesive material or a retaining ring, hence these machines can suffer due to mechanical stresses at high speeds. A SPM machine is magnetically isotropic i.e. direct-axis and quadrature-axis reactances are equal. As a result, SPM machine does not have a reluctance torque component in their output torque. On the other hand, IPM machine does display magnetic anisotropy and consequently produces torque with a contribution from

synchronous torque (produced by the interaction of PM and stator field) as well as reluctance torque (arising due to difference between direct-axis and quadrature-axis reactances).

Most of the losses in the PM machine are iron losses which occur in the stator so designing a mechanism for cooling of this machine is relatively simple. The PM machine, particularly the IPM machine offers an elegant solution for traction applications. However, the cost and fluctuating supplies of PMs are forcing designers to explore magnet-less machines [1, 17, 18]. The dependence of overloading capability of a PM machine on the magnet characteristics is also a limiting factor in its usage.

1.1.4 SWITCHED RELUCTANCE MACHINE

A switched reluctance machine (SRM) bears advantages of simple structure, low manufacturing cost, low rotor losses, fault tolerance and good performance under harsh conditions [1, 16, 18]. Switched reluctance motors do not require PMs or squirrel cage for torque production, instead the difference between d-axis and q-axis reactances allow them to produce a non-zero average torque. Although SR motors are simple in design, their control is much more complicated. Also, they suffer from high torque ripple at low speeds [3]. *Fig. 1-5* depicts the physical construction of a rotor and stator of a SRM.

Fig. 1-5. The rotor and stator of SR motor *[19]*

Table 1-1 provides a comparison of important performance characteristics of the described electric machines with respect to their applicability in traction applications. The comparison shows that the IM ticks the most boxes in terms of required characteristics however power density can be a critical factor for applications with space constraints.

Table 1-1
Comparison of Performance Characteristics of Electric Machines *[3]*

	DC	IM	PMSM	SRM		
power density	⊖⊖	⊙	⊕⊕	⊙	⊕⊕	very good
efficiency	⊖	⊕	⊕⊕	⊕	⊕	good
costs	⊕	⊕⊕	⊖	⊕	⊙	neutral
reliability	⊖	⊕⊕	⊙	⊕	⊖	bad
technical maturity	⊕	⊕	⊙	⊙	⊖⊖	very bad
controlability, costs	⊕⊕	⊙	⊕	⊖		

1.2 PROJECT OVERVIEW

An electric machine is a major component of a hybrid or electric car power train. It lifts the performance of the vehicle and makes it more efficient, therefore it is necessary to optimise the electric

machine design to achieve desired characteristics [20]. This project involves the design and optimization of a switched reluctance machine for the given specifications. This project uses real specifications and data from a company project for automotive drive hybridisation.

1.2.1 AIMS AND OBJECTIVES

The aim is to design, analyse and optimise the switched reluctance machine according to the given specifications.

The following objectives are set to achieve the target:

- To understand main requirements of the traction motor for hybrid drive train
- To develop an analytical design of switched reluctance motor
- To carry out sensitivity analysis on the geometric degrees of freedom for the switched reluctance motor using FEM
- To develop an optimised SRM for a given envelope (specified by the company) and completely characterise its performance.

The design shall be developed, analysed and optimised in Infolytica's MotorSolve. The MagNet software shall then be used for detailed magnetic profiling. For thermal analysis, MotorCAD shall be employed.

1.3 THESIS OVERVIEW

The thesis is arranged in five chapters. The succeeding chapters are summarised below:

Chapter 2: It will cover the theoretical background of SRM. This includes the description of geometry, explanation of its principle of operation and control and details about its advantages and disadvantages.

Chapter 3: This chapter will provide the design procedure adopted in this project. This includes the calculation for the considered design topologies, the improvements made based on simulations and optimisation process of the selected topology based on simulation results.

Chapter 4: It will include the simulations and results for the selected topology and will provide the detailed performance characterisation of the selected design including torque-speed profile, efficiency map and magnetic field density map.

Chapter 5: The last chapter is related to conclusions drawn and recommendations for the future work.

Chapter 2

Switched Reluctance Machine

2.1 INTRODUCTION

A reluctance machine is defined in [21, 22] as:

"*A reluctance machine is an electric motor in which torque is produced by the tendency of its moveable part to move to a position where the inductance of the excited winding is maximised."*

This definition encompasses both switched reluctance (SRM) and synchronous reluctance machine (synRM). A switched reluctance machine has salient stator and salient rotor and both are made of steel laminations. The number of stator poles and rotor poles are generally not equal. The most common configurations of SRM have number of rotor poles as number of stator + 2n, where *n* is an integer. A typical value for *n* is -1. Some configurations are made by repeating a basic configuration e.g. a 12/8 (12 stator and 8 rotor poles) SRM configuration is basically made by repeating 6/4 configuration twice. The stator winding is concentrated i.e. the coil is wound around the stator pole. There are no magnets or any winding on the rotor. This allows the rotor to be simple and prevents the usage of expensive magnets but also makes the control of the machine complex [22]. The fundamental frequency of the stator phase excitation current is given by:

$$f = \frac{N}{60} N_r \tag{2-1}$$

Where N_r is the number of rotor poles and N is the rotor speed in rpm. The step angle or stroke angle (ε) is calculated as:

$$\varepsilon = \frac{2\pi}{N_{ph} N_r} \tag{2-2}$$

Where N_{ph} is the number of phases. The step angle represents the angle, in mechanical radians, between excitation of successive phases. The machine needs to be operated under saturation to maximise its power conversion capability. The non-linearity that accompanies the saturation makes it difficult to develop an analytical model of the machine and accurately predict the output based on the inputs provided.

In the recent years, SRM has emerged as a good candidate for EVs. As a potential replacement to machines with magnets, SRM offers simplicity, ruggedness and low cost but suffers from the problem of large torque ripple because of doubly salient nature and acoustic noise. The torque ripple can be reduced during the design and control stage. In this chapter, basic principles governing the operation of SRM are explained in detail along with summary of its control and converter, and its advantages and disadvantages.

2.2 ENERGY CONVERSION IN SRM

2.2.1 INDUCTANCE VARIATION AND INSTANTANEOUS TORQUE PRODUCTION

Consider a simple single phase SRM as shown in *Fig. 2-1* having 2 stator poles and 2 rotor poles. This simple model is used to explain the aligned and unaligned positions of the rotor. In the *Fig. 2-1*, the rotor poles are aligned with the stator poles. This is said to be the *aligned* position of the rotor. On the other hand, if stator poles are aligned with the inter-polar axis then the rotor is at *unaligned* position as depicted in *Fig. 2-2* [21].

The phase winding inductance is maximum at the aligned position and is minimum at the unaligned position. This is because at aligned position, the stator and rotor iron poles are separated only by a thin airgap so the reluctance to magnetic flux is minimum. At unaligned position stator pole in line with a large airgap so the reluctance is maximum. The aligned inductance is denoted by L_a and unaligned inductance by L_u. The ratio L_a/L_u is termed as inductance ratio. At aligned position, the machine can saturate especially parts like stator back-iron and rotor back-iron. At unaligned position, the chances of saturation are minimal. As the inductance changes with the rotor position, flux linkage varies as well [21, 22]. A typical flux linkage profile of a SRM is presented in *Fig. 2-3*. The lowest curve corresponds to the unaligned position while the top most curve represents the aligned position. In the positions between the two extremes, the machine assumes the curve corresponding to that particular rotor position. As the overlap between stator and rotor poles begin, flux linkage changes more sharply and the characteristics begin to approach the aligned curve. Every rotor pole pitch, the curves repeat [21]. The rotor pole pitch (τ) is defined below in eq. (2-3):

$$\tau = \frac{2\pi}{N_r} \tag{2-3}$$

Where N_r is number of rotor poles.

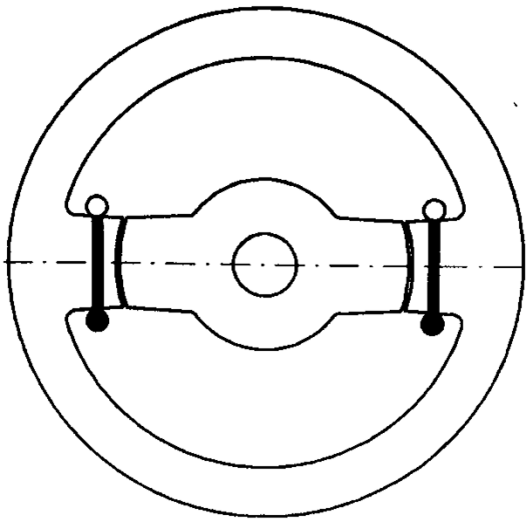

Fig. 2-1. SRM with rotor in aligned position *[22]*

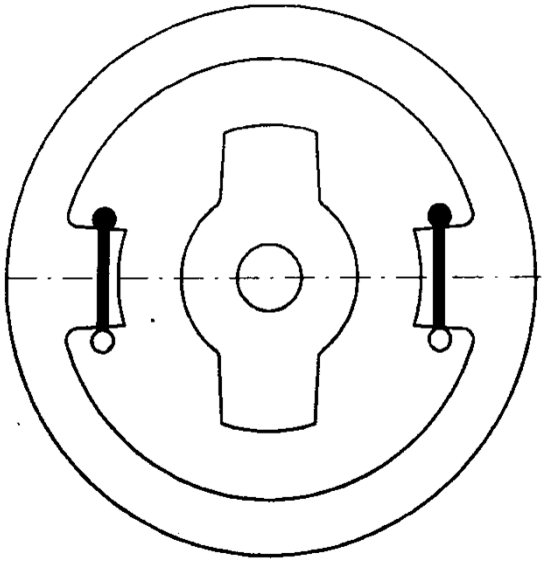

Fig. 2-2. SRM with rotor in unaligned position *[22]*

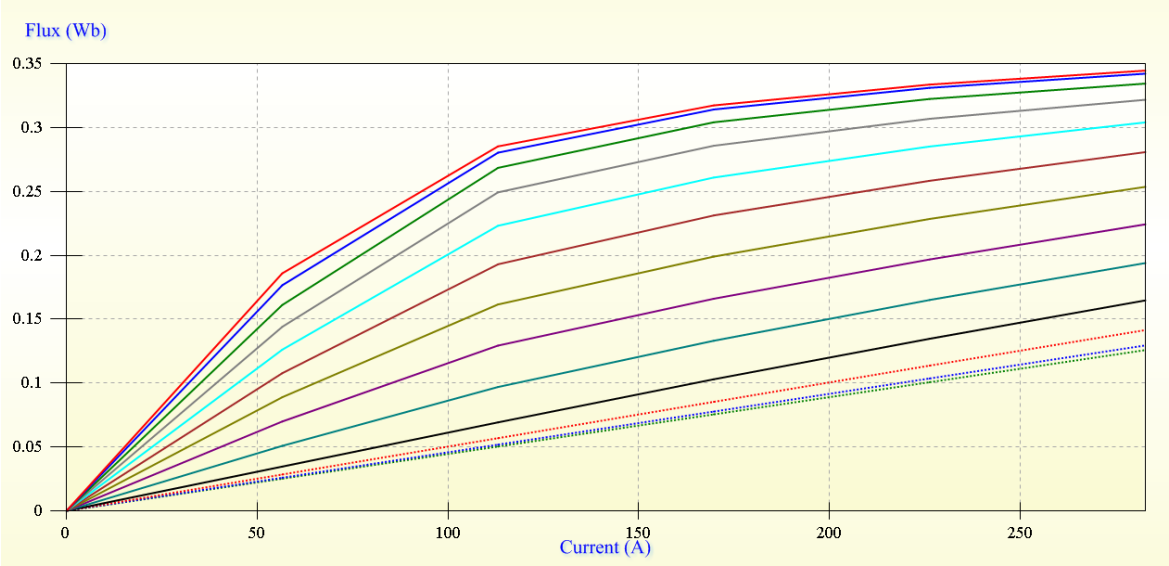

Fig. 2-3. Flux linkage profile of a SRM

Fig. 2-4 shows the inductance variation and torque pulses with rotor motion. The small bars in the picture depict the position the relative position of the stator and rotor poles. The torque at the aligned position (A) is zero because inductance has achieved its maximum value and the change in inductance is zero. However, if the rotor is displaced to either side of the aligned position, a restoring torque will arise that will tend to move the rotor towards the aligned position. At exactly unaligned position (U) the torque is also zero because the inductance reaches the minimum value and the change in inductance reduces to zero. However, in between the aligned and unaligned position (J to A or A to K), there is a change in inductance and exciting the phase winding in this region of rotor movement produces torque. In case of motoring operation, current is supplied when the rotor is moving from unaligned to aligned position (J to A). Alternatively, for operation in generator mode, current must be supplied when the rotor is moving from aligned to unaligned position (A to K). In this way torque pulses are produced with the movement of the rotor. With the constant current, as is the case in *Fig. 2-4*, the torque pulses produced would be opposite and equal and hence average torque would be zero. However, with unidirectional current the machine produces a non-zero average torque as shown in *Fig. 2-5*.

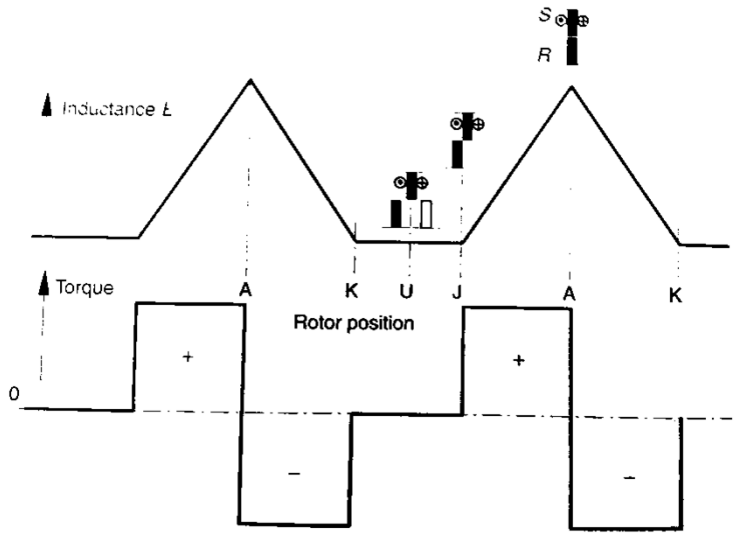

Fig. 2-4. Inductance and torque variation with rotor motion and constant current *[22]*

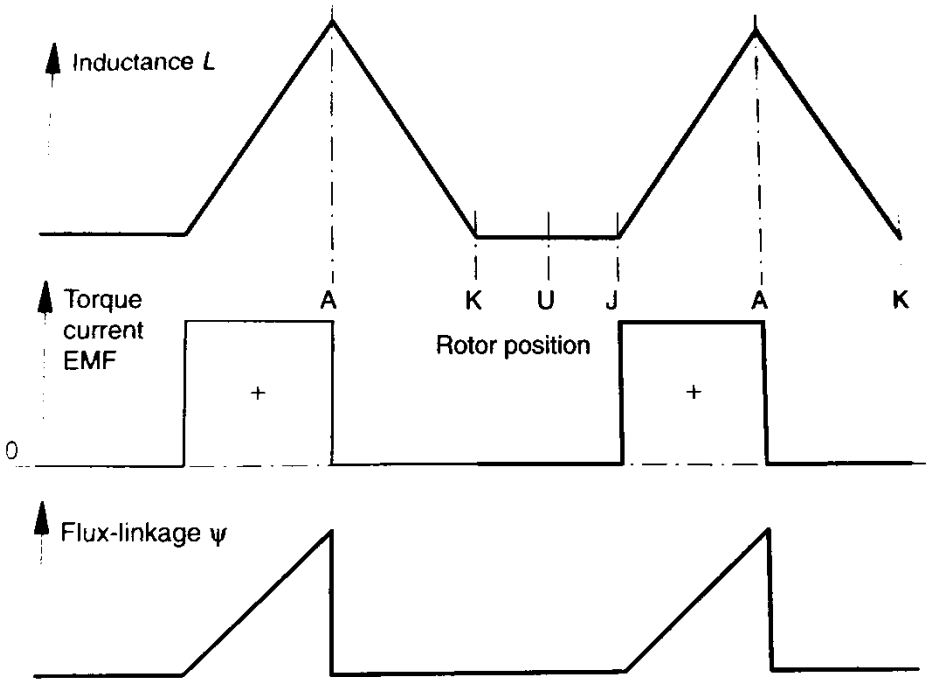

Fig. 2-5. Inductance and torque variation with rotor motion and unidirectional current *[22]*

2.2.2 LINEAR ANALYSIS OF SRM

A relationship can be developed for instantaneous torque in terms of current and change in inductance with the rotor position. To begin, we assume that machine does not saturate i.e. machine operates in the linear region of flux linkage-current characteristics. This means that inductance only changes with the rotor positions and does not change with the current. We can write the phase voltage equation as:

$$v = Ri + \frac{d\psi}{dt} \tag{2-4}$$

Where v is the voltage at the terminals, R is the phase resistance, i is the current and ψ is the flux-linkage. At the constant angular speed ω, we can write:

$$dt = \frac{d\theta}{\omega} \tag{2-5}$$

Where θ is the rotor position. Since we assume the machine to be operating in the linear region, therefore following relationship also holds true:

$$\psi = Li \tag{2-6}$$

Where L is the phase inductance. Eq. (2-4) can be rewritten as:

$$v = Ri + \omega \frac{d\psi}{d\theta} = Ri + \omega \frac{d(Li)}{d\theta}$$

$$v = Ri + \omega i \frac{dL}{d\theta} + L \frac{di}{dt} \tag{2-7}$$

The term with ω represents the back-emf e i.e.:

$$e = \omega i \frac{dL}{d\theta} \tag{2-8}$$

To find the instantaneous power, we multiply both sides of eq. (2-7) by i:

$$vi = Ri^2 + \omega i^2 \frac{dL}{d\theta} + Li \frac{di}{dt} \tag{2-9}$$

The time rate of change of stored energy in the magnetic field can be calculated as:

$$\frac{dW_f}{dt} = \frac{d}{dt}(\frac{1}{2} Li^2) = Li \frac{di}{dt} + \frac{1}{2} i^2 \frac{dL}{dt}$$

$$\frac{dW_f}{dt} = \frac{d}{dt}(\frac{1}{2} Li^2) = Li \frac{di}{dt} + \frac{1}{2} \omega i^2 \frac{dL}{d\theta} \tag{2-10}$$

Where W_f represents the stored magnetic field energy in the machine. As the instantaneous electromechanical power balance for a machine, neglecting losses, can be written as:

$$vi = \frac{dW_f}{dt} + T\omega \tag{2-11}$$

Where T is the instantaneous output torque. Equating eq. (2-9) and (2-11) and putting the value of change in magnetic energy from eq. (2-10) we can write:

$$T\omega = \frac{1}{2} \omega i^2 \frac{dL}{d\theta}$$

$$T = \frac{1}{2} i^2 \frac{dL}{d\theta} \tag{2-12}$$

A machine operating in linear region has poor energy conversion. This can be explained with the help of *Fig. 2-5* and *Fig. 2-6*. The energy conversion diagram in *Fig. 2-6* is shown for motoring operation. At the aligned position (A), the flux linkage is maximum and the hence the energy stored in the magnetic field is also at its peak. After reaching the aligned position (A), current should be driven

back to zero to prevent the development of negative torque and to reduce the flux linkage back to zero and return the energy stored in the magnetic field to the source.

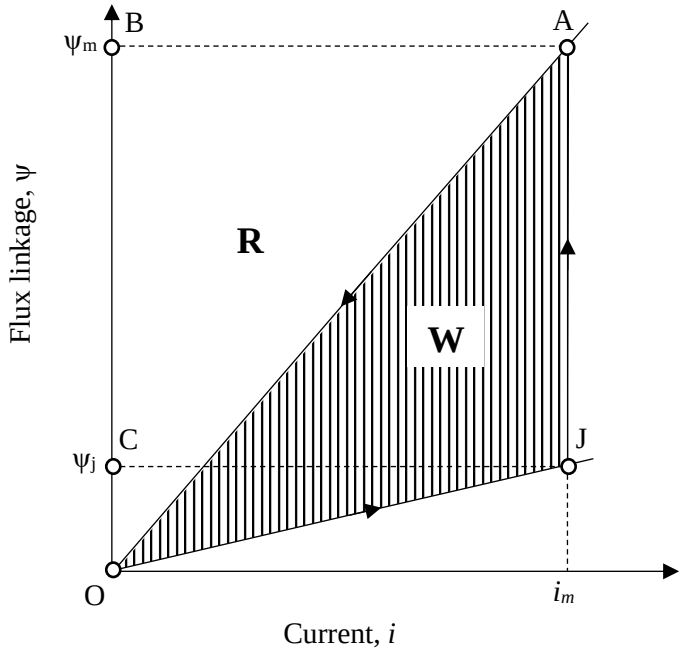

Fig. 2-6. Energy conversion for a machine operating in linear region

From *Fig. 2-5*, we can see that at position J, current pulse is applied and current rises to i_m. This change is represented as OJ in *Fig. 2-6*. The energy supplied in traversing from O to J is:

$$S_1 = \frac{1}{2} i_m^2 L_u \tag{2-13}$$

From J to A, a back-emf develops in accordance with eq. (2-8) due to change in the inductance. This back-emf absorbs energy given by:

$$S_2 = e i_m \Delta t = \omega i_m^2 \frac{dL}{d\theta} \Delta t = \omega i_m^2 \frac{dL}{d\theta} \frac{d\theta}{\omega}$$

$$S_2 = i_m^2 \Delta L \tag{2-14}$$

Where dL = ΔL is L_a - L_u i.e. the difference between aligned and unaligned inductance. In moving from J to A, the torque is developed according to eq. (2-12) and the converted output energy is given by:

$$W = T\Delta\theta = \frac{1}{2} i_m^2 \frac{dL}{d\theta} \Delta\theta$$

In this case since dθ = Δθ and dL = ΔL so we can write:

$$W = \frac{1}{2} i_m^2 \Delta L \tag{2-15}$$

The input energy (S) is given by the sum of S_1 and S_2 so:

$$S = S_1 + S_2$$

$$S = \frac{1}{2} i_m^2 L_u +_m^2 \Delta L \tag{2-16}$$

The energy ratio (Q) i.e. ratio of converted energy to the supplied energy can be written as:

$$Q = \frac{W}{S} = \frac{W}{W + R} \tag{2-17}$$

The half of the energy supplied during the rotor's motion from unaligned position (J) to aligned position (A), is converted to output mechanical energy. However, since some additional energy (S_1) was also supplied in traversing from O to J hence the overall energy ratio is less than 0.5. For this reason, SRM does not operate in the linear region. The torque production of an actual SRM requires non-linear analysis of the torque production process [22].

2.2.3 NON-LINEAR ANALYSIS OF SRM

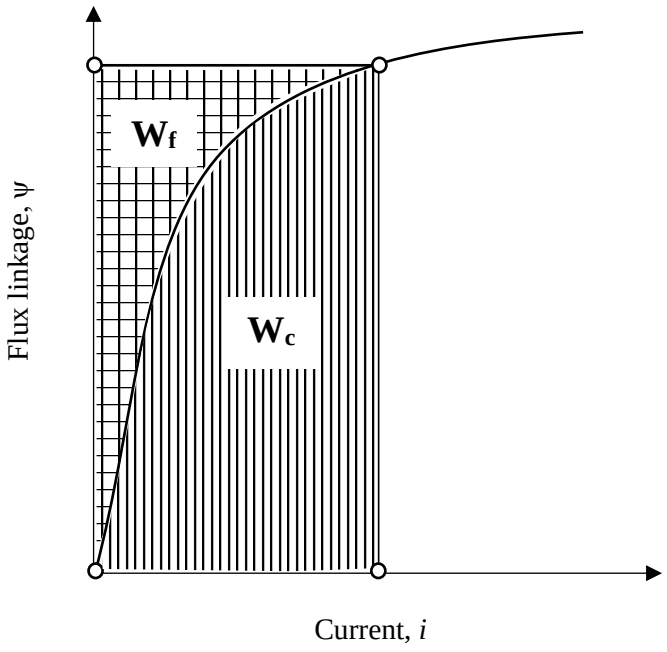

Fig. 2-7. Energy (W_f) and Co-energy (W_c)

To carry out the non-linear analysis, the concept of co-energy is used. From the magnetization curve shown in *Fig. 2-7*, we can see that:

$$i\psi = W_f + W_c \tag{2-18}$$

Mathematically, co-energy is a state function that allows us to calculate the torque as a function of the current instead of flux linkage. Neglecting the copper losses, putting the value of *v* from eq. (2-4) into eq. (2-11) gives:

$$i\frac{d\psi}{dt} = \frac{dW_f}{dt} + T\frac{d\theta}{dt}$$

$$id\psi = dW_f + Td\theta$$

$$dW_f = id\psi - Td\theta \tag{2-19}$$

Eq. (2-18) can be re-written as:

$$dW_f = d(i\psi) - dW_c$$

$$dW_f = \psi di + id\psi - dW_c \tag{2-20}$$

Equating eq. (2-19) and eq. (2-20), we get:

$$dW_c = \psi di + Td\theta \tag{2-21}$$

Calculus dictates that equivalent form of eq. (2-21) is as follows:

$$dW_c = \frac{\partial W_c}{\partial i}\Big|_{\theta=const} di + \frac{\partial W_c}{\partial \theta}\Big|_{i=const} d\theta \tag{2-22}$$

Comparing eq. (2-21) and (2-22), we can express the torque as:

$$T = \frac{\partial W_c}{\partial \theta}\Big|_{i=const} d\theta \tag{2-23}$$

Eq. (2-23) is the most general expression of the torque valid for linear and non-linear machines. In a linear machine, $W_f = W_c$ however in case of saturable machine, as is the case in *Fig. 2-7*, $W_c > W_f$. The saturation improves the energy conversion ratio of SRM hence a SRM should always be operated in non-linear region to get the most out of it. *Fig. 2-8* shows the energy conversion loop of SRM operating in non-linear machine. Every step or stroke, this cycle is executed once. If the number of steps in each rotor revolution is S, W is the energy converted in one step then the average torque can be calculated as:

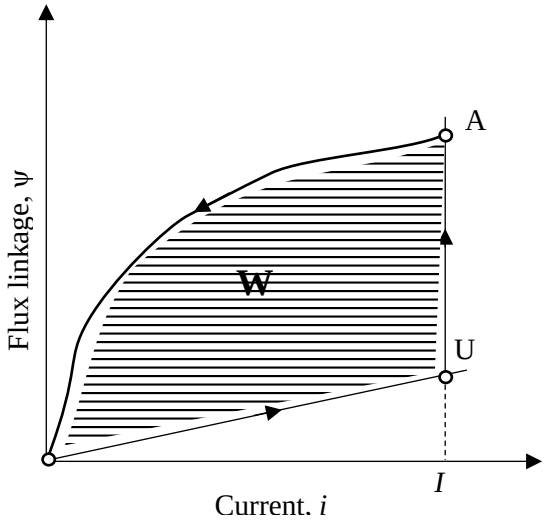

Fig. 2-8. Energy conversion in non-linear SRM

$$T_{avg} = \frac{SW}{2\pi} \tag{2-24}$$

2.3 DESIGN OF SRM

The performance of a SRM depends on the choice of the parameters used in the design. Depending on the type of the application, a SRM can have various configurations of stator and rotor

poles, number of phases and pole arcs etc. In this section, we identify and review the impact of a few important parameters for the design of a SRM.

2.3.1 NUMBER OF PHASES AND POLES

The selection of number of phases and number of poles determines the step angle of the SRM. Increasing the number of steps improves the average torque of the machine as suggested by eq. (2-24). To increase the number of steps, step angle needs to be reduced i.e. increase the number of phases or rotor poles in accordance with eq. (2-2). Increasing the number of steps also reduces the torque ripple. Torque ripple is defined as:

$$T_{ripple} = \frac{T_{\max} - T_{\min}}{T_{avg}} \tag{2-25}$$

Torque ripple is maximum at the commutation, where one phase hands over the responsibility of producing torque to the succeeding phase. Increasing the number of steps increases the torque overlap between phases and hence reduces the ripple [23]. However, increasing the number of steps also increases the fundamental frequency of phase currents thereby increasing the copper losses and core losses.

Increasing the number of poles reduces the step angle but also reduces the pole widths. Reduction in pole widths reduces the aligned inductance of the machine so decreases the inductance ratio. Also, the clearance between rotor and stator poles reduces, which increases the unaligned inductance. The decrease in inductance ratio means a reduction in energy conversion per each step. So pole numbers can only be increased to the limit where the reduction in energy conversion is compensated by the increased number of steps [21, 23].

Increasing the number of phases provides a way to decrease the step angle without increasing the number of rotor poles. It also improves the ability of the machine to start from any rotor position. The increase in phase numbers has a smaller effect on inductance ratio than the increase in the number of poles. So, the average torque increases due to reduction in torque ripple. The disadvantage of increasing phase number is the added complexity on the drive side [21, 23].

A good way to decrease the step angle is to repeat a basic configuration. As an example, a three-phase SRM with 12 stator poles and 8 rotor poles can perform better than a three-phase machine with 6 stator poles and 4 rotor poles. Multiplying a basic configuration in this way should affect the inductance ratio ideally [23]. This multiplication also shortens the flux paths hence this can serve well to reduce the core losses [21].

2.3.2 POLE ARCS

Pole arcs play an important role in determining the torque ripple of a SRM. This can be explained in a better way by defining the *inductance overlap ratio* (K_L) [23]. It is defined in eq. (2-26):

$$K_L = 1 - \frac{\varepsilon}{\min(\beta_r, \beta_s)} \tag{2-26}$$

Fig. 2-9 graphically explains the importance of K_L. Widening of the pole arcs means better inductance overlap between the adjacent phases and lesser the torque ripple. However, widening of the stator poles also implies reduced slot area which can increase copper losses. On the other extreme, narrow pole widths reduce the aligned inductance thereby reducing the energy conversion. In general, stator and rotor pole widths are set similar however following conditions are generally applied to pole widths:

- Rotor pole arc (β_r) is made slightly larger than stator pole arc (β_s). This allows us to maintain the value of aligned inductance without reducing the slot area. The difference between the pole arcs ($\beta_r - \beta_s$) creates a torque dead zone at the aligned rotor position. This dead zone serves no purpose other than allowing more time for current to be reduced back to zero as the rotor moves away from aligned position [21].

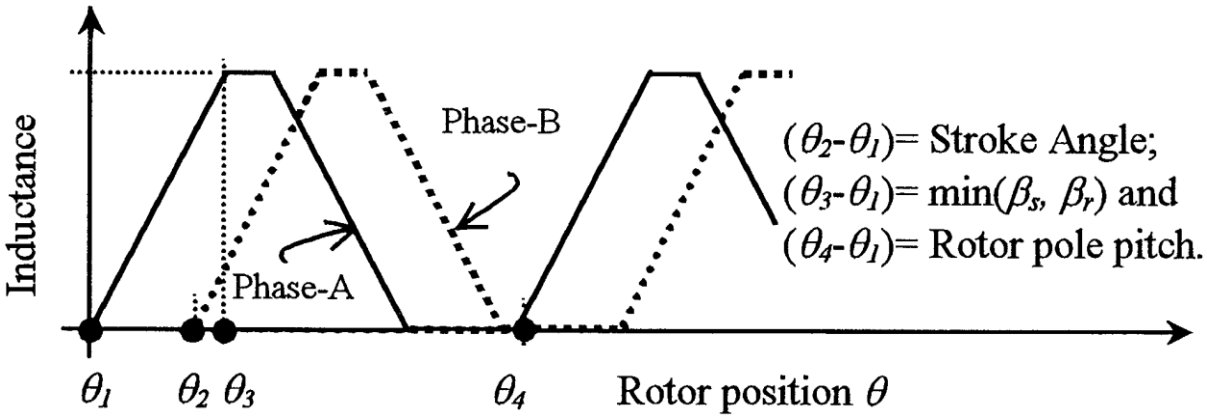

Fig. 2-9. Phase overlap with rotor movement *[23]*

- Min (β_r, β_s) ≥ ε (step angle). This is to ensure that motor has can start from all rotor positions [21] and this condition should be met to reduce the torque ripple as dictated by eq. (2-26).
- Stator pole arcs should be set in such a way that there is some gap between stator and rotor poles. Maintaining a small gap makes the unaligned inductance smaller and improves inductance ratio [21]. This condition can be mathematically written as:

$$\beta_s < \frac{2\pi}{N_r} - \beta_r$$

2.3.3 WINDINGS

The windings in a SRM are simple and concentrated. Generally, a phase consists of two opposite poles with one coil on each pole. The coil can be connected either in series or in parallel. The coils need not to be wound after the assembling the stator. They can be wound separately and then mounted on the poles later. All winding terminals are connected to the external terminal box for connection as there is no internal neutral point for SRM. These extra connections increase the copper losses [21].

2.3.4 CORE MATERIAL

The excitation currents in a SRM have high fundamental frequency compared to an induction machine. The high frequency implies that eddy current losses are going to dominate. The shape of the currents is also not sinusoidal. Therefore, the currents have high harmonic content as well. Since the machine needs to be operated in the non-linear region of magnetization curves so the saturation levels are high. This makes the stator core and rotor core material selection an important aspect of SRM design. A thin lamination is preferable for SRM so Silicon steel is a suitable candidate for core material. In performance-intensive application cobalt based metal alloys are used [21].

2.4 SRM DRIVE AND CONTROL

Fig. 2-10 shows one leg of the drive circuit for a SRM. The drive circuit is different than other machine drives. The switches Q1 and Q2 help applying positive voltage across the winding as the rotor moves from unaligned to aligned position for motoring operation. As the motor reaches the aligned position, Q1 and Q2 are turned off and with the help of diodes D1 and D2, negative voltage is applied

to suppress the current to zero. This circuit is valid for operation as a generator as well. The relative magnitudes of the energy supplied and absorbed determine the operation as a generator or a motor [22]. A leg of switches is added for each phase.

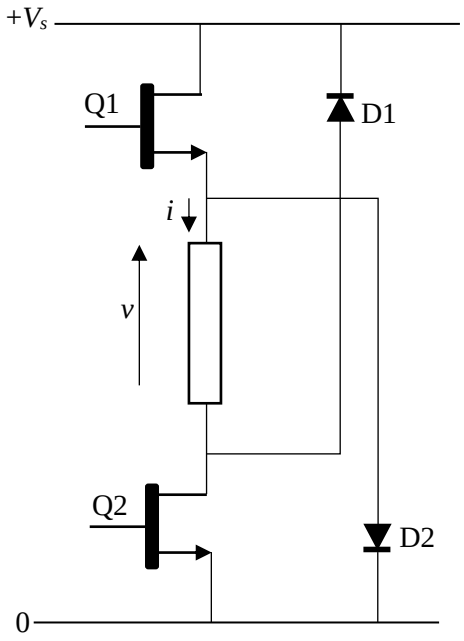

Fig. 2-10. A phase-leg of SRM drive circuit

Due to the non-linear nature of operation, the SRM drive is not easy to control. There is no simple relationship between torque and current like DC machine or synchronous field orientation control method as in induction machine drives to help in simplification of the control strategy. A high-resolution position sensor is required for a SRM drive as the control of the machine is heavily reliant on the information about rotor position. However sophisticated sensor-less control methods have also been reported [24, 25].

The control parameters for a SRM drive are turn-on (θ_{on}) and turn-off (θ_{off}) angles for Q1 and Q2, the conduction period represented by θ_{dwell} which is given by $\theta_{off} - \theta_{on}$ and the phase current. These control parameters determine the torque, efficiency, ripple and other parameters. The control methods of SRM can be broadly categorized as average torque control and instantaneous torque control. In average torque control, average torque produced is controlled by controlling the exciting phase current. For instantaneous torque control, a complex analytical model of the machine is required [22]. The control methods can also be divided into: Voltage controlled drives, current controlled drives and complex controllers e.g. torque ripple minimization controller [26].

2.4.1 TORQUE-SPEED CHARACTERISTICS

The torque-speed characteristic of a SRM is presented in *Fig. 2-11*. There are three regions of the characteristic as shown in the figure. Based on the average torque control method, the control in the three regions is explained as below:

In the constant torque region, rated torque can be delivered with rated voltage and current. The rated speed (point B in *Fig. 2-11*) is maximum speed at which the rated torque can be delivered. For operation in this region, torque is controlled by current which in turn can be limited using reduced voltage by use of pulse width modulation (PWM) [22].

With the increasing speed, we enter the constant power region. In this region, the dwell angle is increased with speed to maintain the flux level in the machine. The longer dwell is achieved by

advancing the θ_{on}. When θ_{dwell} (magnetizing period) is equal to the difference between the angle where the current reaches zero and θ_{off} (de-fluxing period), this state is termed as continuous conduction i.e. the current does not reach zero. With the increasing θ_{dwell} the energy conversion loop area decreases so the average torque decreases but the power is kept constant by the increasing speed [22].

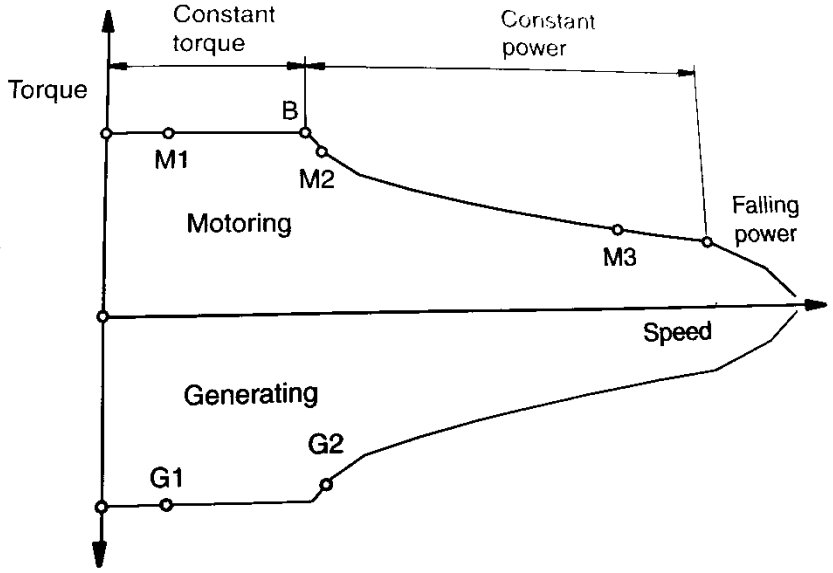

Fig. 2-11. Torque-speed characteristic of a SRM *[22]*

With the further increase in the speed, θ_{on} reaches the limit of its advancement and loop area further decreases to the point where constant power cannot be delivered. The drive enters continuous conduction mode and current never reaches zero. As the current does not reduce to zero, energy is stored in the magnetic field which is not returned to the source so the energy conversion moves away from the origin. Distance between aligned and unaligned magnetization curves increase and torque per ampere rises. Thus, the continuous conduction method can be used to increase power density in high speed regions [22].

2.5 LOSSES IN SRM

The copper losses can be calculated for a SRM as for any other machine using I^2R, where R is the phase resistance. As the commutation frequency of phase currents is high so copper losses in SRM are increased due to the skin effect. The additional copper losses are also due to presence of harmonic content in the phase currents compared to other AC machines. Since there are no magnets so an additional component of the current is required to setup the magnetic field in the machine so SRM suffers a bit because of this additional current as compared to PM machines [21].

Core losses in SRM can be lower than other AC machines. Although switching frequency of current is high and current waveform is non-sinusoidal but the volume of the iron used is less so core losses are controlled [21].

2.6 ADVANTAGES AND DISADVANTAGES OF A SRM DRIVE

A comprehensive list of advantages and disadvantages of a SRM drive is present in [21]. The pros and cons of the machine and the controller are covered separately. A summary is provided here.

2.6.1 MACHINE

SRM offers the following advantages:

- ✓ A SRM is cheap to manufacture. It does not need sophisticated manufacturing methods. It is simple in construction and as it does not require magnets, it avoids all magnet related problems during manufacturing to operation at high speeds.
- ✓ A SRM does not need expensive materials. It only needs thinner laminations to cope with the effects of high frequency currents.
- ✓ SRM is sturdier than induction machine or PM machine in working under high temperatures. The absence of magnets in SRM means that it is not vulnerable to the problem of demagnetization in soaring temperatures. Unlike IM, there is no winding or squirrel cage on the rotor so rotor losses are low and mechanical integrity issues are avoided.
- ✓ SRM can achieve high speeds. The speed limit is set by losses, converter rating, bearings, shaft and rotor strength. At very high speeds, the laminations are not thin enough to contain eddy currents. The rotor faces very large centrifugal force as well. So, at very high speeds, lamination and rotor strength need to be carefully designed.
- ✓ SRM has low inertia as the rotor has significant spaces between its poles.
- ✓ SRM is easy to repair as the winding is concentrated on the pole. This makes the possibility of changing a coil without removing other coils a reality.
- ✓ The end-turn length in SRM is shorter than other AC machines. This implies less losses in end windings. An added advantage is that shorter end turns are mechanically more stable. Also as the winding is concentrated so coils of different phases do not come in contact in their path so probability of phase-phase fault is reduced.
- ✓ SRM has lower rotor losses than IM as there is no winding. The commutation frequency is higher than IM but the volume of material used is less than IM.
- ✓ As there is no internal source of magnetization in SRM so if a winding coil is open circuited or short-circuited, there will be no induced voltages in the faulty winding unlike PM machine. From this point of view, SRM is fault tolerant.

Below is a list of a few disadvantages:

- × The need to design a SRM with sufficiently thick stator and rotor core sections means that shaft diameter is smaller compared to other machines. Smaller shaft diameter results in lower value of critical speed as well which could make the rotor vulnerable to lateral deflection.
- × SRM requires a small airgap to be efficient in its operation. It also needs the air gap to be smooth with least possible variations. Controlling the airgap smoothness to this strict requirement can increase the price of a machine.
- × Hot spots can develop due to large cross section of the coil. This is somewhat compensated by shorter end-turns.
- × Although sensor-less control is possible, the dependency of SRM control on the information about rotor position means that in the drive where a sensor is installed, it needs to be of high-precision and reliable.
- × The biggest disadvantage of SRM lies in the downside of its simple geometry. The doubly salient nature of the nature leads to high torque ripple and noise. Noise reduction requires control of firing angles and current ripple. The torque ripple however needs complex control algorithms to minimise it.
- × The shape of a SRM rotor can cause high windage losses at high speeds.
- × Some configurations of SRM can have long flux paths. This means mmf drop in the core material and reduction in flux linkage.
- × SRM cannot be directly connected to the grid. It needs a converter for its operation.

2.6.2 CONTROLLER

SRM controller has following points in its favour:

- ✓ Number of switching devices per leg is the same as other AC machine drives.
- ✓ As the phase winding of SRM is connected between the switching devices so a shoot-through is not possible unless the phase winding is short-circuited.
- ✓ Different phases of a SRM work almost independently. Loss of one phase does not affect the operation of other phases.
- ✓ Many circuit topologies are available for a variety of applications.
- ✓ Digital implementation of SRM control relatively simpler than IM.
- ✓ SRM has a large constant power area which makes it suitable for traction applications.

The disadvantages of a SRM controller are:

- × SRM needs its own drive circuit. The circuit used by other AC machines cannot be used.
- × All terminals of the windings need to be wired to the drive due to lack of an internal star-point. This results in additional losses and more number of cables.
- × As the unaligned inductance of a SRM can be very low so in systems with low voltage levels the supply wires can cause large voltage drops and affect the machine performance.
- × Commutation frequency is higher than other AC machines.

Chapter 3

Machine Design Calculations and Analysis

3.1 DESIGN SPECIFICATIONS

The design specifications for the project are tabulated in *Table 3-1*.

Table 3-1
Design Specifications

Rated Operating Voltage	345.6 VDC
Operating Voltage Range	240 VDC – 400 VDC
Stator Cooling	Type: Liquid Flow Rate: 6L/min – 12L/min
Peak Power	≥85 kW from 2460 rpm - 6000 rpm for ≥20 s
Continuous Power	≥45 kW from 2456 rpm - 6000 rpm
Peak Torque	≥275 Nm from 0 rpm - 2460 rpm for ≥20 s
Continuous Torque	≥137 Nm from 0 rpm – 2456 rpm
Speed Range	0 rpm - 7000 rpm
Maximum Efficiency	>90% from 350 rpm – 3500 rpm @ 50 Nm – 100 Nm >95% from 3500 rpm - 7000 rpm @ 100 Nm - 275 Nm
BackEMF	<100Vpk/1000rpm @ 25°C
Peak Current	<400 Arms
Continuous Current	<200 Arms
Torque Ripple	≤2.5% * 275Nm
Motor Diameter	270 mm (outside of stator)
Stator Length	107 mm (excluding end turns)
Airgap length	1 mm

The specifications suggest a rated power of about 35 kW at rated speed of 2456 rpm and rated torque of 137 Nm. However, the continuous power is given as 45 kW. In consultation with the supervising professors, it was decided to set rated torque 137 Nm at 3000 rpm which gives rated power of about 43 kW.

3.2 DESIGN CALCULATIONS

Three different topologies were selected for the base design of the machine to satisfy the requirements. These topologies include 3-phase 6/4[1], 3-phase 12/8 and 4-phase 8/6. 3-phase 6/4 is the simplest topology of the proposed ones. It is capable to provide the required torque but the torque ripple would be high. 3-phase 12/8 topology is considered as it offers lower torque ripple and potentially more average torque without adding additional phase. 4-phase 8/6 topology offers reduced torque ripple, higher torque with lower commutation frequency as compared to 3-phase 12/8 machine. However, it adds complexity to the drive because of additional phase leg. Other topologies with higher phase or pole numbers were not considered because the drive would become more complex for higher phase numbers. High pole numbers increase the strokes per revolution so they improve energy conversion but at the same time inductance ratio decreases. With narrower poles, poles tend to saturate more quickly

[1] Number of stator poles / number of rotor poles

and higher rotor pole numbers increase the commutation frequency of the currents as well which results in higher core losses. Therefore, the advantages of higher pole numbers tend to balance out their disadvantages.

The design calculations for each of the topologies tested include calculation of geometric parameters such as rotor diameter, shaft diameter, rotor slot depth, stator slot depth, rotor pole arc, stator pole arcs, rotor pole width and stator pole width etc. The calculation of each of these parameters is based on the procedure described in [21] and are used in [27] as well.

All design calculations begin with the torque equation:

$$T = KD_r^2 L \tag{3-1}$$

Where D_r is rotor diameter, L is stack length and K is output coefficient. K represents the product of electric and magnetic loading and as suggested in [27], K should be determined based on Finite Element Analysis (FEA) therefore in this project we begin by dimensioning the machine based on the method of [21] and then improve the design according to simulation results to get the required torque. The details of calculating the parameters is provided below.

3.2.1 ROTOR DIAMETER

T. Miller [21] has provided some recommended rotor diameter (D_r) to stator diameter (D_s) ratios for each of the topologies described above. The recommended ratios are tabulated in *Table 3-2* and based on these ratios respective rotor diameters are calculating considering that D_s is 270 mm.

Table 3-2
Recommended Rotor Diameter to Stator Diameter Ratios *[21]*

	3-PHASE 6/4	**3-PHASE 12/8**	**4-PHASE 8/6**
D_r/D_s	0.5	0.53	0.57

3.2.2 POLE ARCS

Ref. [21] recommends pole arcs for the selected topologies. The pole arcs are denoted by β_r and β_s for rotor and stator respectively. These are listed in *Table 3-3*. The pole arc widths are given by the equations (3-2) and (3-3):

$$t_r = 2R_r \sin\frac{\beta_r}{2} \tag{3-2}$$

$$t_s = 2(R_r + g)\sin\frac{\beta_s}{2} \tag{3-3}$$

Where R_r is rotor radius and g is airgap length.

3.2.3 YOKE WIDTH

The yoke width should be at least half the pole width. There is a margin added as well to avoid localised saturation. The recommended value for the yoke width is 2/3 of respective pole width [21] i.e.

$$y_r = \frac{2}{3}t_r \tag{3-4}$$

$$y_s = \frac{2}{3}t_s \tag{3-5}$$

3.2.4 SLOT DEPTH

The rotor slot depth (d_r) is recommended in [21] to be one half of t_s. The stator slot depth (d_s) is calculated by the already calculated parameters. Higher slot depth increases slot area thereby allowing reduction in copper losses.

$$d_r = \frac{t_s}{2} \tag{3-6}$$

$$d_s = \frac{1}{2}\{D_s - D_r - 2(g + y_s)\} \tag{3-7}$$

3.2.5 SHAFT DIAMETER

By calculating rotor slot depth and rotor yoke width the shaft diameter (D_{sh}) is then given by the eq. (3-8):

$$D_{sh} = D_r - 2(d_r + y_r) \tag{3-8}$$

The shaft diameter should be made as large as possible to ensure mechanical integrity and increase the first critical speed [21].

3.2.6 NUMBER OF TURNS PER PHASE

To calculate the approximate number of turns, assume that at certain speed the conduction angle for the transistors is equal to the step angle. Assuming the linear increase in flux linkage we can write:

$$\psi = \frac{V}{\omega}\varepsilon \tag{3-9}$$

Where V is the rated voltage, ω is rated speed and ε is step angle. We can also write the equation for flux linkage in terms of flux density and number of turns per phase as:

$$\psi = t_s L B_s n_c N_p \tag{3-10}$$

Where t_s is stator pole width, L is stack length, B_s is maximum flux density, n_c is number of coils per phase and N_p is number of turns per phase. Equating eq. (3-9) and (3-10) we get,

$$\frac{V}{\varepsilon}\omega = t_s L B_s n_c N_p$$

Rearranging gives,

$$N_p = \frac{V\varepsilon}{\omega t_s L B_s n_c} \tag{3-11}$$

3.2.7 END-TURN OVERHANG LENGTH

The end-turn overhang length (L_{oh}) is suggested to be 1.2 times the stator pole width [21].

This completes the parameter calculation process. All the calculated parameters are presented in *Table 3-3*.

Table 3-3
Calculated Parameters for the Considered Design Topologies

Parameter	Design Topology					
	3-Phase 6/4		3-Phase 12/8		4-Phase 8/6	
Rotor Diameter (D_r)	135 mm		143.1 mm		153.9 mm	
Pole Arcs (β_r, β_s)	32°	30°	16°	15°	23°	21°
Pole Widths (t_r, t_s)	37.21 mm	35.46 mm	21.42 mm	20.35 mm	28.53 mm	26.44 mm
Yoke Widths (y_r, y_s)	24.81 mm	23.64 mm	14.28 mm	13.57 mm	19.02 mm	17.63 mm
Slot Depths (d_r, d_s)	17.73 mm	42.86 mm	10.17 mm	43.48 mm	13.22 mm	44.82 mm
Shaft Diameter (D_{sh})	49.93 mm		104.99 mm		78.62 mm	
Number of Turns Per Phase (N_p)	40		35		27	
End-turn Overhang length (L_{oh})	42.55 mm		24.42 mm		31.73 mm	

3.3 PRELIMINARY SIMULATIONS

Based on the calculations above, a preliminary design was created for each topology in Motor Solve software for analysis. Initial analysis and results are detailed below for each topology. The selected material for stator and rotor core is M300-35A. Epoxy resin is selected as stator slot liner material. The winding is set to have slot fill factor of 0.5. For easy referencing, 3-phase 6/4 design will be designated as D-1, 3-phase 12/8 design as D-2 and 4-phase 8/6 as D-3.

Fig. 3-1, *Fig. 3-2* and *Fig. 3-3* show Motor Solve machine models. As a preliminary design, all parameters are set as calculated above. Firstly, firing angles were found by repeated simulations for each design to find angles which produced the maximum torque under given conditions. Initial analysis was performed with the aim to get the rated torque of 137 Nm at the rated speed of 3000 rpm.

Table 3-4 presents a comparison of the results for the three designs. The comparison shows that D-1 is offering better torque while D-3 is giving significantly better efficiency. D-2 and D-3 designs need considerable improvement so that they give the expected better overall performance than D-1.

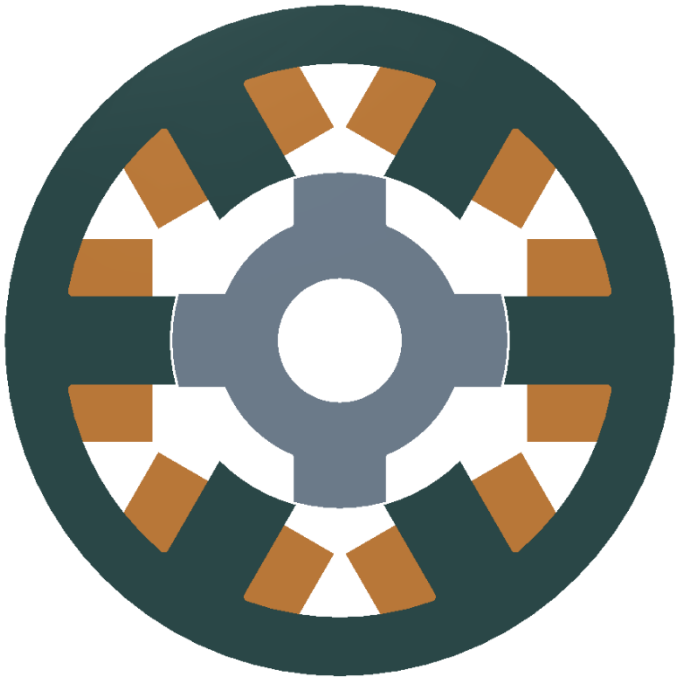

Fig. 3-1. 3-phase 6/4 model

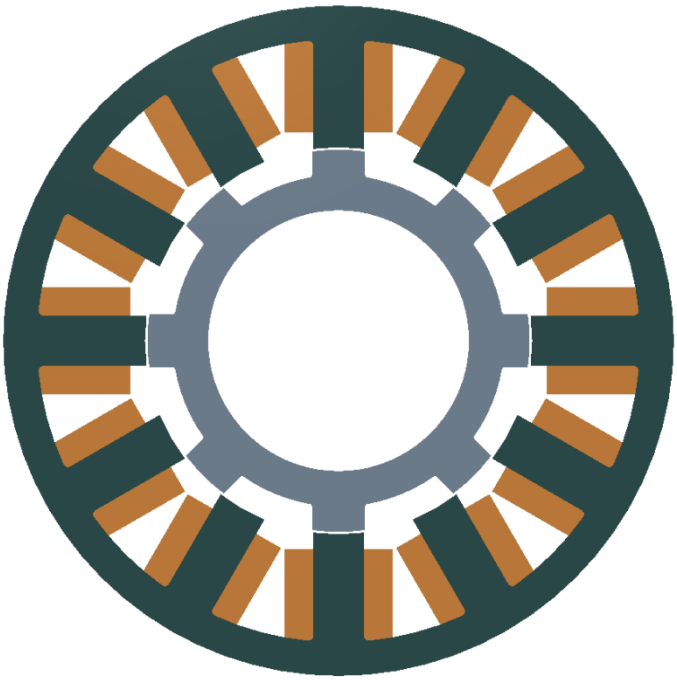

Fig. 3-2. 3-phase 12/8 model

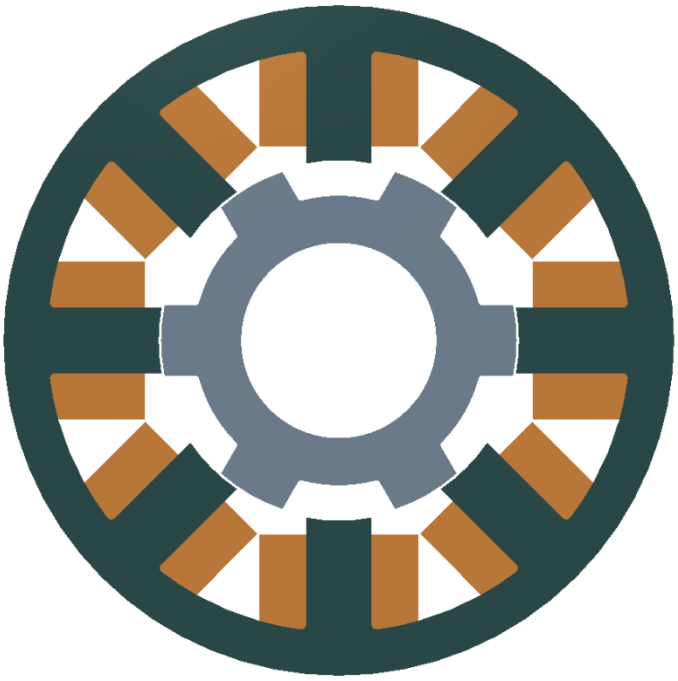

Fig. 3-3. 4-phase 8/4 model

The result parameters included in *Table 3-4* not only show the important performance parameters such as torque and efficiency but also include a breakdown of the losses in the machine. This breakdown can help us to study the effects of different fundamental frequencies on the portions of the iron losses as well as copper losses in the SRM.

After improvement, based on the performance characteristics, one of these proposed topologies will be selected as the primary design. The primary design shall then be thermally analysed, optimised and completely characterised using FEA.

Table 3-4
Comparison of Preliminary Simulation Results

Parameter	Design		
	3-phase 6/4	3-phase 12/8	4-phase 8/6
Torque (N·m)	132	108	105
Input power (kW)	48.1	39.2	35.8
Output power (kW)	41.5	33.9	32.9
Efficiency (%)	86.3	86.4	92
Torque per unit volume (N·m/mm³)	8.63E-05	5.42E-05	6.09E-05
Loss - Total (kW)	6.58	5.3	2.85
Loss - Winding (kW)	6.15	4.79	2.13
Loss - Stator back iron hysteresis (W)	148	135	213
Loss - Stator back iron eddy current (W)	43.2	50.0	130
Loss - Stator teeth hysteresis (W)	84.4	130	135
Loss - Stator teeth eddy current (W)	17.1	32.5	55.6
Loss - Rotor back iron hysteresis (W)	49.4	58.6	76.6
Loss - Rotor back iron eddy current (W)	14.7	27.5	41.2
Loss - Rotor teeth hysteresis (W)	49.9	48.0	45.8
Loss - Rotor teeth eddy current (W)	16.0	25.3	21.9

3.4 DESIGN IMPROVEMENTS

As evident through the preliminary simulation, the proposed designs, in particular D-2 and D-3 need improvement. The following paragraphs explain the step-by-step procedure adopted to improve these designs. Considering the specifications for this project, the key goal is recognised as to obtain the required torque with the required efficiency. Therefore, during each step of the design improvement, the values of the parameters are selected to give the best combination of torque and efficiency. As a secondary part of sensitivity analysis, effect of each parameter variation on the torque ripple is also graphically presented. The data related to torque ripple variation would enable us to identify the parameters that need to be optimised for torque ripple minimisation. Rather than looking at variation of all important parameters such as rotor diameter, stator and rotor pole arcs, stator core thickness etc. altogether on the characteristics of the machine, here a simplistic approach is adopted. All parameters are changed one by one while keeping other parameters fixed except for the case of rotor diameter. At the end of the improvement process, one design out of these three will be selected based on the generated results.

3.4.1 3-PHASE 6/4 MACHINE

The D-1 design has high inductance. The unaligned inductance is 1.8 mH and the aligned inductance is 2.51 mH. *Fig. 3-4* shows the inductance profile. Although the inductance is high, but still the current rises to its rated value at rated speed of 3000 rpm. This is because since this is a three-phase

machine with only 4 rotor poles, so number of steps per revolution are only 12 compared to 24 for D-2 and D-3. Therefore, the conduction time for each phase is more than available in D-2 and D-3 so current finds enough time to rise to its value.

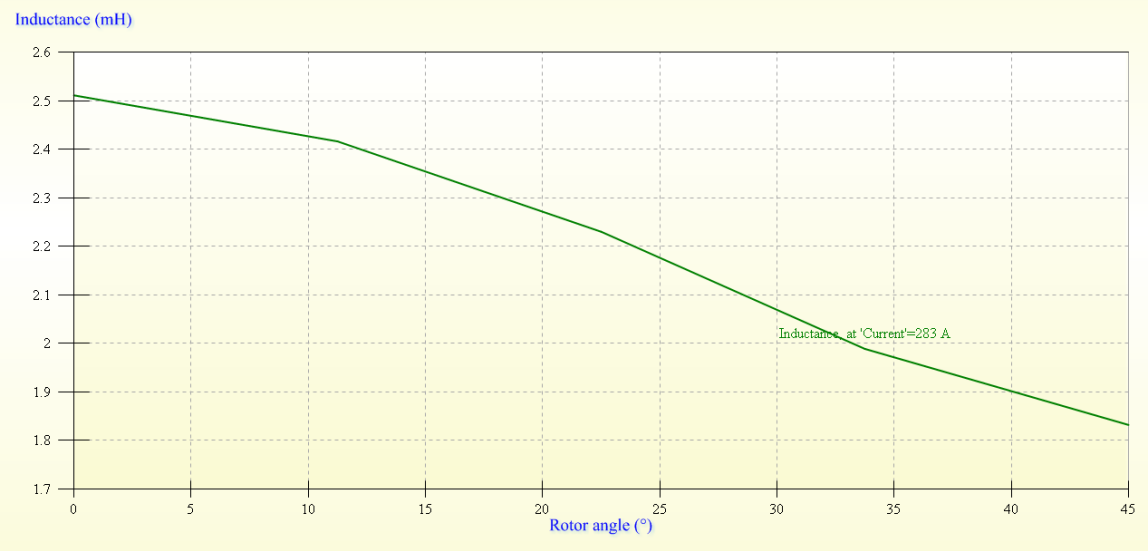

Fig. 3-4. Inductance profile of D-1

The improvement process began by trying to find the best combination of rotor diameter and shaft diameter. Other parameters are calculated using the design equations based on the simulated values of rotor diameter and shaft diameter. *Fig. 3-5* shows the results of changing D_r and D_{sh}. The range for shaft diameters selected was 50-80 mm. However, shaft diameters above 60 mm do not produce results worthy enough of consideration so results produced by only 50-60 mm are shown here. The range for rotor diameter was selected to be 130-180 mm. However, looking at results produced by rotor diameter = 170 mm showed that increasing further the rotor diameter would have deteriorated the efficiency more. So, the limit was set to consider results till 170 mm. The selected values for rotor diameter and shaft diameter were 160 mm and 50 mm respectively. With these values, the torque produced was 187 Nm at an efficiency of 85.9%. A higher value of torque with small decrease in efficiency is preferred as having more torque than required allows current to be dropped to improve efficiency.

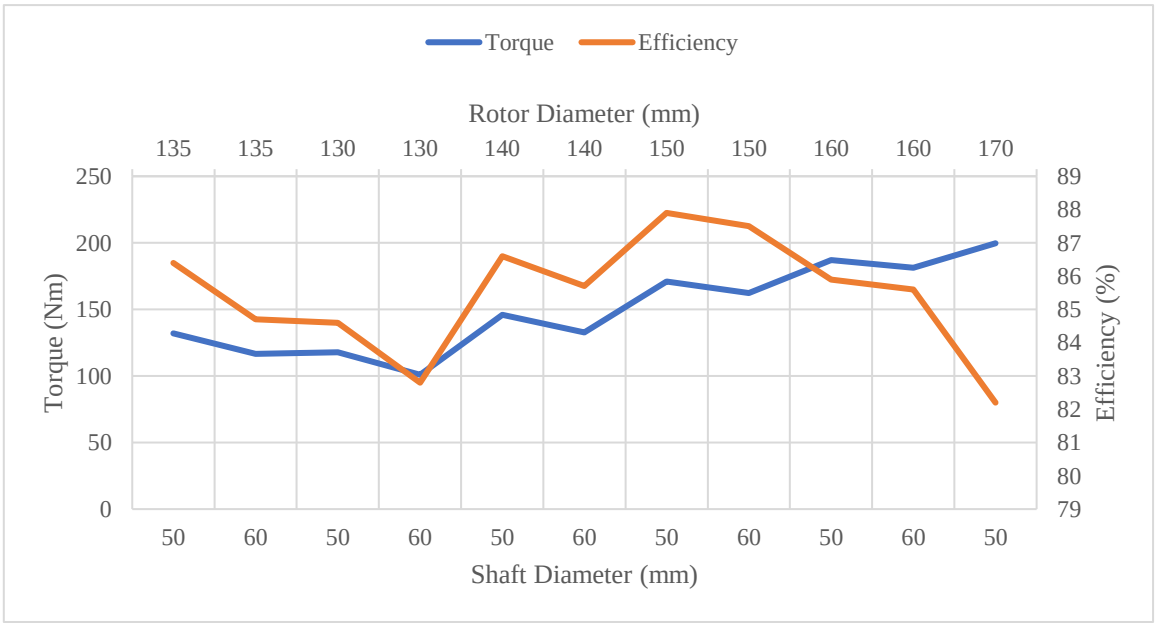

Fig. 3-5. Variation of rotor diameter and shaft diameter vs. Torque and Efficiency for D-1

The pole arcs for D-1 were kept to the values used in the preliminary design. This is because the end-turn overhang length is determined by the stator pole arc. With stator pole arc of 30° the sum of overhangs of both sides of the machine is just below the stator length. So, any increase would have made the end-turns lengthier than the stator itself. Values below 29° were not considered to preserve the machine's ability to develop torque from any rotor position and also not to increase the torque ripple. As an extension to the selection of pole arcs, skew angles for poles were also selected. The results are similar for skew angle values of (87, 93), (87, 96) and (84, 96), refer to *Fig. 3-6*. However, rotor pole skew is selected as 87° and stator pole skew angle as 93° to give maximum possible space for the winding. As pole arcs have the major impact on torque ripple so effect on torque ripple is also considered here. *Fig. 3-7* shows variation of torque ripple with pole skew angles.

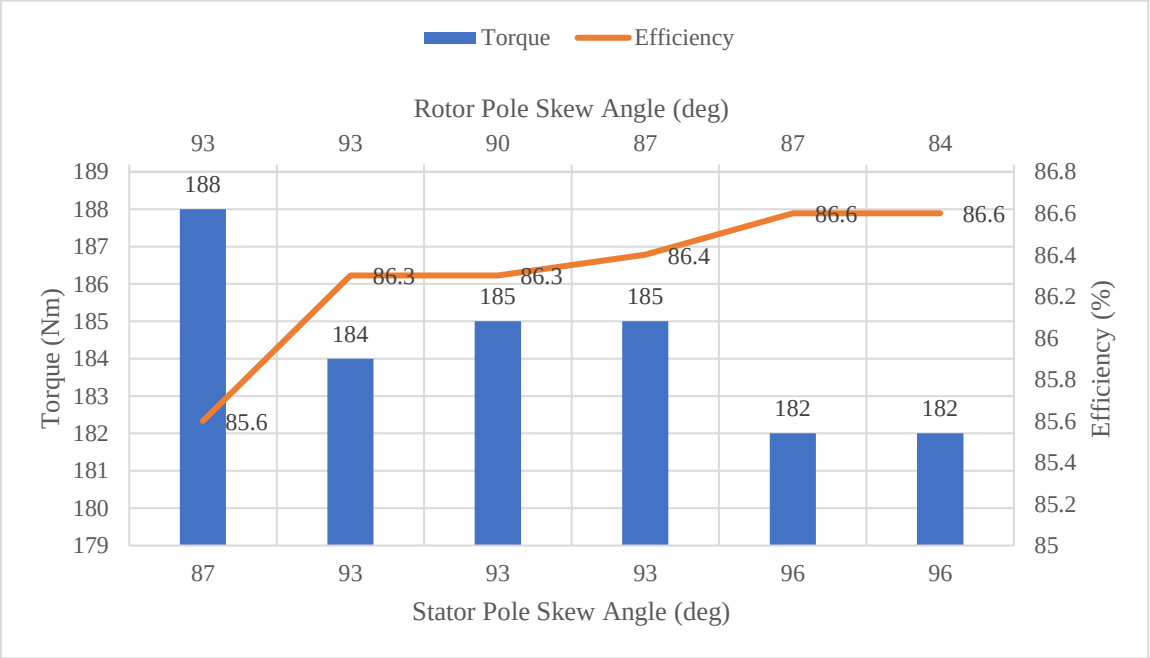

Fig. 3-6. Pole skew angles vs. Torque and Efficiency for D-1

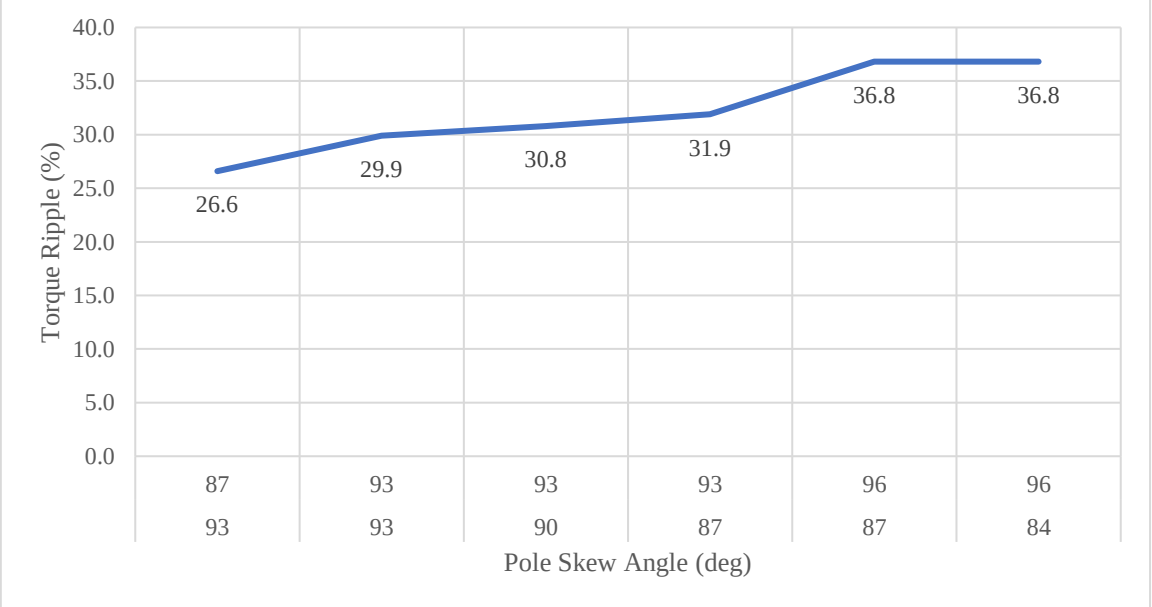

Fig. 3-7. Variation of torque ripple with pole skew angle (top row: stator, bottom row: rotor)

Third step in this improvement process for D-1 involved selecting the stator pole depth. The value in preliminary design was calculated to be 26 mm. In this set of simulations, values above and below 26 mm were tested. Referring to *Fig. 3-8*, the calculated value produces better results than other values. Hence this value is retained. *Fig. 3-9* shows the impact of stator pole depth on the torque ripple.

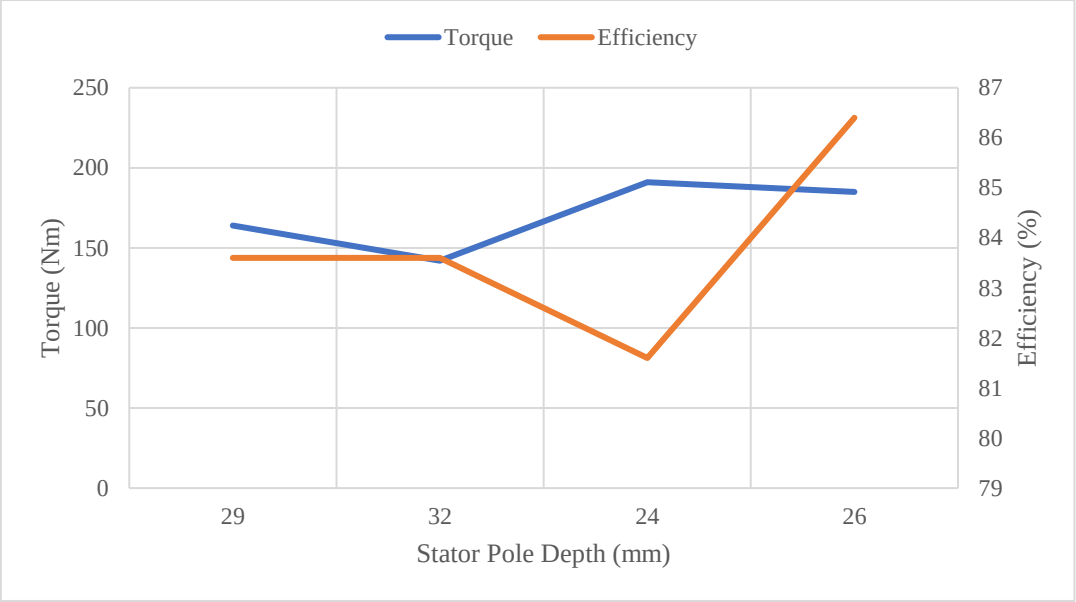

Fig. 3-8. Stator pole depth vs. Torque and Efficiency

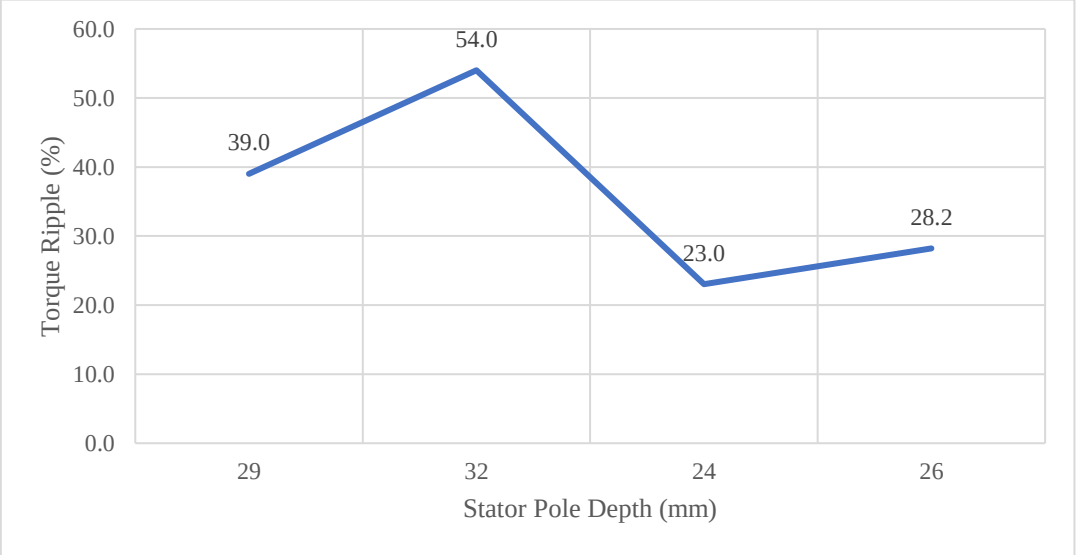

Fig. 3-9. Variation of torque ripple with change in stator pole depth

Following selection of stator pole depth, different values of rotor pole depth are simulated for selection of best value. The calculated value used in preliminary design is 29.4 mm. As shown in *Fig. 3-10*, rotor pole depth of 29.4 mm produces the suitable values of torque and efficiency. *Fig. 3-11* shows the variation of the torque ripple with the change in rotor core thickness. The calculated value produces the lowest ripple. Rotor core thickness has perceptible influence on the torque ripple for D-1.

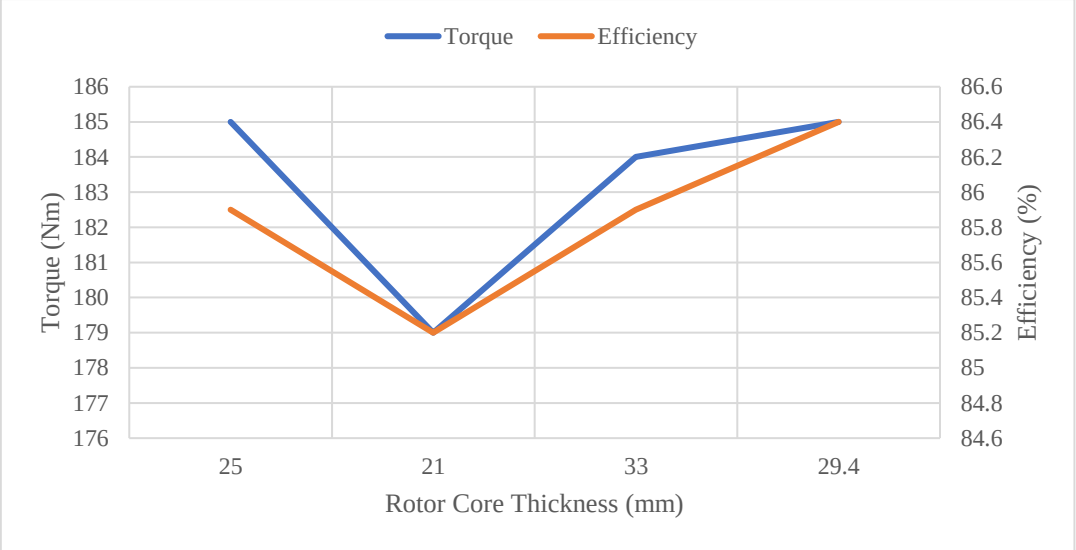

Fig. 3-10. Rotor core thickness vs. Torque and Efficiency

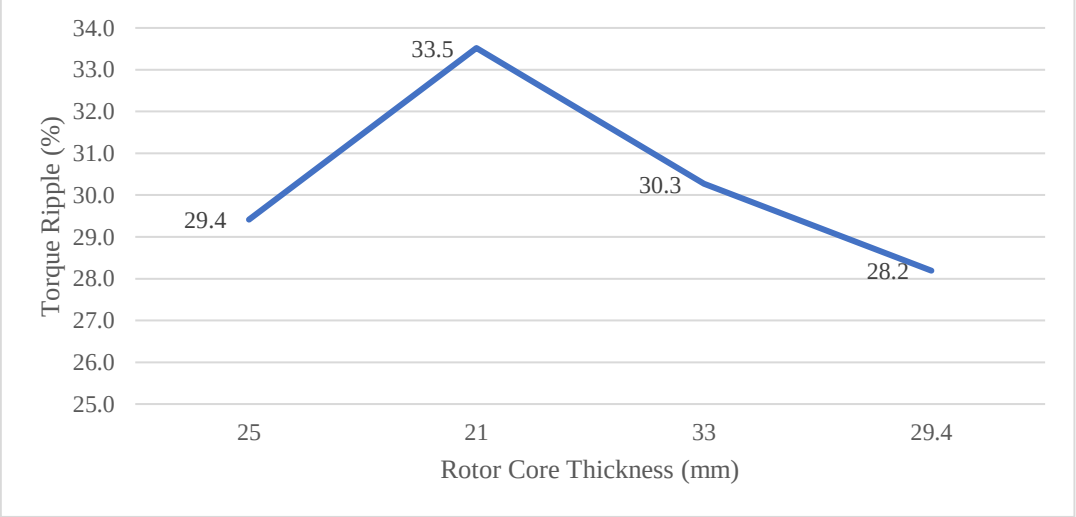

Fig. 3-11. Rotor core thickness vs. torque ripple

As the final step of the design, coil size is increased to occupy the available space as much as possible. This reduces the copper losses and improves efficiency. Number of turns were also reduced to 23 not only to improve efficiency but also to reduce the inductance. Lower inductance would help the machine to develop the required torque at higher speeds. The current was only reduced by 2% so the rated torque is produced using 98% of rated current.

Fig. 3-12 shows the improved D-1 model after all the modifications done in the process explained above. *Fig. 3-13* displays inductance profile of D-1 after improvement. The unaligned inductance is 0.48 mH and aligned inductance is 1.59 mH. This gives the inductance ratio of 3.3 compared to 1.4 before improvements. The flux linkage at aligned and unaligned rotor positions is provided in *Fig. 3-14*. Torque waveform is given in *Fig. 3-15*. The magnitude of torque ripple is 62.9 Nm or 45% of the average torque. *Table 3-5* provides the results of motion analysis of D-1 at 3000 rpm. To complete the characterisation, *Fig. 3-16* presents the torque-speed profile of D-1.

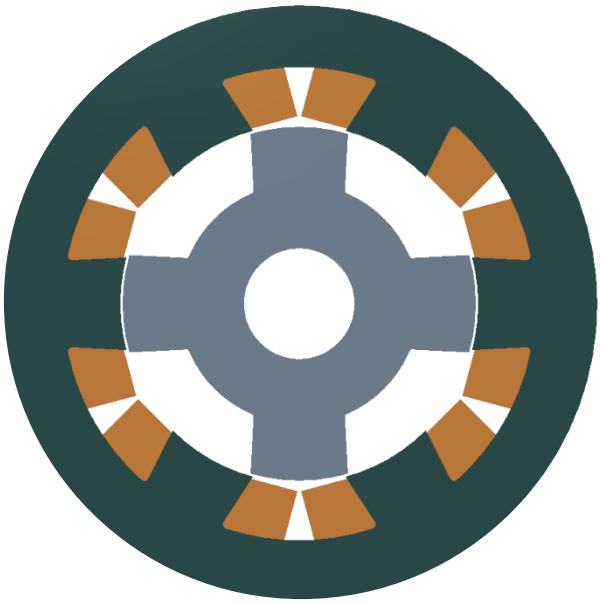

Fig. 3-12. Improved model of D-1

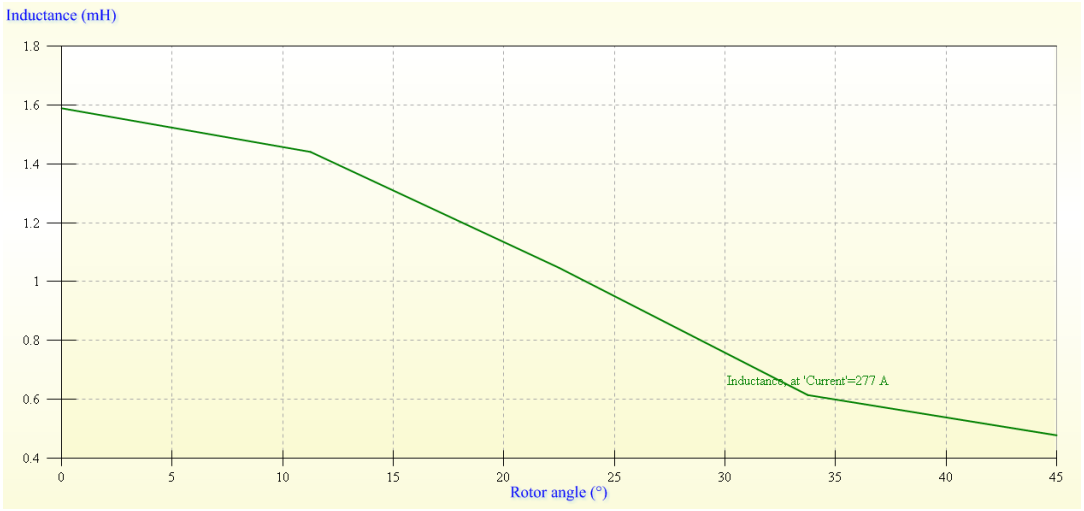

Fig. 3-13. Inductance profile of D-1 @ current = 98%

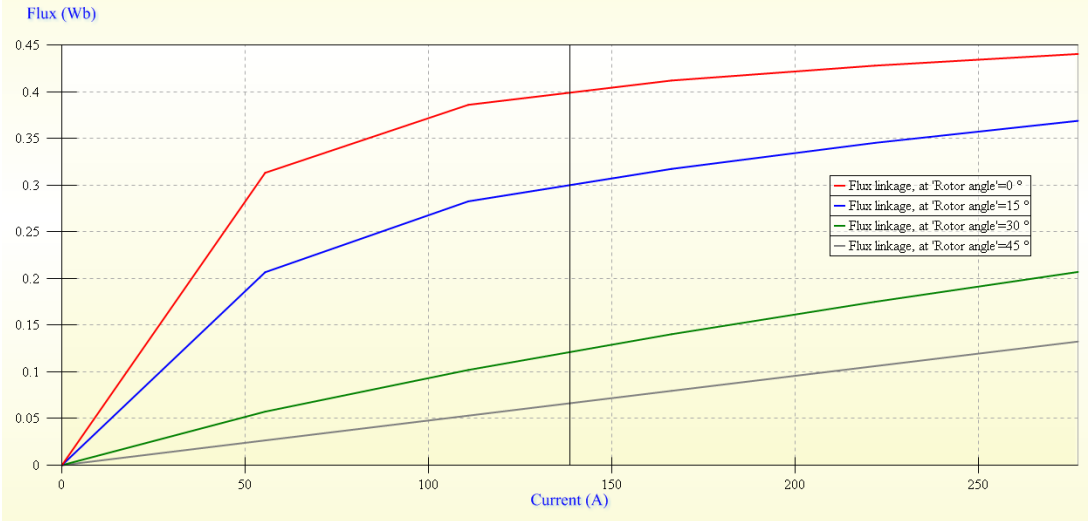

Fig. 3-14. Magnetization curves for D-1 @ current = 98%

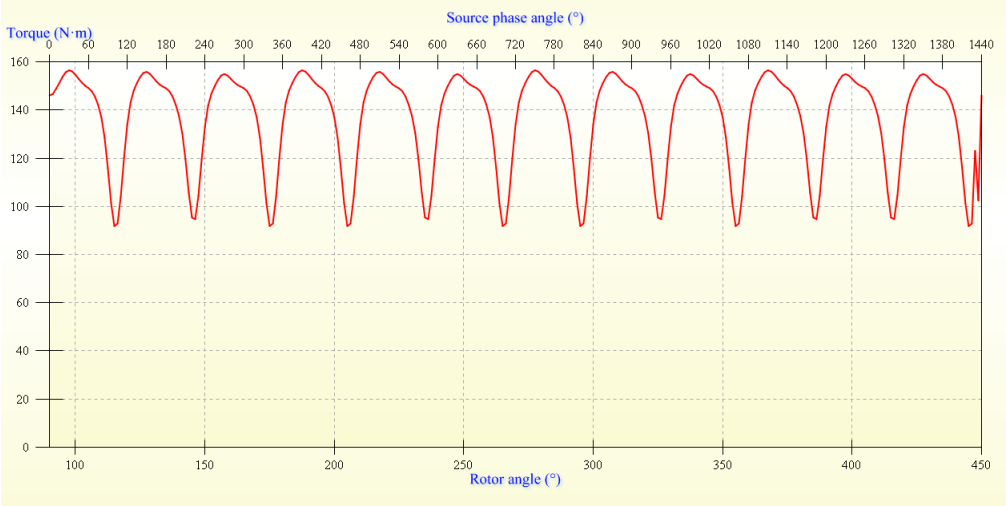

Fig. 3-15. Torque waveform of D-1 at rated speed

Table 3-5
Motion Analysis of D-1 at Rated Speed

Torque (N·m)	137
Input power (kW)	46.4
Output power (kW)	43
Efficiency (%)	92.8
Torque per unit volume (N·m/mm³)	6.36E-05
Loss - Total (kW)	3.4
Loss - Winding (kW)	2.82
Loss - Stator back iron hysteresis (W)	191
Loss - Stator back iron eddy current (W)	79.0
Loss - Stator teeth hysteresis (W)	67.7
Loss - Stator teeth eddy current (W)	21.5
Loss - Rotor back iron hysteresis (W)	67.2
Loss - Rotor back iron eddy current (W)	22.4
Loss - Rotor teeth hysteresis (W)	67.0
Loss - Rotor teeth eddy current (W)	22.9

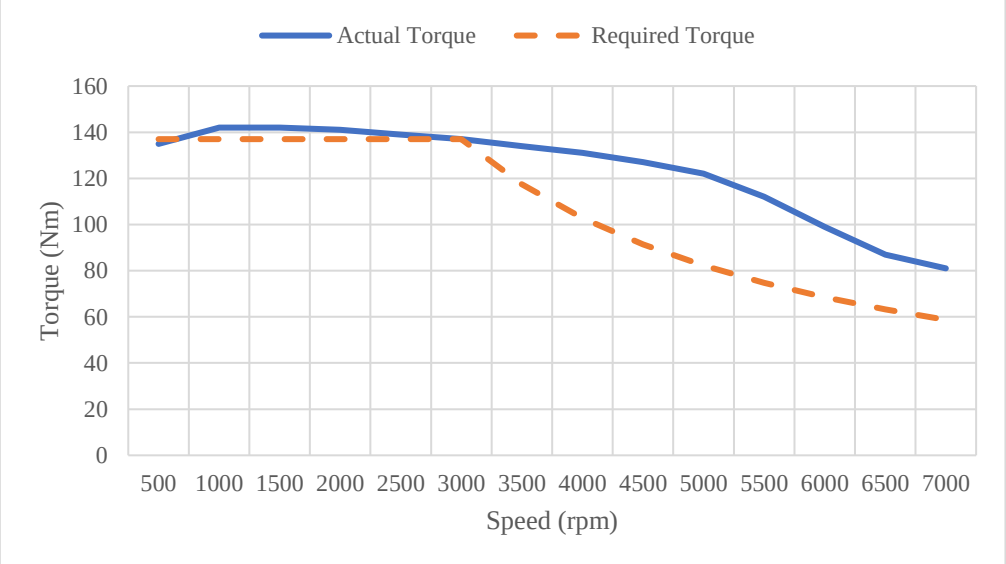

Fig. 3-16. Torque-speed profile of D-1

3.4.2 3-PHASE 12/8 MACHINE

Fig. 3-17 shows the inductance profile of the D-2. The unaligned inductance for D-2 is around 2.2 mH which is too high. This high value of inductance does not let the current to rise to the desired level hence the torque production is compromised. The high inductance also pushes the machine into continuous conduction mode at much lower speeds than required. Therefore, the first step in improving D-2 is to get lower inductance levels so that current can rise to the required level and then other parameters be selected to get the required performance.

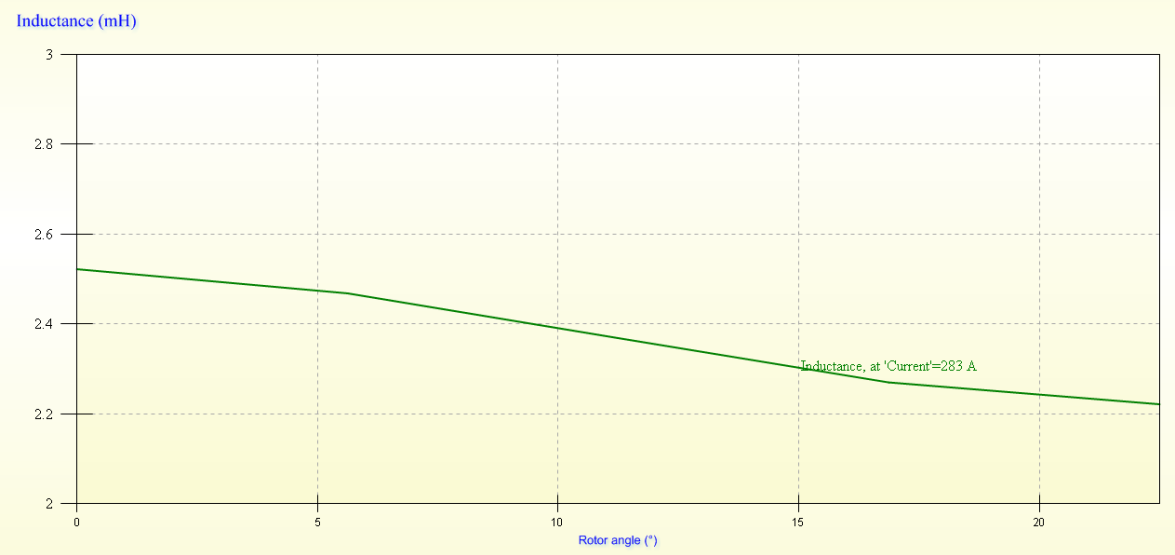

Fig. 3-17. Inductance profile of D-2

To reduce the inductance, number of turns were reduced to 15 instead of 35 as calculated. *Fig. 3-18* shows the inductance profile of D-2 after reduction in number of turns. The unaligned inductance has been reduced to 0.6 mH and aligned inductance is 0.97 mH. This give the inductance ratio of 1.6 which is also better than the preliminary model.

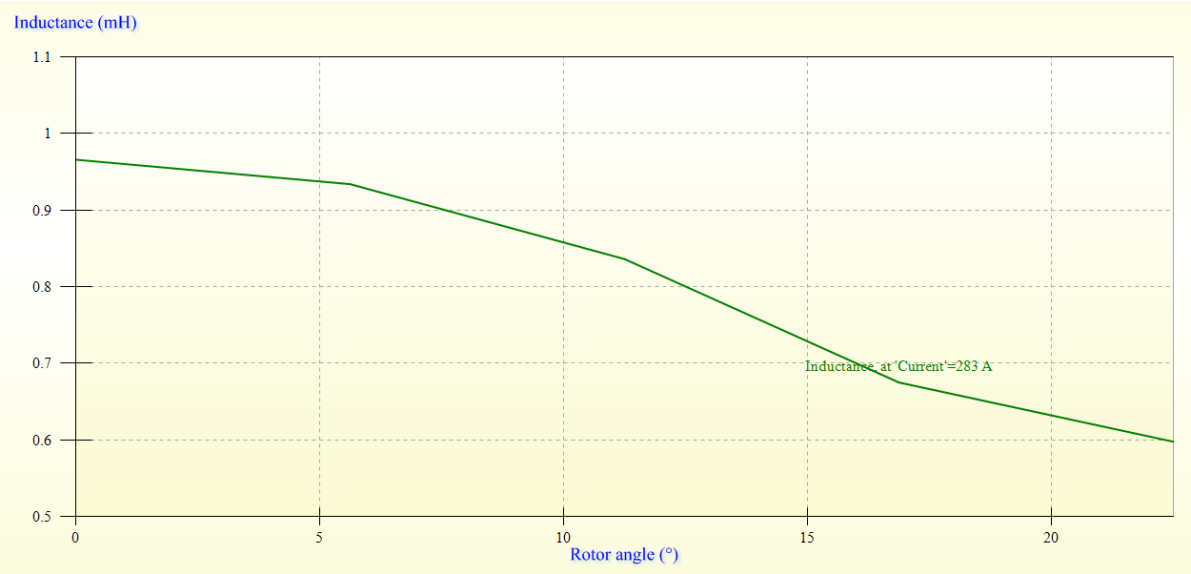

Fig. 3-18. Inductance profile of D-2 with reduced inductances

To find the best combination of rotor diameter and shaft diameter for this design, the values of these diameters are fixed and other parameters are calculated using the design equations. The number of turns are kept constant at 15. The stator back iron and rotor back iron thicknesses were allowed a

value of at least 15 mm. A higher width for back-iron should prevent the machine from going too deep into saturation under rated conditions and could help in dealing with peak load conditions. Thickness of back-iron also makes it stiff which helps it against the mechanical forces [21]. However, it also means that the machine does not utilise its full potential under the rated conditions. Decreasing back-iron thickness increase stator pole depth thereby increasing space for the coil but at the same time worsens the acoustic noise problem. Back-iron thickness should be at least 15 mm to ensure mechanical integrity [18]. So, the cases where stator back iron was too thin (<15mm), stator pole depth was adjusted to keep the stator back iron of at least minimum width. *Fig. 3-19* shows the results of changing shaft diameter and rotor diameter. The chosen values for (D_r, D_{sh}) are (180,60) as these values provide the best combination of torque and efficiency.

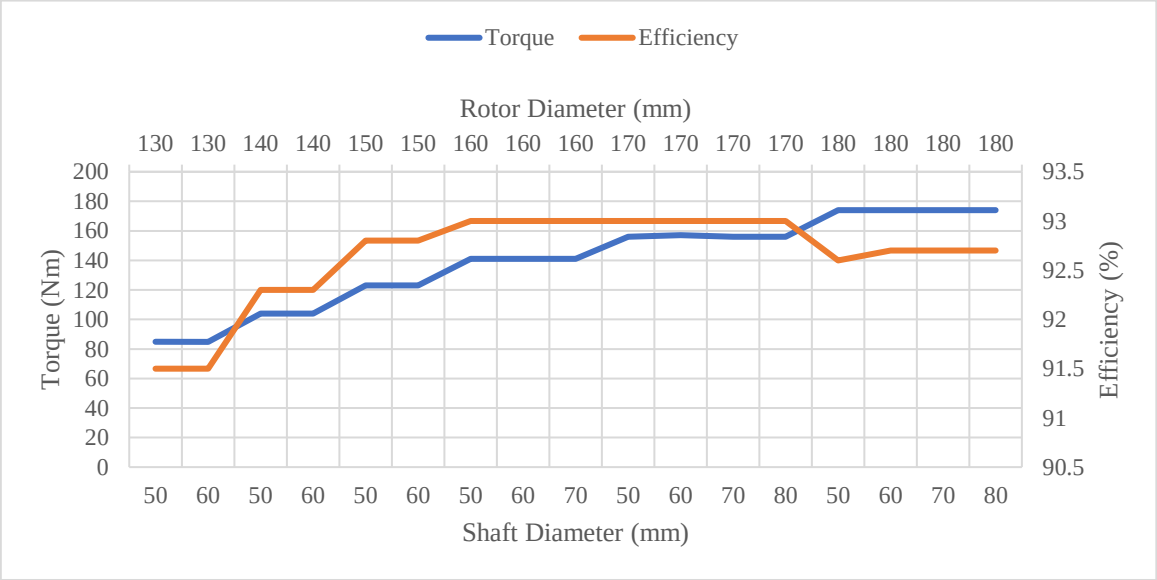

Fig. 3-19. Effect of changing rotor diameter and shaft diameter on Torque and Efficiency for D-2

Moving forwards, variation of stator pole depth was simulated. With the changing stator pole depth, the variation of torque and efficiency is plotted in *Fig. 3-20*. The value selected for stator pole depth is 26 mm as it offered more torque but at slightly lower efficiency. The torque margin allows the current to be reduced to lower the copper losses. *Fig. 3-21* shows the effect of stator pole depth on the torque ripple.

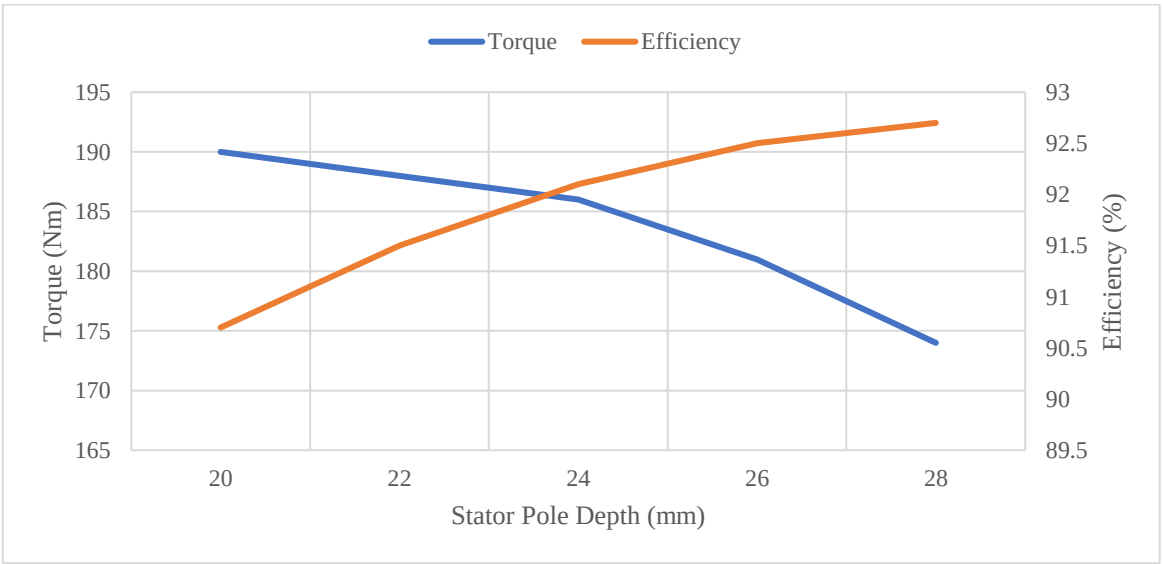

Fig. 3-20. Effect of variation of stator pole depth on D-2

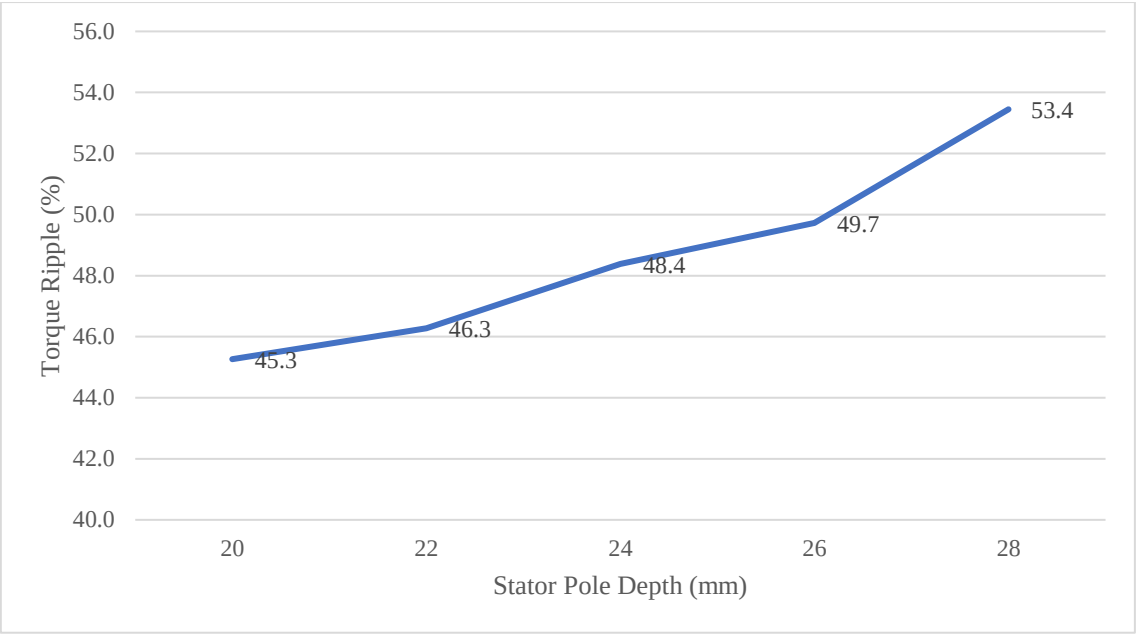

Fig. 3-21. Change in torque ripple with variation of stator pole depth

Rotor core thickness has very little influence on the torque or efficiency of the machine as shown *Fig. 3-22*. Rotor core thickness was selected to be 25 mm to make the rotor core neither too thin or unnecessarily thick. This value should help the rotor to not become saturated at lower speeds. *Fig. 3-23* shows the variation of the torque ripple for different rotor core thickness values. The effect of rotor core thickness in this case is not very significant on torque ripple as well.

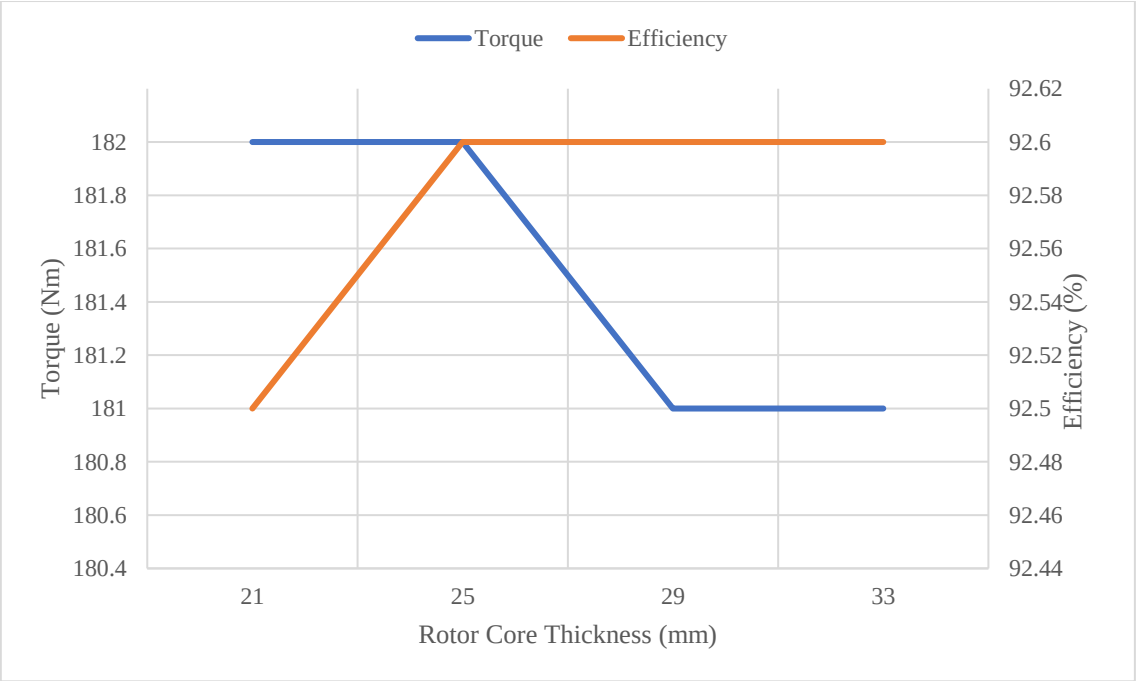

Fig. 3-22. Effect of rotor core thickness on D-2

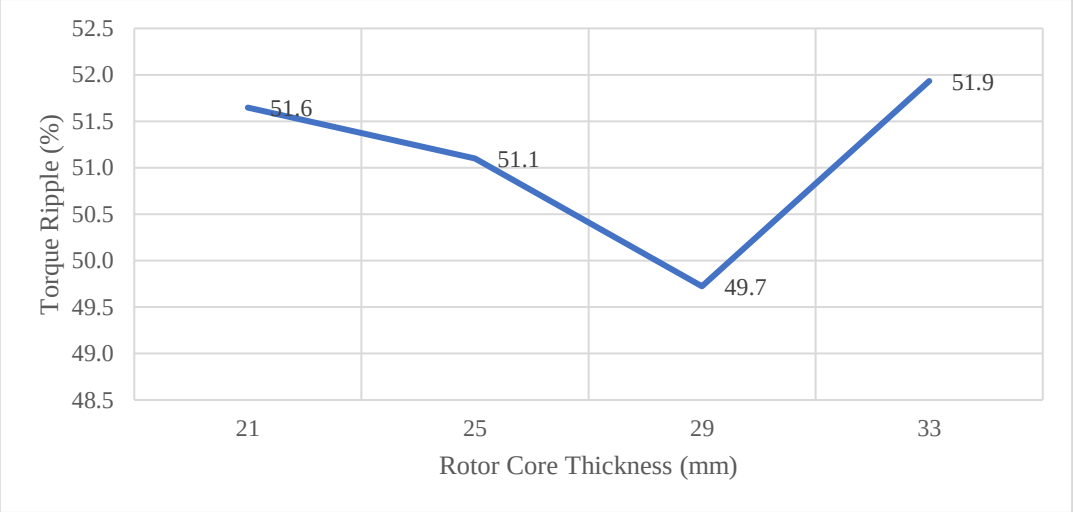

Fig. 3-23. Rotor core thickness vs. torque ripple

As the next step, we select the stator and rotor pole arcs that maximise the torque and efficiency. The range of values for rotor pole arc was set as 16°-19° and stator pole arc was adjusted such that the difference between pole arcs never exceeded 2° and lower limit on stator pole was set at 15°. The values for stator pole arc less than 15° are not considered as min (β_r, β_s) should be greater than or equal to the step angle which is 15° in this case. While changing the pole angle values, all parameters except for end-turn length are kept constant. The end-turn length was calculated from stator pole width. *Fig. 3-24* depicts the result of changing the pole arcs. The chosen values for rotor pole arc and stator pole arc are 17° and 16° respectively. Increasing the min (β_r, β_s) reduces the torque ripple but also decreases efficiency so setting 16° as minimum of pole arcs is a reasonable compromise. Skewing the pole arcs had adverse effects either on torque or efficiency as shown in *Fig. 3-25* therefore, skew angles were kept to default value of 90°.

As already explained in chapter 2, pole arcs play an important role in determining the torque ripple of the machine. Therefore, changing the arcs should affect the torque ripple. *Fig. 3-26* and *Fig. 3-27* capture this phenomenon. As expected ripple is lower for higher values of min (β_r, β_s) which in this case is β_s.

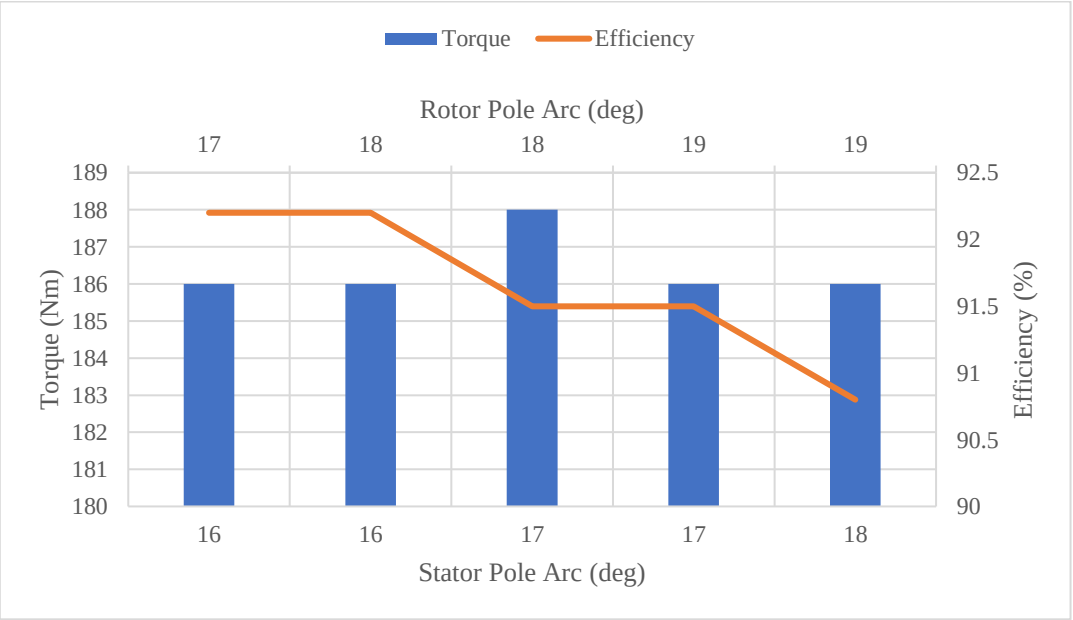

Fig. 3-24. Pole arcs vs. Torque and Efficiency for D-2

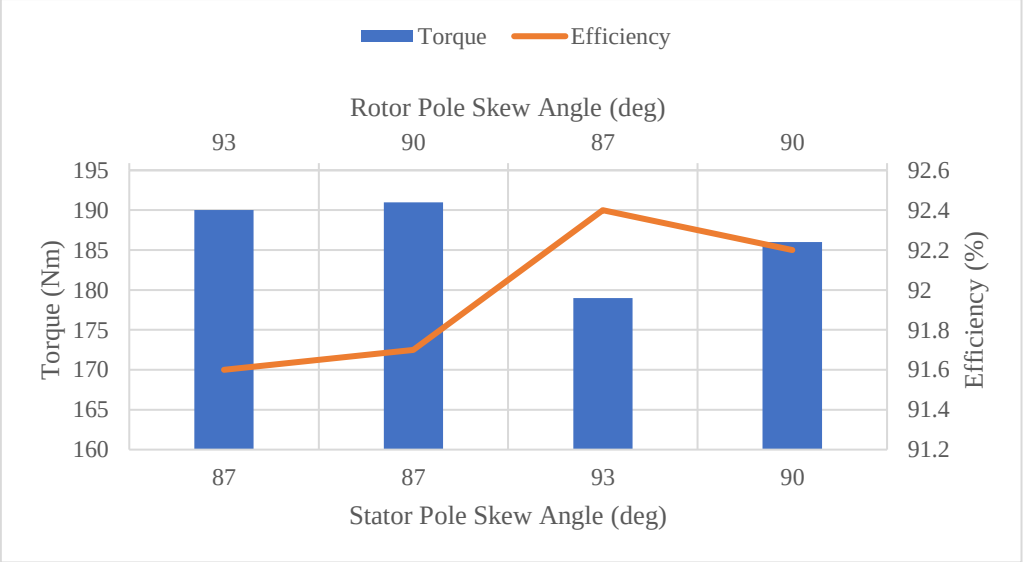

Fig. 3-25. Effects of skewing the poles on D-2

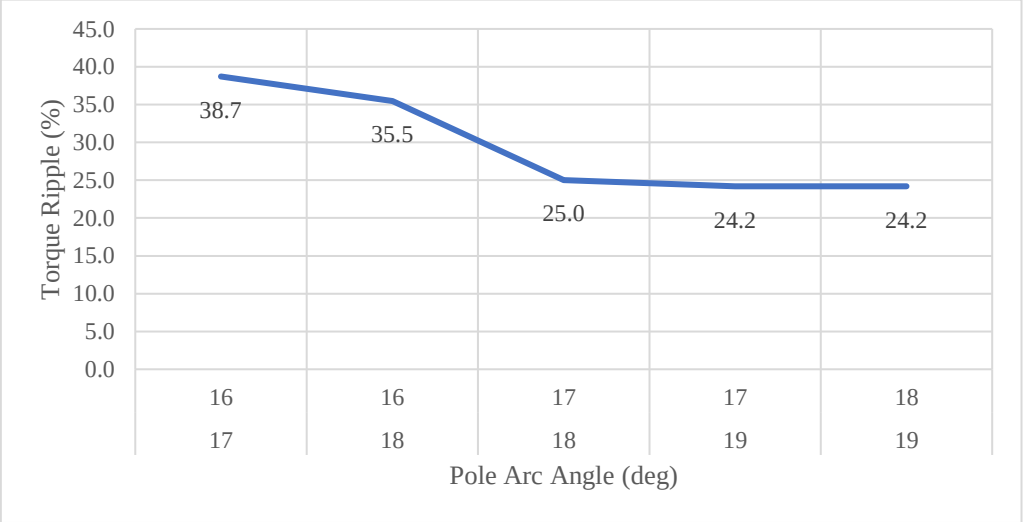

Fig. 3-26. Torque ripple vs. pole arcs (top row: stator, bottom row: rotor)

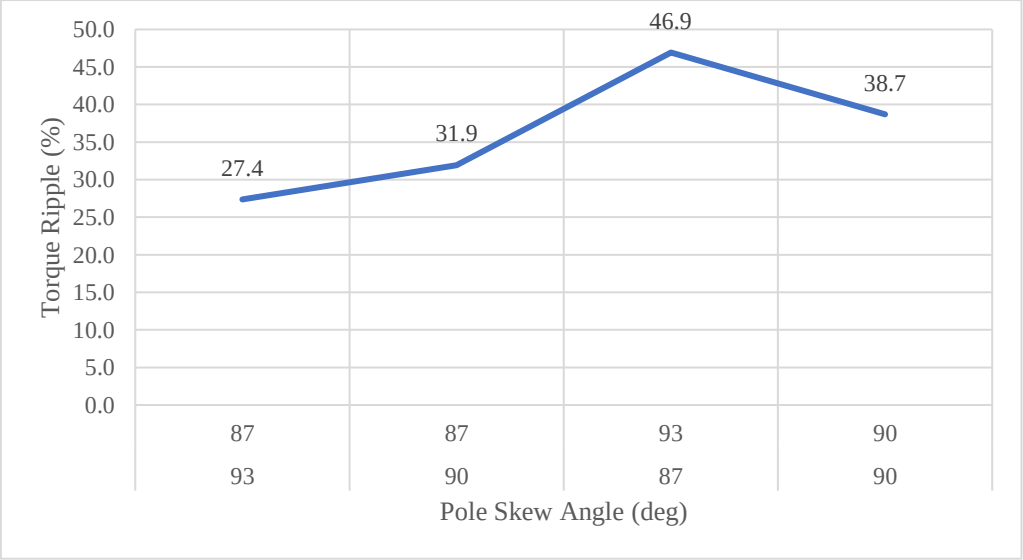

Fig. 3-27. Torque ripple vs. pole skew angle (top row: stator, bottom row: rotor)

Finally, after selecting all the parameters, the coil is sized to occupy maximum available space. This allows the copper losses to be reduced. Afterwards, current is reduced to get the required torque of 137 Nm and increase the efficiency by reducing the copper losses. The current is reduced to 77% to produce exactly the required torque. At the end of the improvement process, D-2 looks as depicted in *Fig. 3-28*.

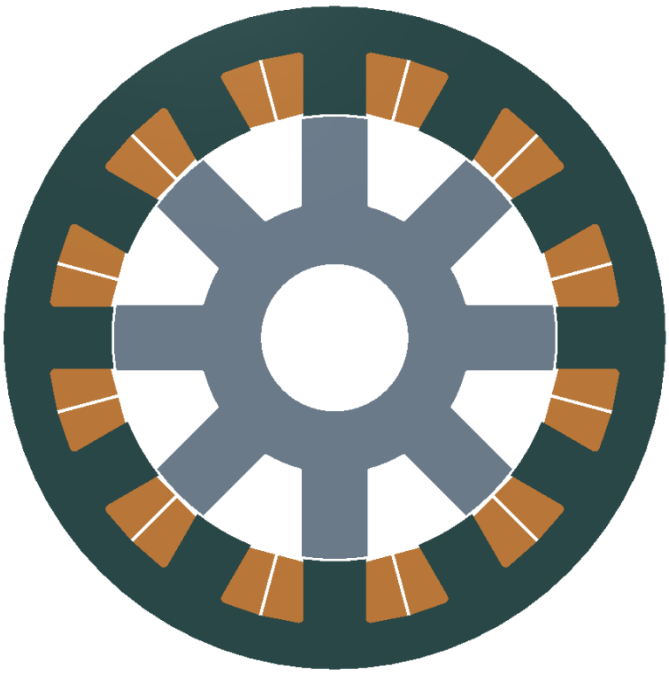

Fig. 3-28. D-2 model after improvement

Fig. 3-29 shows the inductance profile of the improved D-2. The unaligned inductance is 0.45 mH and aligned inductance is 1.53 mH which gives the inductance ratio of 3.4. The improvement process has more than doubled the inductance ratio compared to the profile shown in *Fig. 3-18*. The flux linkage vs current profiles, shown in *Fig. 3-30*, with changing rotor positions give the machine operating characteristics in the unaligned and aligned positions.

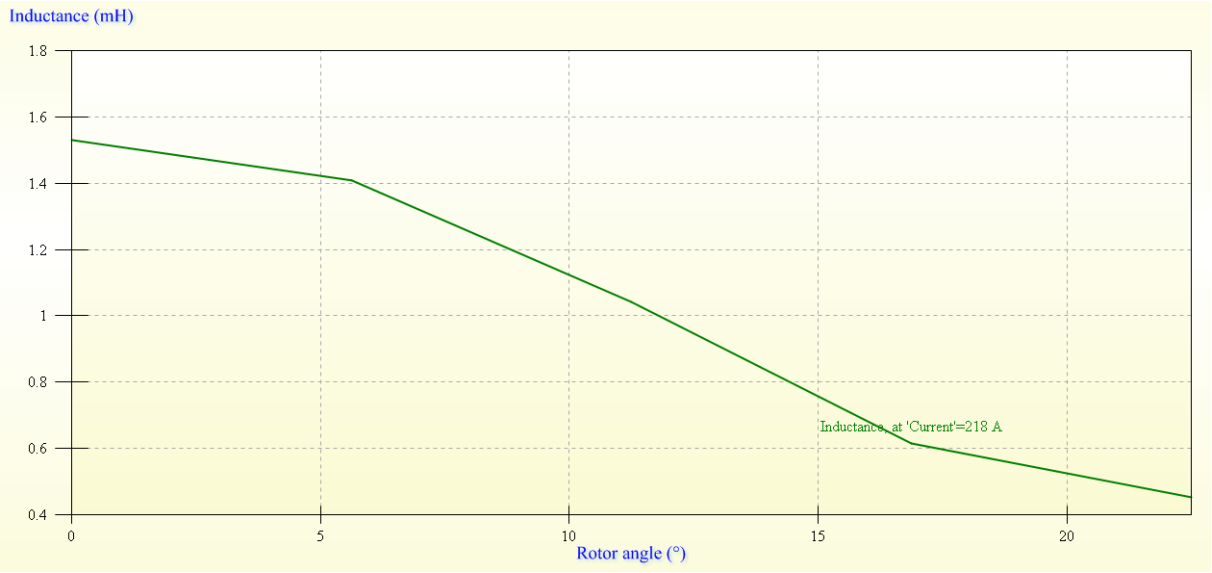

Fig. 3-29. Inductance profile of improved D-2 @ current = 77% of rated value

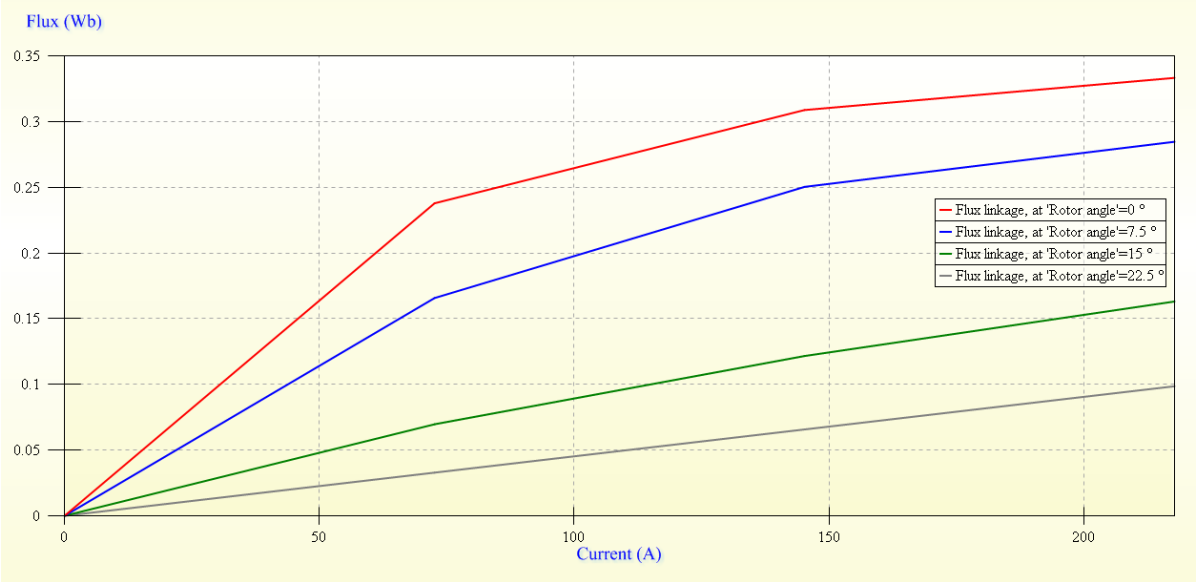

Fig. 3-30. Magnetization curves for D-2 at aligned and unaligned rotor positions

The torque waveform of D-2 is presented in *Fig. 3-31*. The torque ripple as can be seen in the torque waveform, given in *Fig. 3-31*, is small. The value of torque ripple is 41 Nm or 29.3% of the average torque. *Table 3-6* provides the results generated by the motion analysis of design D-2. The average torque produced is 140 Nm with an efficiency of 94.3%. *Fig. 3-32* displays the torque-speed profile of D-2 with current set at 77%. With increasing speed, turn-on and turn-off angles were increasingly advanced to get the required torque at the given speeds. Clearly, D-2 is capable to produce the required torque throughout the considered speed range.

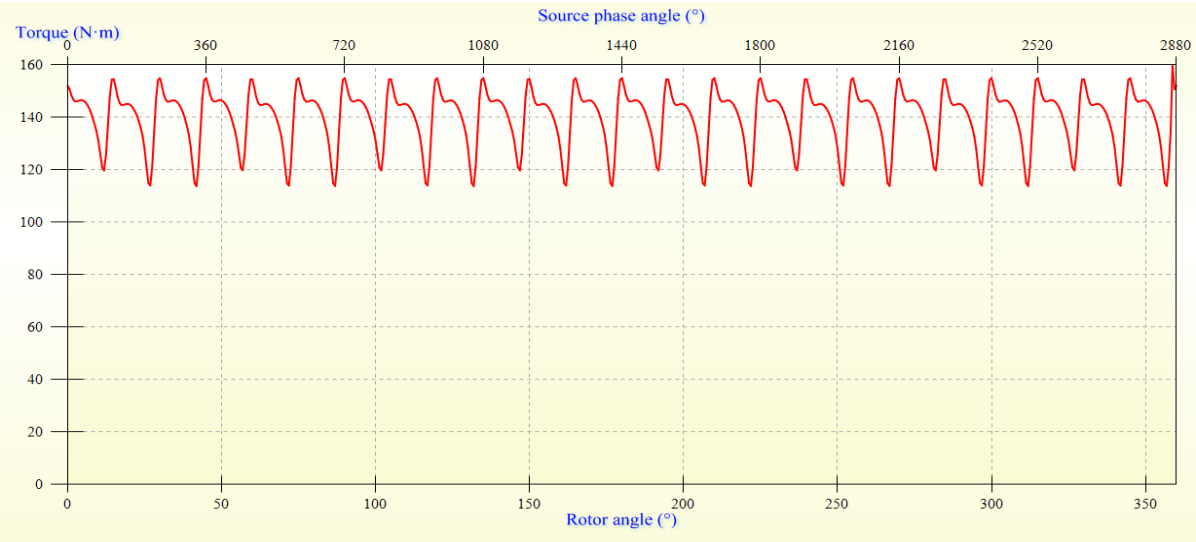

Fig. 3-31. Torque waveform of D-2

Table 3-6
Motion Analysis of D-2 at rated speed with current = 77%

Torque (N·m)	139
Input power (kW)	46.1
Output power (kW)	43.5
Efficiency (%)	94.3
Torque per unit volume (N·m/mm³)	5.14E-05

Loss - Total (kW)	2.60
Loss - Winding (kW)	1.67
Loss - Stator back iron hysteresis (W)	232
Loss - Stator back iron eddy current (W)	142
Loss - Stator teeth hysteresis (W)	141
Loss - Stator teeth eddy current (W)	62.5
Loss - Rotor back iron hysteresis (W)	79.0
Loss - Rotor back iron eddy current (W)	35.1
Loss - Rotor teeth hysteresis (W)	155
Loss - Rotor teeth eddy current (W)	77.6

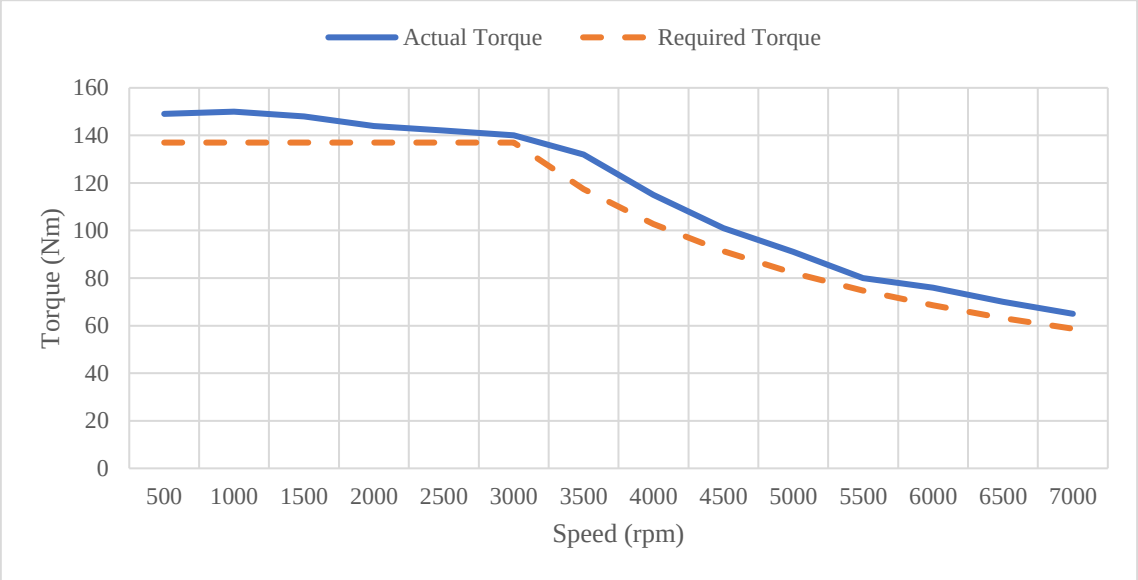

Fig. 3-32. Torque-speed profile of D-2

3.4.3 4-Phase 8/6 Machine

The D3 design does not have high aligned and unaligned inductance problem as other designs *Fig. 3-33* shows the inductance profile of D-3 at 100% of the rated value of the current. The unaligned inductance is below 1 mH so setting up the current through the windings does not require large advancements in turn-on angles and current should be able to reach the required level during the conduction period. The aligned inductance is 1.21 mH which is not high as well thereby allowing the current to decrease to zero without the need to advance the turn-off angle too much except for if the machine is operating at higher speeds.

The first step for D-3 is to identify the best combination of rotor diameter and shaft diameter. To achieve this purpose, rotor diameter was varied between 130 mm and 170 mm while shaft diameter was moved in the range of 50 mm to 80 mm. The rest of the parameters were calculated from the equations used in the design calculations as described above. The resulting data is plotted in *Fig. 3-34*. The best values for rotor diameter and shaft diameter are chosen as 160 mm and 60 mm respectively. This combination gives more than the required torque while providing the highest efficiency. The combination (160,50) also gave same values for torque and efficiency however higher value for shaft diameter was chosen to aid mechanical stability.

In the second step, most suitable combination of stator and rotor pole arc angle is selected. All parameters are set as calculated with rotor diameter set at 160 mm and shaft diameter as 60 mm. The only parameter changes with stator pole arc angle is end-turn overhang length. Rotor pole arc variation range was set between 20° to 23°. The reason is that beyond 23°, rotor pole will further increase the

between rotor and stator poles at the unaligned position. This overlap will reduce the ratio between the

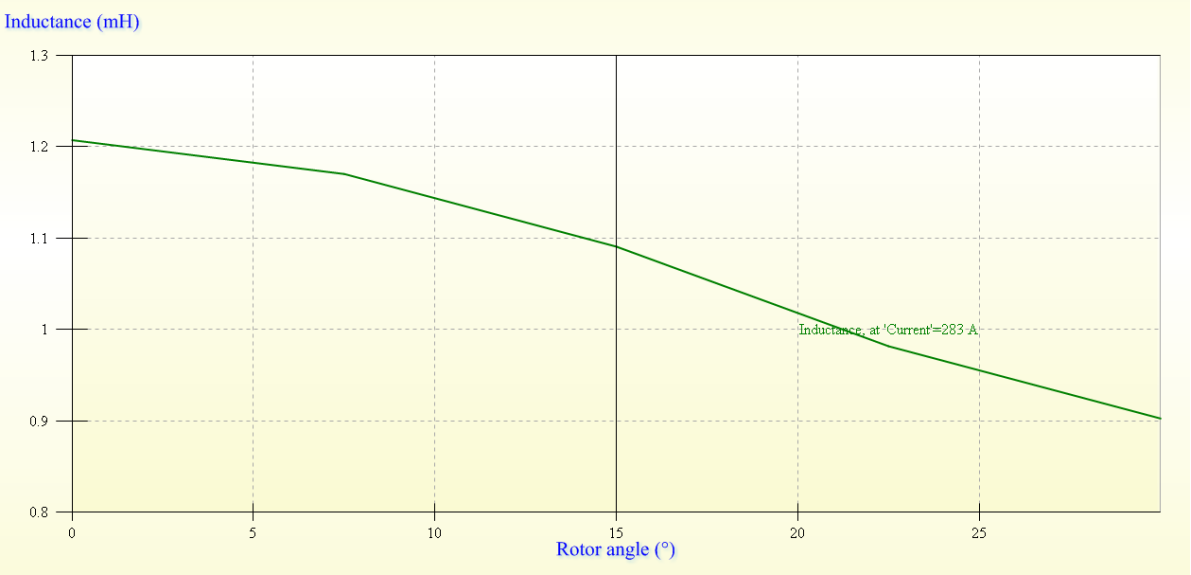

Fig. 3-33. Inductance profile of D-3

aligned inductance and unaligned inductance, thereby reducing the torque output. The stator pole angle in turn was selected so that the difference between rotor pole angle and stator pole angle does not exceed 3°. The rotor pole angle is always set to be greater than stator pole angle. The results are shown in *Fig. 3-35*. The selected values for rotor and stator pole angles are 20° and 19° respectively. As an extension of this step, skew angles (or alternatively *tooth angles* as used in Motor Solve) for stator and rotor poles are also determined. Skewing should help to better direct the flux from stator to rotor pole and vice versa, so it should reduce leakage flux and improve the torque output. The default value for both stator and rotor skew angle was 90°. After simulations, as shown in *Fig. 3-36*, the selected skew angles are 93° for rotor pole and 80° for stator pole. A smaller skew angle is chosen for rotor pole to make it less eccentric. The effects of changing the pole arcs and pole skew angles on the torque ripple are presented in *Fig. 3-37* and *Fig. 3-38* respectively.

The sum of stator pole depth and stator back-iron is given by the one half the difference of outer stator diameter, which is 270 mm as per specifications, and stator bore diameter, which is the sum of rotor diameter and airgap width. This difference comes out to be 108 mm so sum of stator pole depth and stator back-iron is 54 mm. The range for stator pole depth has been selected as 31-36 mm to keep the stator back-iron width more than 15 mm and have sufficient clearance between the winding top portion and stator pole top. The results are plotted in *Fig. 3-39*. With decreasing stator pole depth, torque and efficiency are increasing so stator pole depth is set as 31 mm. As shown in *Fig. 3-40*, the selected value of stator pole depth also results in the lowest torque ripple.

Next the best value of rotor core thickness is determined. As per selected rotor diameter and shaft diameter, sum of rotor yoke thickness (y_r) and rotor pole depth (d_r) is 50 mm. Therefore, y_r is varied between 20-28 mm to check the result above and below the 25 mm which is one-half the sum of y_r and d_r. In these set of simulations, since the change of rotor thickness values only changes the rotor pole depth therefore all other parameters are same as obtained in the last step. The results are plotted in the *Fig. 3-41*. There is no significant change in either torque or efficiency however the chosen value for rotor yoke is 26 mm. This value is selected to make rotor core as thick as possible without compromising on either torque or efficiency. The results plotted in *Fig. 3-42* show that rotor core thickness has considerable effect on the torque ripple.

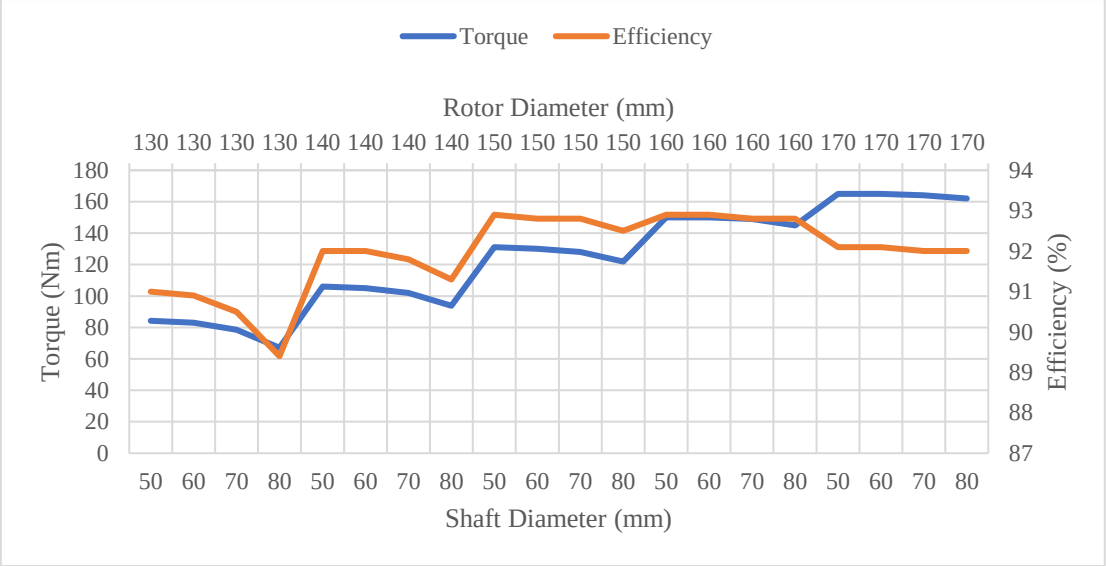

Fig. 3-34. Variation of torque and efficiency with rotor and shaft diameter for D-3

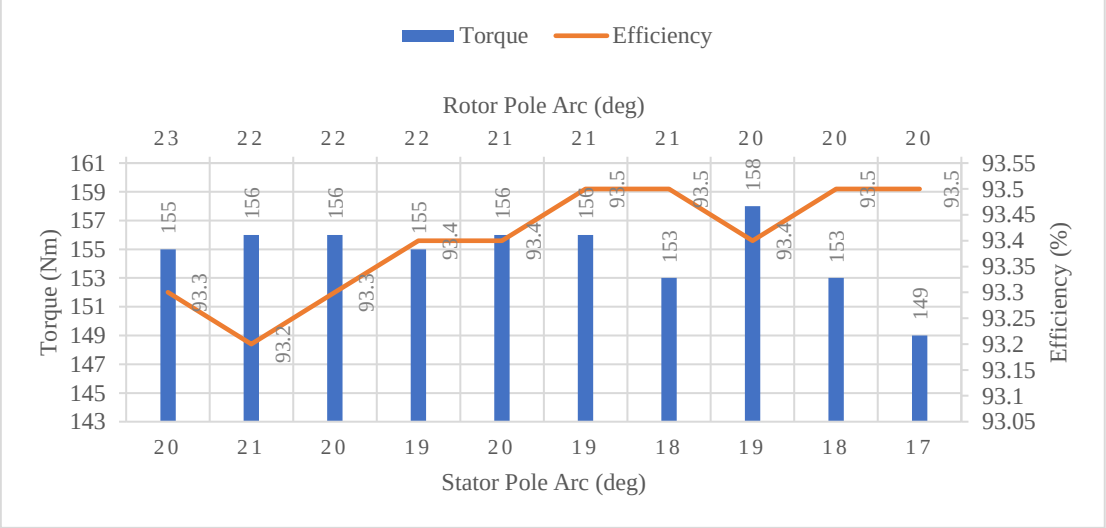

Fig. 3-35. Variation in Rotor pole angle and Stator pole angle vs Torque and Efficiency

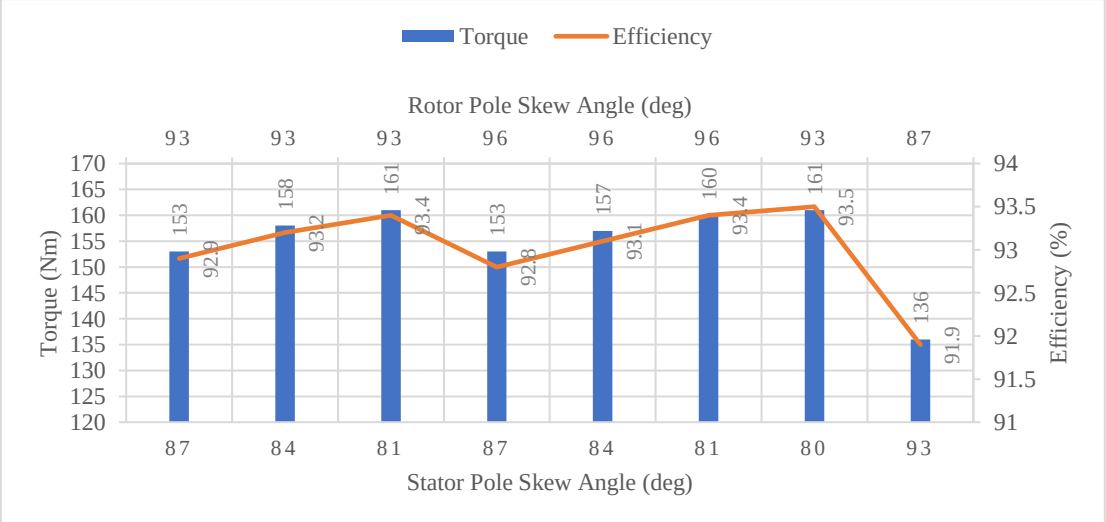

Fig. 3-36. Variation in Rotor pole skew angle and Stator pole skew angle vs Torque and Efficiency

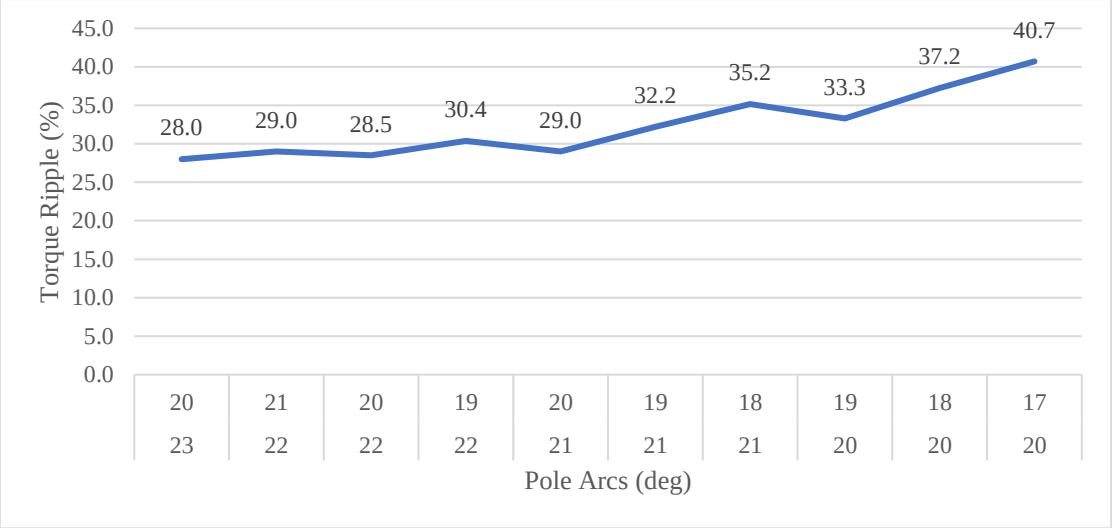

Fig. 3-37. Torque ripple variation with pole arcs (top row: stator, bottom row: rotor)

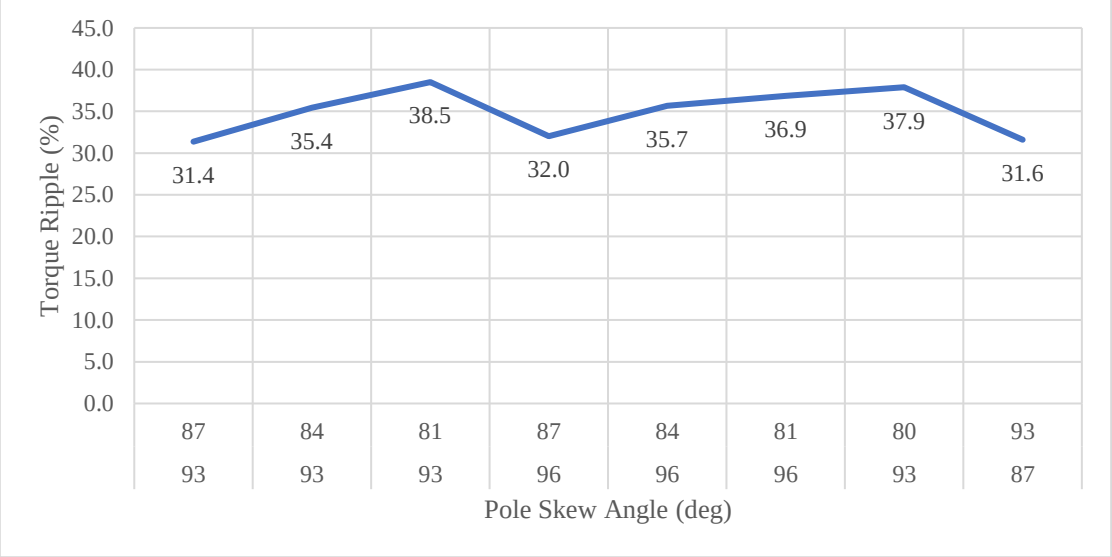

Fig. 3-38. Effect of changing pole skew angle on torque ripple (top row: stator, bottom row: rotor)

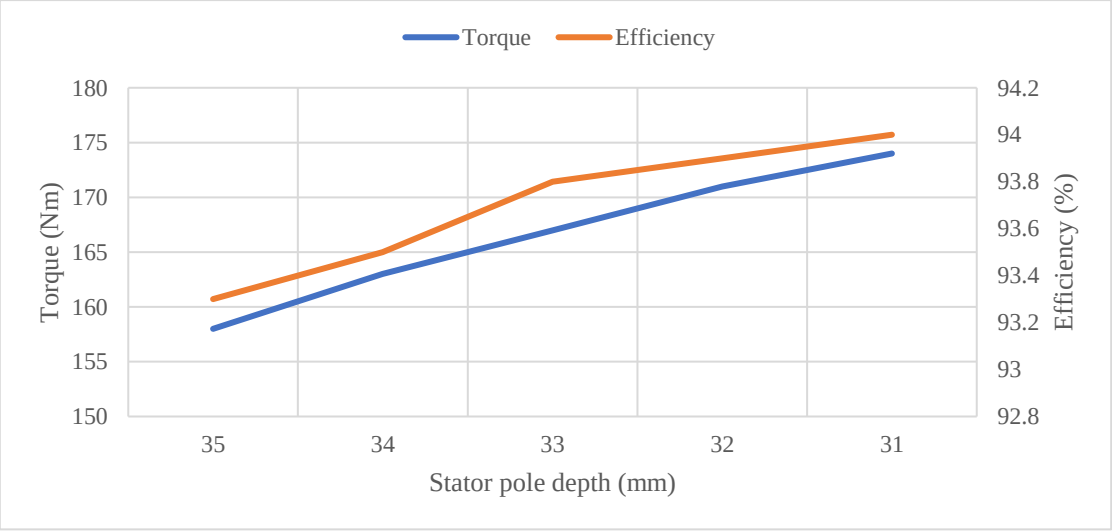

Fig. 3-39. Effect of variation of stator pole depth

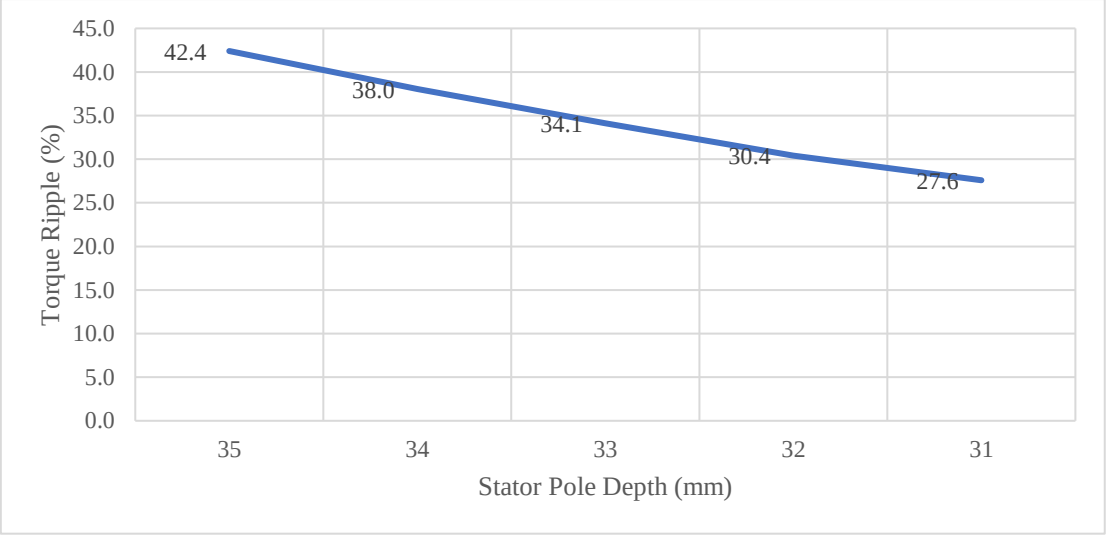

Fig. 3-40. Stator pole depth vs. torque ripple

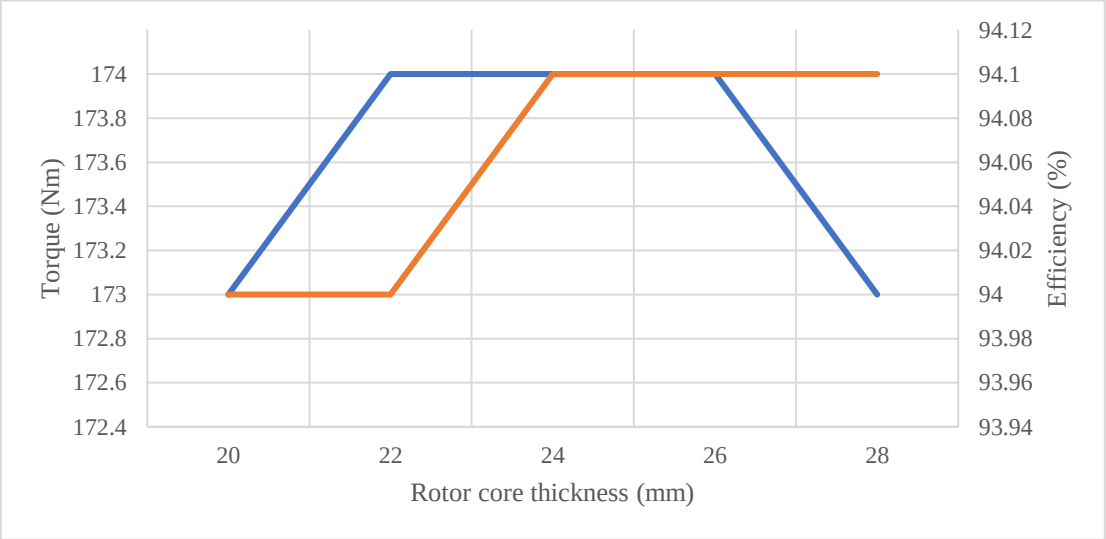

Fig. 3-41. Effect of variation of rotor core thickness

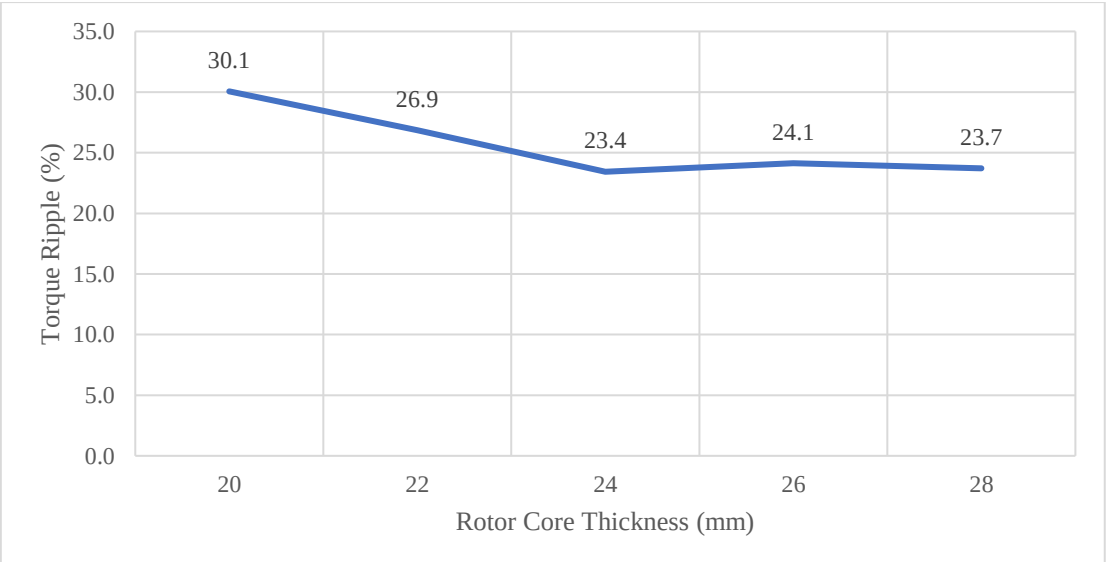

Fig. 3-42. Rotor core thickness vs. torque ripple

After having selected all the parameters, since the required torque is much more than the required value of 137 Nm, number of turns and current can be reduced to get the required torque and to push the efficiency further up. Now more number of turns provide higher torque at low speeds but they decrease the speed range. While less number of turns reduce the starting torque, the speed range increases [28]. In this case, as torque is significantly higher so the current is reduced to 80% and number of turns are maintained at 24 as calculated earlier. The final model is shown in *Fig. 3-43*. The inductance profile of the improved design is shown in *Fig. 3-44*. The unaligned inductance is now reduced to 0.53 mH compared to 0.9 mH before improvement. The aligned inductance to unaligned inductance ratio is 2.85. Flux linkage of improved D-3, at different rotor positions, is exhibited in *Fig. 3-45*.

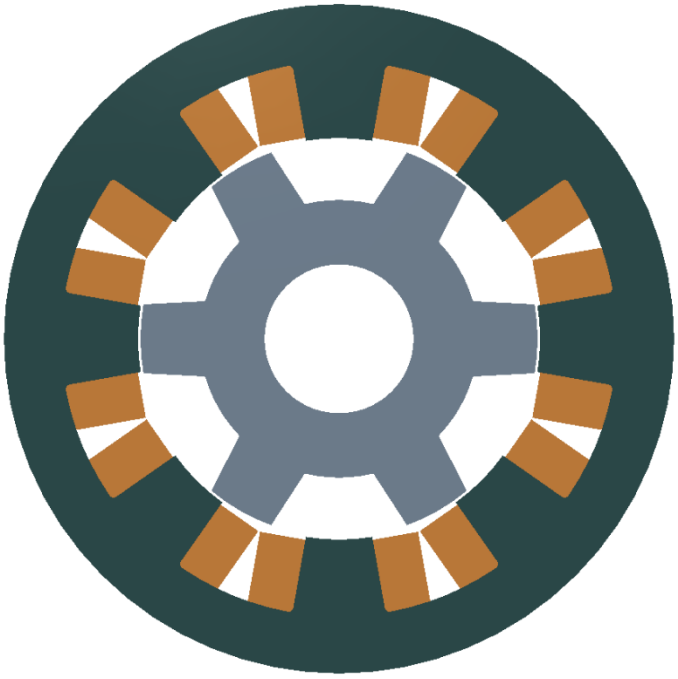

Fig. 3-43. The improved model of D-3

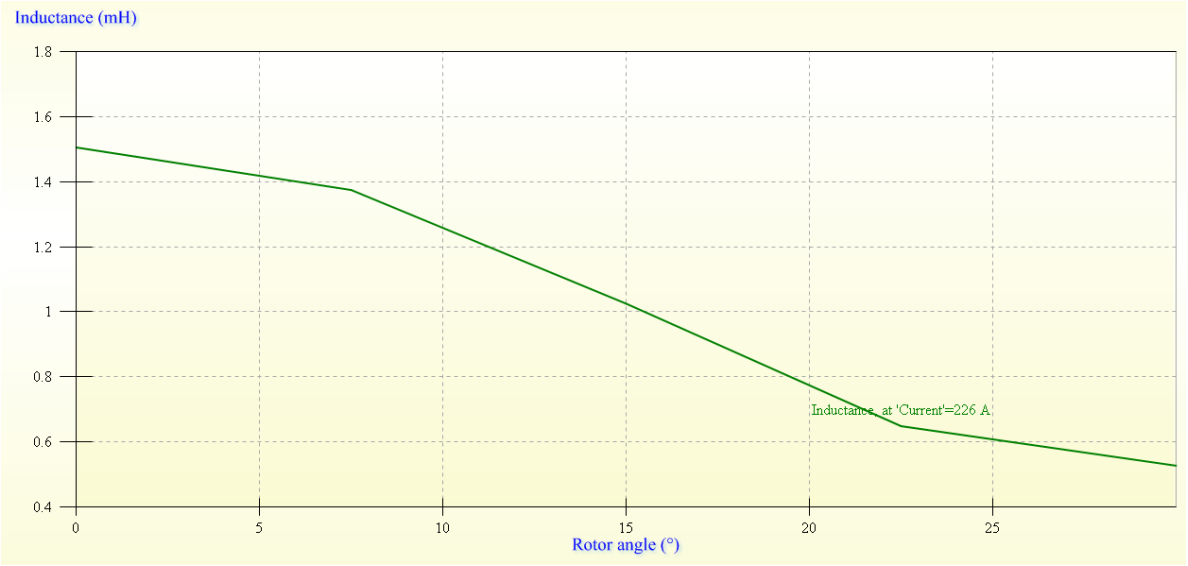

Fig. 3-44. Inductance profile of improved D-3 design @ current = 80%

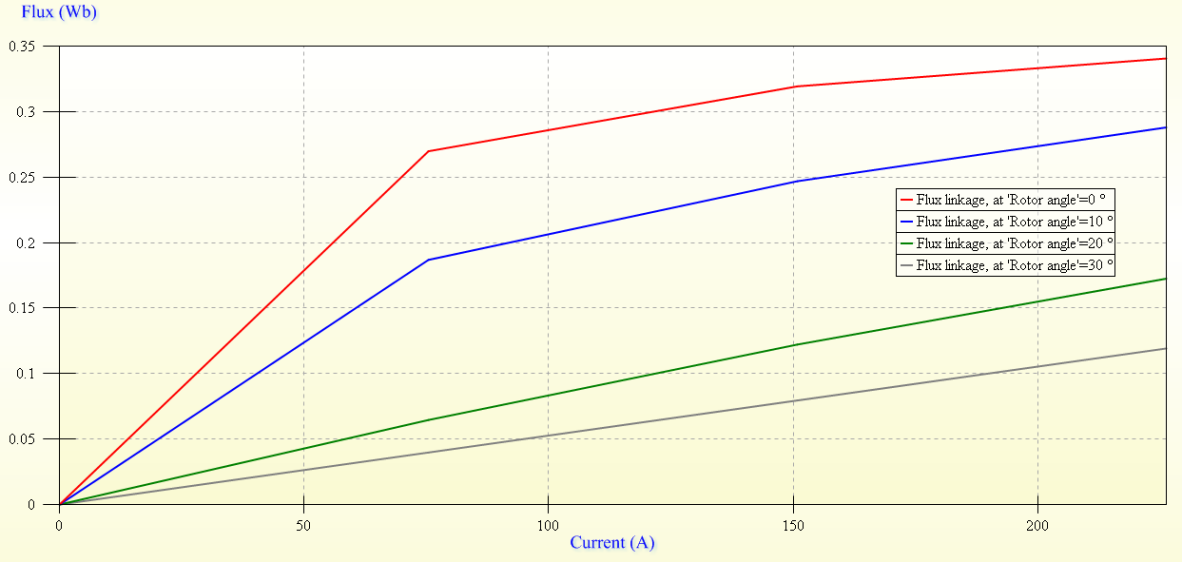

Fig. 3-45. Magnetization curves of D-3 at unaligned and aligned rotor positions with current = 80%

Fig. 3-46 shows the torque waveform of improved D-3 plotted against the rotor angle. The average torque is 141 Nm. The magnitude of the ripple is 39 Nm or 27.7% of the average torque which is the least among the designs considered. *Table 3-7* provides the results of motion analysis of D-3. Torque-speed profile of D-3 is presented in *Fig. 3-47*. Like other two designs, D-3 is also producing the required torque throughout the speed range.

This completes the improvement process for the considered design topologies. In the next section, a comparison has been done to determine the best design for this application considering the results obtained in this section. The complete design data for the three design topologies is presented in Appendix A.

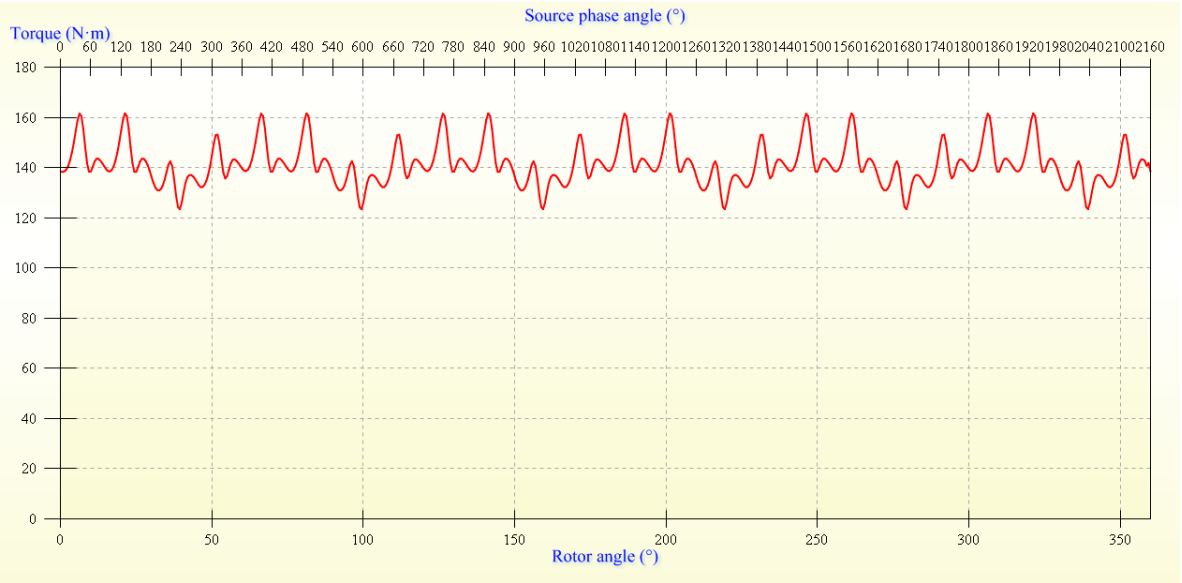

Fig. 3-46. Torque waveform of improved D-3

Table 3-7
Motion Analysis of Improved D-3 at rated speed

Torque (N·m)	141
Input power (kW)	46.9
Output power (kW)	44.4
Efficiency (%)	94.7
Torque per unit volume (N·m/mm³)	6.57E-05
Loss - Total (kW)	2.48
Loss - Winding (kW)	1.84
Loss - Stator back iron hysteresis (W)	198
Loss - Stator back iron eddy current (W)	104
Loss - Stator teeth hysteresis (W)	93.2
Loss - Stator teeth eddy current (W)	38.1
Loss - Rotor back iron hysteresis (W)	71.9
Loss - Rotor back iron eddy current (W)	32.8
Loss - Rotor teeth hysteresis (W)	67.8
Loss - Rotor teeth eddy current (W)	28.8

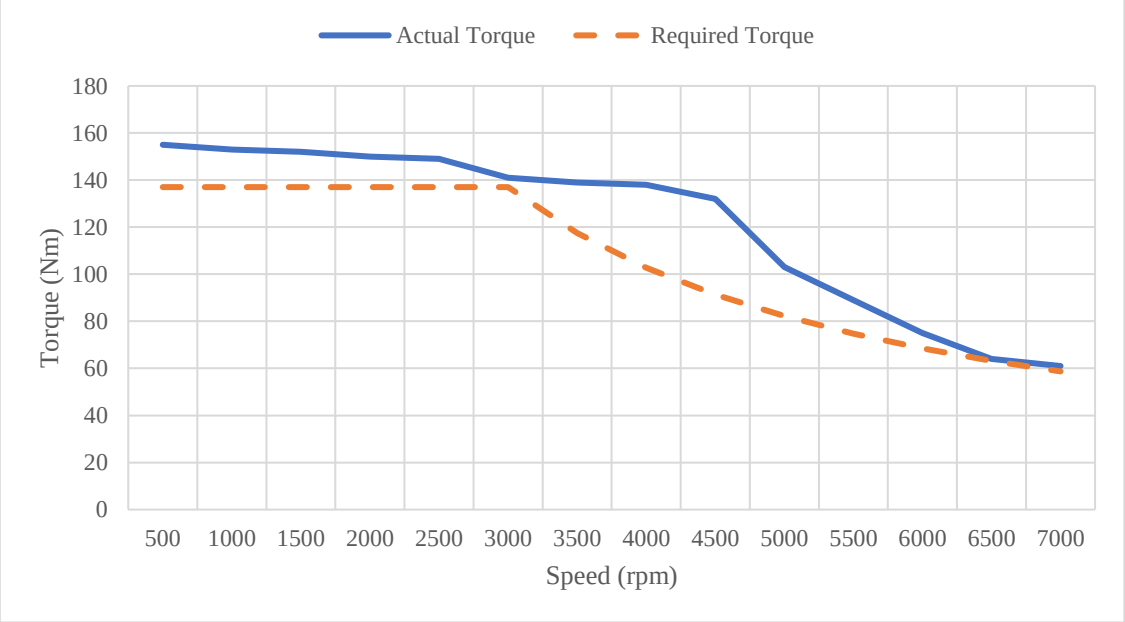

Fig. 3-47. Torque-speed profile of D-3

3.5 Final Selection of The Design

Based on the results obtained for D-1, D-2, D-3 designs, D-2 design has been chosen as the design suitable for this application. It offers higher efficiencies at lower speeds, has low torque ripple and requires the three-phase drive. Although D-3 offers highest efficiency and lowest torque ripple at higher speeds, however, it would require an extra leg in the converter which would make the converter more expensive and the drive more complex. D-1 offers the lowest efficiencies among all designs throughout the speed range and has the highest torque ripple. *Fig. 3-48* provides a comparison of efficiencies delivered by the designs under consideration.

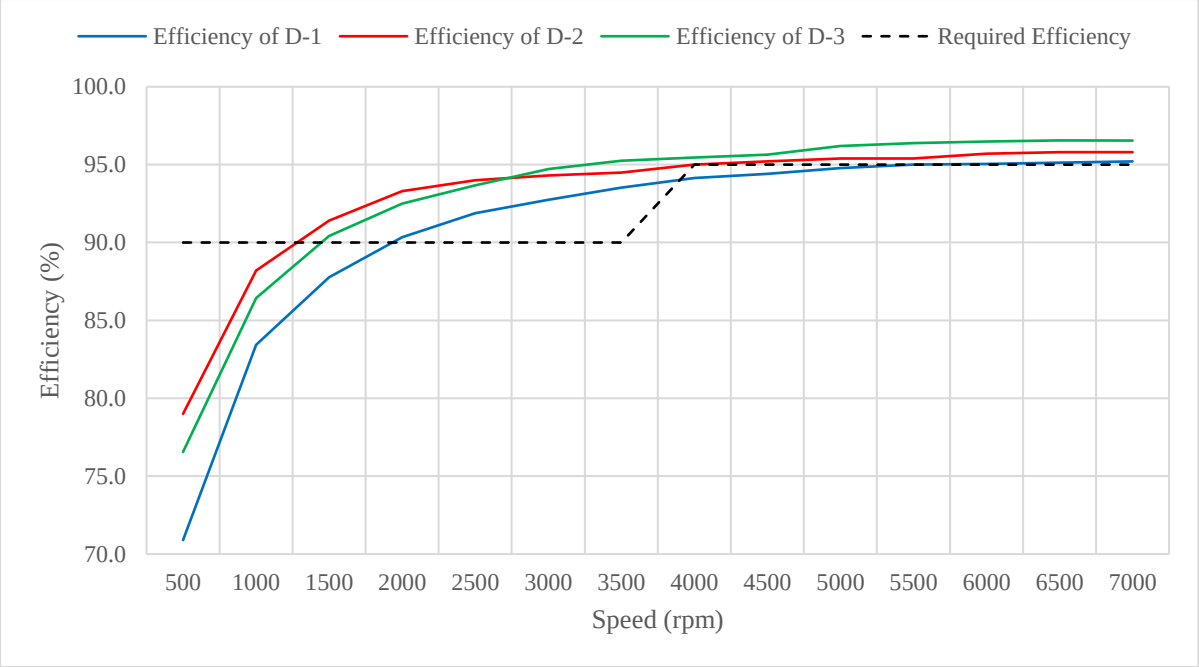

Fig. 3-48. Comparison of efficiencies of D-1, D-2 and D-3 in the considered speed range

Chapter 4

Performance Characterisation

As 3-phase 12/8 SRM has been chosen as the machine topology best suited for this project, we now proceed with detailed performance characterisation of this design.

4.1 Thermal Analysis

Heat removal from the machine is an important design aspect. Ideally all the heat generated due to losses should be removed from the machine and the heat should be uniformly distributed to avoid formation of the hot spots. In general, there are three heat removal methods: conduction, radiation and convection [21]. Thermal modelling depicts the behaviour of the system with respect to heat distribution and heat removal considering the geometry of the machine [29].

Thermal analysis for the selected machine has been carried out in MotorCAD. MotorCAD uses lumped circuits for the thermal analysis of a machine [30]. Lumped parameter modelling means to represent the properties of a body in realisable quantities e.g. volume, average temperature etc. In developing thermal nodal network, the objects are broken down into smaller elements and one or few nodes then represent those smaller elements [29]. Motor CAD selects the location of the nodes in the machine automatically. These nodes are connected to the thermal resistances based on heat removal methods. At the pertinent nodes, the losses are introduced [30].

As the specifications provided in *Table 3-1* suggest, liquid cooling is available for the stator. To begin the machine was simulated without using any liquid cooling in a round housing without any fins. *Fig. 4-1* shows the result of this simulation. Looking at the results we can safely assume that the machine needs liquid cooling.

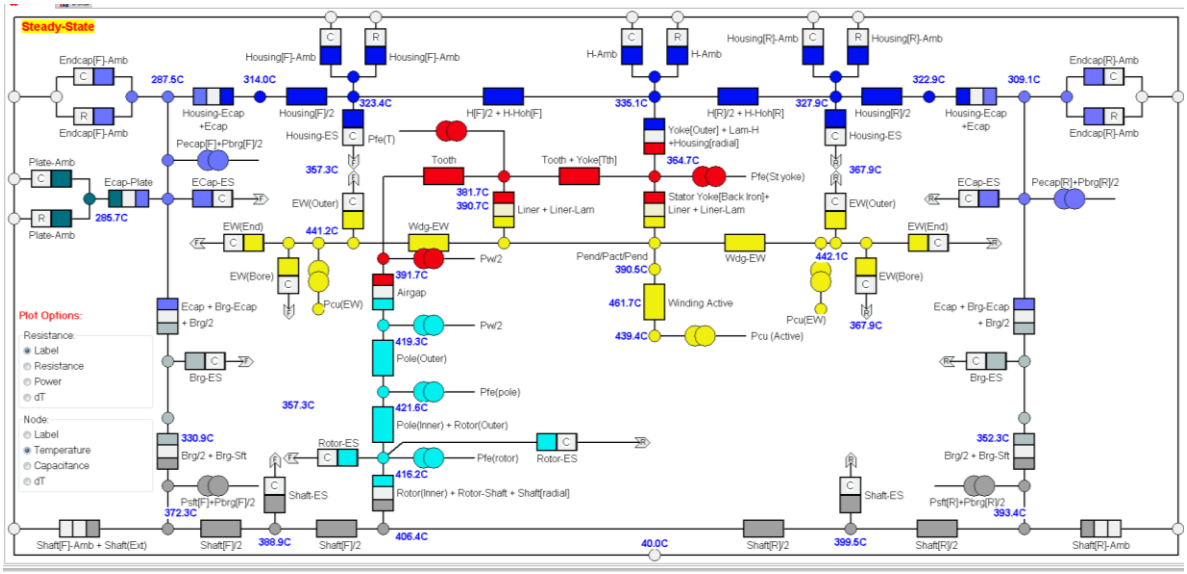

Fig. 4-1. Thermal analysis without using liquid cooling

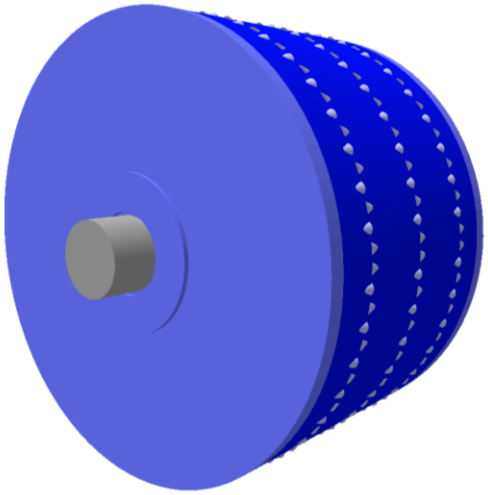

Fig. 4-2. Machine model with stator cooling

In the next step, a water jacket has been added outside the stator as a part of housing. *Fig. 4-2* shows the machine 3D model with cooling jacket. The cooling liquid used for this set of simulations is water. Simulations are first done at the minimum value of liquid flow rate i.e. 6 litre/min. As results at this flow rate indicate, refer *Fig. 4-3*, the maximum winding temperature is 182.7° C. The maximum allowed temperature for insulation class H is 180° C so maximum winding temperature needs to be reduced [31].

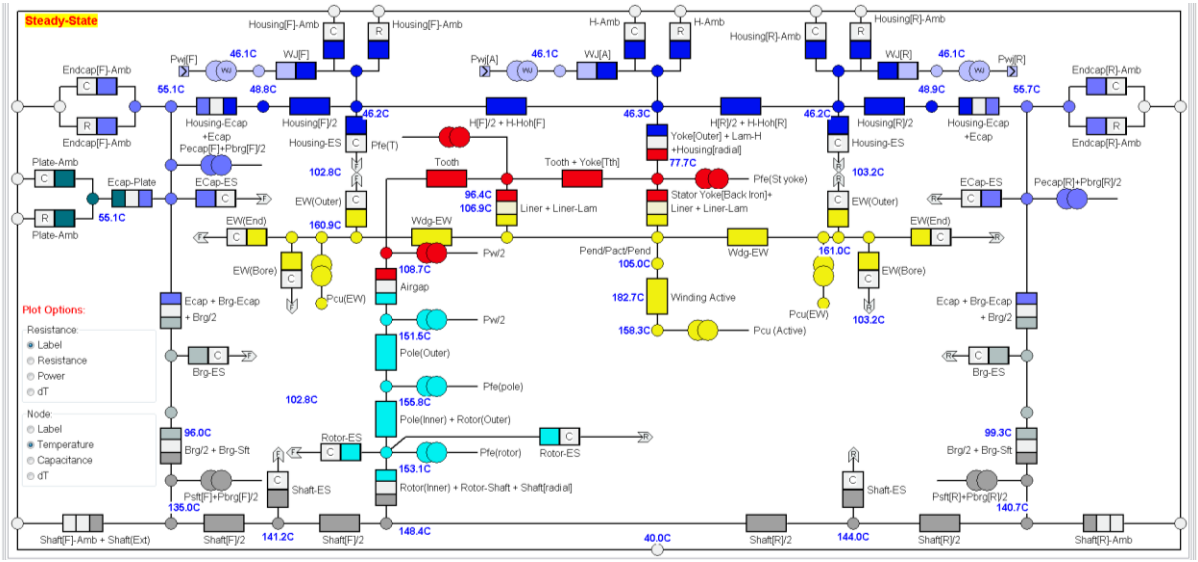

Fig. 4-3. Thermal analysis results with 6 litre/min flow rate

Simulating with the maximum value of liquid flow provided in specifications i.e. 12 litre/min reduces the maximum winding to temperature to just below 180° C which meets the insulation requirement. However, it would be recommendable to increase the liquid flow rate to get some margin between maximum winding temperature and 180°C mark. For example, increasing the liquid flow rate to 24 litre/min reduces the maximum winding temperature to 178° C as shown in *Fig. 4-5* and adds a 2°C margin. So higher flow rate is recommended for this project.

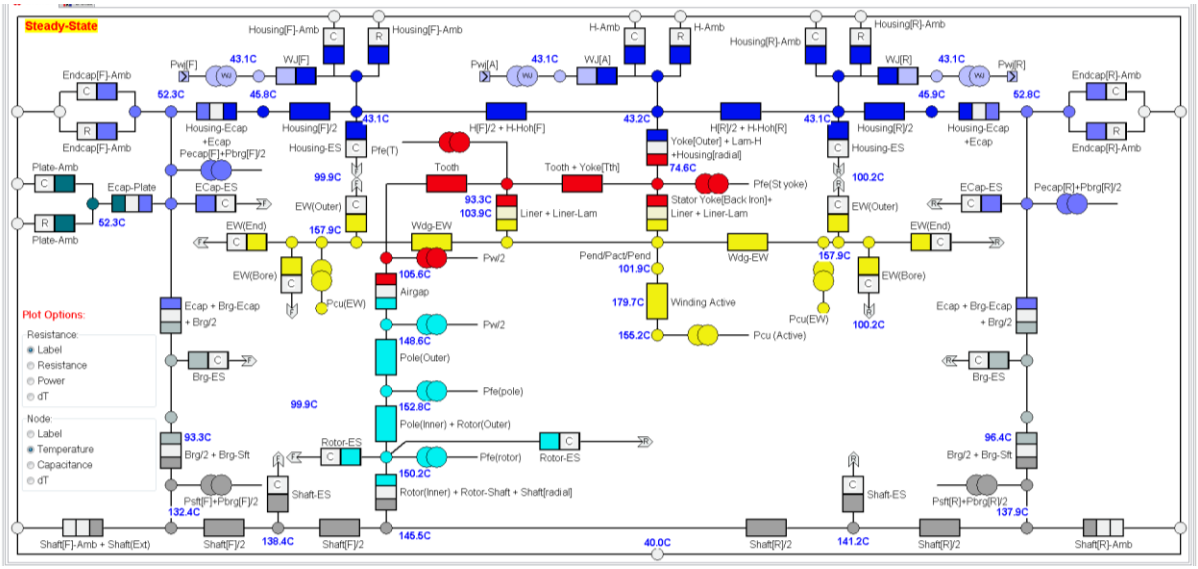

Fig. 4-4. Thermal analysis results with 12 litre/min flow rate

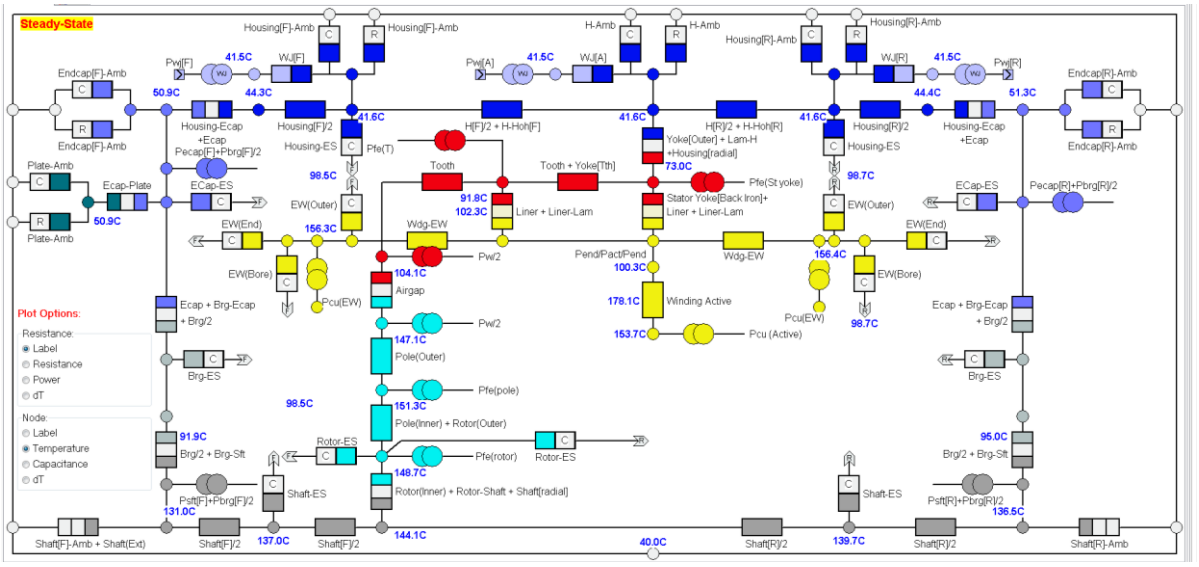

Fig. 4-5. Thermal analysis results with 24 litre/min flow rate

4.2 EFFICIENCY MAP

An efficiency map provides efficiency curves plotted over the torque-speed profile of a machine. It gives information about the efficiency of the machine at different power levels throughout the speed range under consideration. To build an efficiency map for the selected SRM, torque-speed profiles were developed at different current levels. Current levels used were 100%, 77% (value of the current used to get rated power), 50% and 20% of the rated value of current. To develop torque-speed profile, the turn-on and turn-off angles were advanced with the speed. The optimum values of these angles were found by repeated simulations.

Fig. 4-6 presents the torque-speed profiles of the selected 3-phase 12/8 SRM. As expected torque reduces by reducing the current however the relationship is not direct due to nonlinearity. Based on these profiles, an efficiency map is produced as shown in *Fig. 4-7*. An important thing to be kept in mind is that efficiency at a particular speed is not only affected by the current but also by the turn-on and turn-off angles as well. As the speed increases, the rise time for the current to the required level gradually decreases. So, to allow enough time for the current to rise, turn-on angle needs to be advanced

as well. Similarly, turn-off angles need to be advanced according to the speed to allow the current to reduce to zero.

The map shows that the efficiency of the SRM keeps on increasing with the speed. However, the efficiency at higher speeds decreases with the decreasing current. This is due to the fact at lower levels of the current, machine is less saturated so the energy conversion process is not as efficient as it is at higher levels of current. The reduction in copper losses achieved by reducing the current does not compensate the loss of output power due to reduced saturation. The map also shows that efficiency is higher at lower speeds (< 1000 rpm) for lower values of injected current.

The torque-speed profiles and the efficiency map give a comprehensive overview of the performance of the machine. The complete data obtained while developing these curves is available in Appendix A.

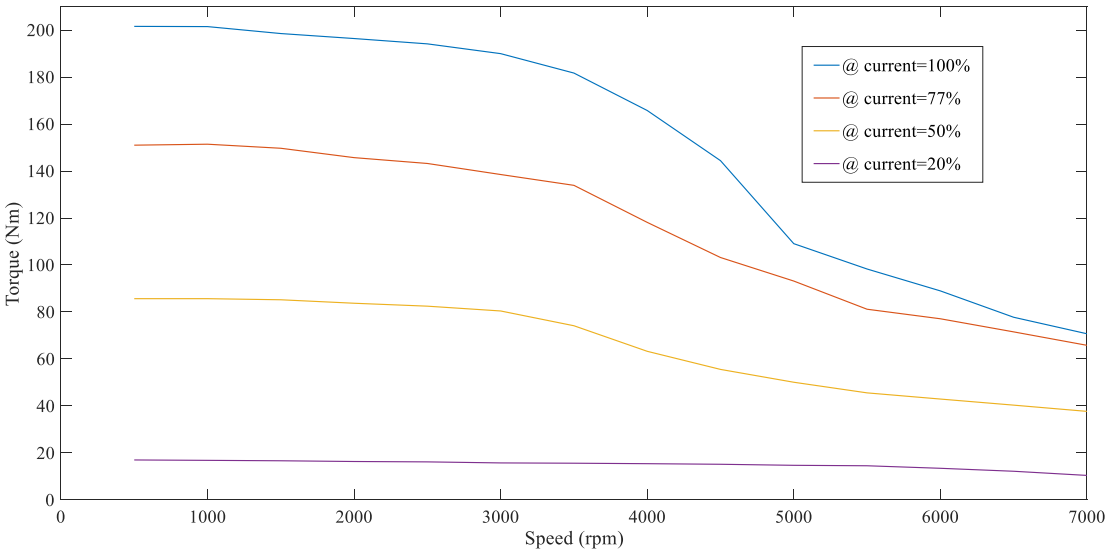

Fig. 4-6. Torque-speed profiles at different current levels of selected SRM

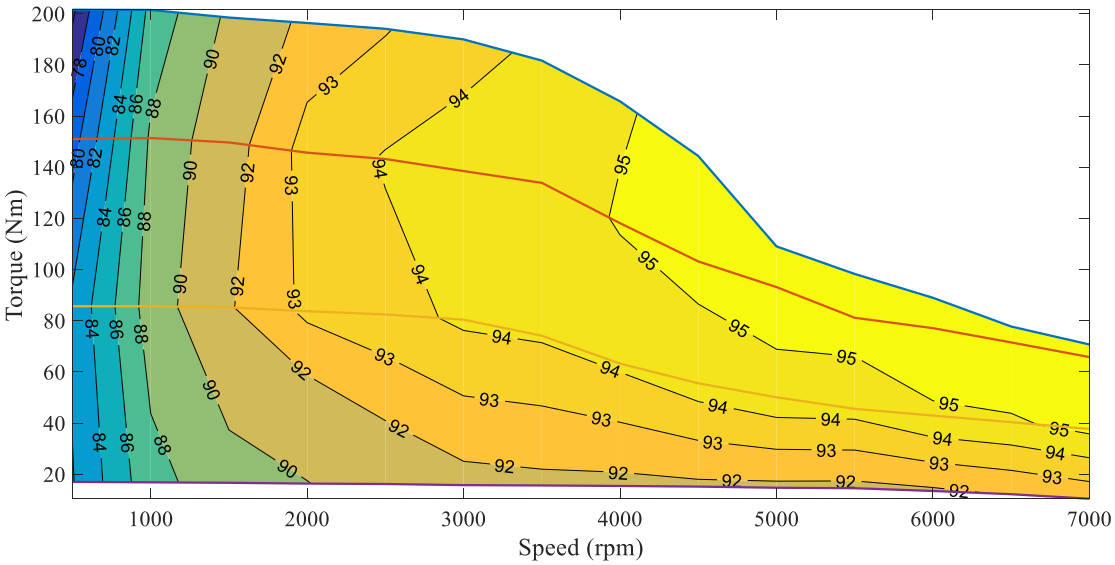

Fig. 4-7. Efficiency map of the selected SRM

4.3 FINITE ELEMENT ANALYSIS

MagNet is used to perform finite element analysis to check electromagnetic profile of the machine and to verify the results of MotorSolve. Data of the three phase currents used by MotorSolve was exported and used in MagNet. *Fig. 4-8* shows the torque waveform produced by MagNet. The average torque is calculated as 137 Nm. The torque waveform is of same shape as generated by MotorSolve as shown in *Fig. 3-31*. The only difference is the magnitude of the ripple. The torque ripple in the waveform generated by MagNet is about 44% of the average torque compared to 29% reported by MotorSolve.

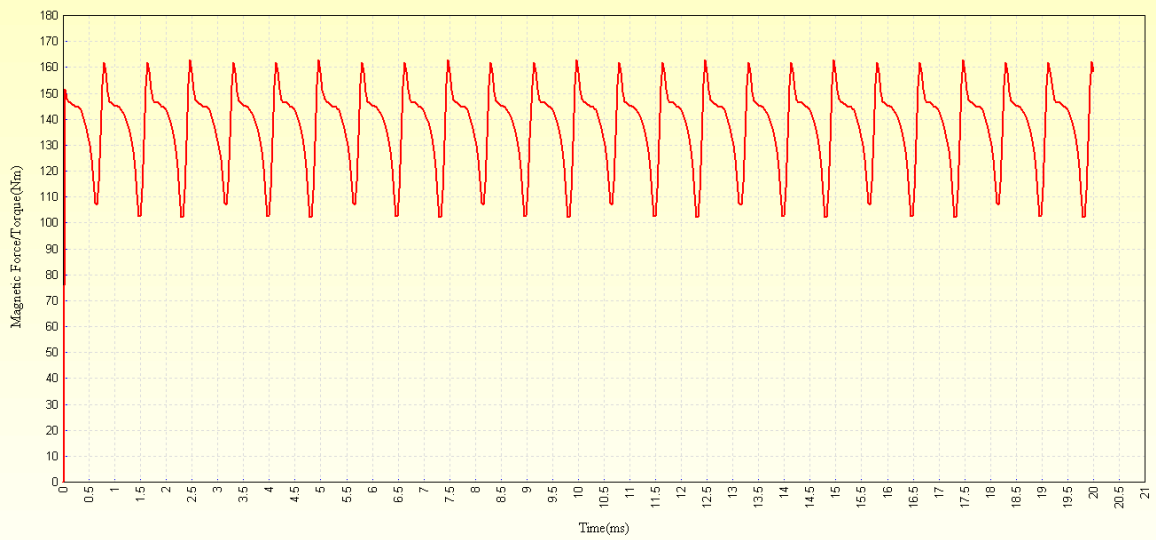

Fig. 4-8. Torque waveform generated by Magnet

Fig. 4-9 to *Fig. 4-12* show magnetic field density distribution in the machine at different rotor positions with respect to phase A under rated power conditions. As the rotor begins, the pole corners get saturated. The peak of magnetic field density occurs in the first few degrees of alignment process. As the alignment between rotor and stator poles increases the flux sharing area increases and the density drops. At the aligned position, the density falls to 1.4 T in stator pole. Stator poles of other phases also have the same distribution.

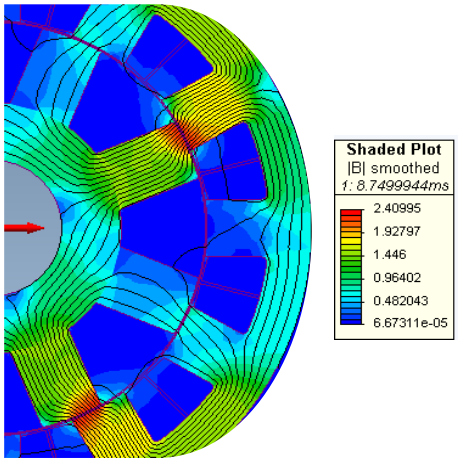

Fig. 4-9. Magnetic field density distribution when phase A is unaligned

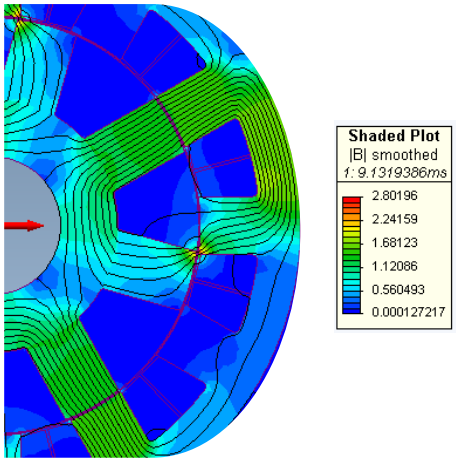

Fig. 4-10. Magnetic field density distribution when phase A begins to align

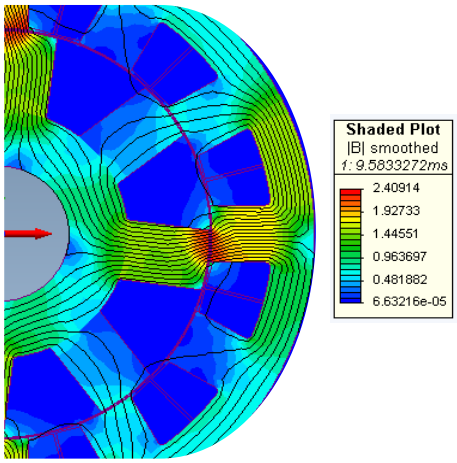

Fig. 4-11. Magnetic field density distribution when phase A is half aligned

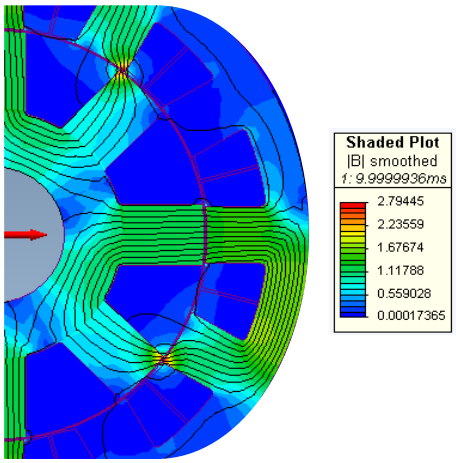

Fig. 4-12. Magnetic field density distribution when phase A is aligned

The machine produces the peak torque and hence peak power at 3000 rpm with 200% of the rated current. The magnetic field density under peak power conditions at the pole corners goes as high

as 2.8 T. The peak field density only occurs at the stator pole corners. Other parts of the machine such as stator back iron experience a maximum of 1.8 T and peak density in rotor back iron is 0.8 T. *Fig. 4-13* to *Fig. 4-16* show field density distribution under peak conditions.

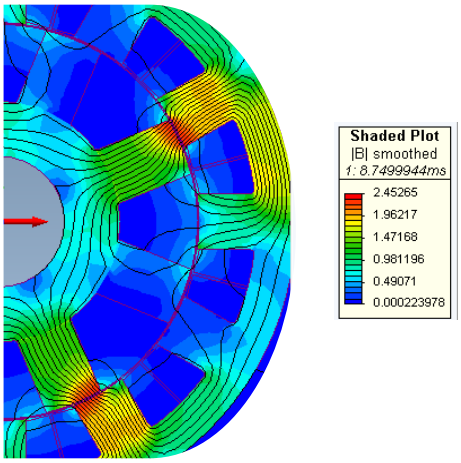

Fig. 4-13. Magnetic field density distribution under peak power conditions with unaligned phase A

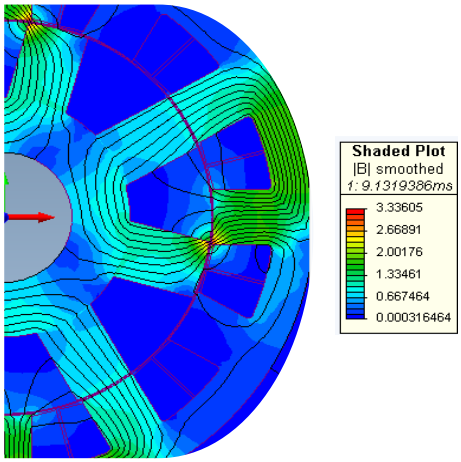

Fig. 4-14. Magnetic field density distribution under peak power conditions as phase A begins to align

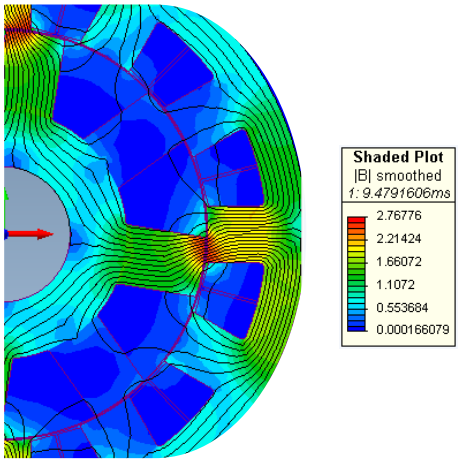

Fig. 4-15. Magnetic field density distribution under peak power conditions with partially aligned phase A

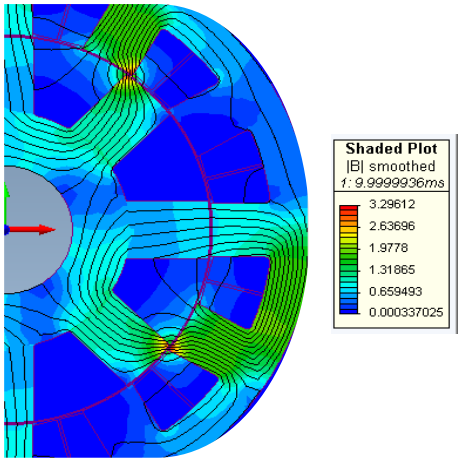

Fig. 4-16. Magnetic field density distribution under peak power conditions with partially aligned phase A

The FEA shows that pole corners in the selected SRM have maximum magnetic flux density while stator and rotor back iron are way less saturated which bodes well for the design.

Chapter 5

Conclusions and Future Work Recommendations

5.1 CONCLUSIONS

- The important characteristics required of an electric machine for traction application are high power and torque density, high efficiency, low cost, robustness and wide constant power speed range.
- As the SRM is non-linear machine therefore developing a comprehensive analytical model in the short duration of this project was not possible. Hence the focus of this project shifted to develop a SRM that could satisfy the requirements laid down in the specifications.
- Three topologies: 3-phase 6/4, 3-phase 12/8 and 4-phase 8/6 were considered as potential solutions for the problem under consideration. Based on the results obtained during the design process, 3-phase 12/8 machine was selected as the most suitable SRM for this project. For sensitivity analysis, effects on torque, efficiency and torque ripple, of the variation of rotor and shaft diameter, stator and rotor pole arcs, stator and rotor back iron thicknesses were considered.
- Some important conclusions drawn during the design process of the SRM are as follows:
    - The rotor and shaft diameter values have the major impact on the torque output so their values should be optimised to maximise it.
    - Stator and rotor pole arcs, stator and rotor pole skewing angles, and stator and rotor back iron thicknesses in general have a slight influence on the torque or efficiency but exhibit a stronger influence on the torque ripple. Therefore, to reduce the torque ripple these parameters should be optimised.
    - Pole corners face the highest flux density in the machine and it occurs when the rotor pole just starts aligning with the stator pole. Stator and rotor back iron in comparison have lower values of maximum flux density.
    - The selected 3-phase 12/8 SRM needs a higher cooling liquid flow rate than the specified 12 litre/min to have some safety margin above its maximum winding temperature.
- As the SRM is simple in construction, cheap to manufacture, robust and as the design results reveal it can satisfy the requirements for a traction application. Therefore, it can be concluded that the SRM possesses the full potential to be a competent option for electric vehicles.

5.2 FUTURE WORK RECOMMENDATIONS

Some recommendations are provided here to build on the work done in this project:

- Analytical model of the machine can be developed to predict the machine performance. Based on the model, switching angles for the transistors in each leg should be found to maximise the performance.
- As pointed out in the conclusions, machine parameters can be optimised to further improve the performance parameters.
- As the machine was designed based on the specified outer dimensions, further work can be done to reduce the volume of the machine thereby increasing the torque density per volume.
- Other machine types such as induction machine or PM machine can be developed for the same specifications and a comparison can be done among all machine types to put the performance of SRM into perspective.

References

[1] E. Bostanci, M. Moallem, A. Parsapour and B. Fahimi, "Opportunities and Challenges of Switched Reluctance Motor Drives for Electric Propulsion: A Comparative Study," *IEEE Transactions on Transportation Electrification,* vol. 3, no. 1, pp. 58-75, 2017.

[2] K. Chau and W. Li, "Overview of electric machines for electric and hybrid vehicle," *International Journal of Vehicle Design,,* vol. 64, no. 1, pp. 46-71, 2014.

[3] T. Finken, M. Felden and K. Harmeyer, "Comparison and design of different electrical machine types regarding their applicability in hybrid electrical vehicles," in *Proc. 18th International Conference on Electrical Machines,* Vilamoura, 2008.

[4] Z. Q. Zhu and D. Howe, "Electrical machines and drives for electric hybrid and fuel cell vehicles," *Proc. IEEE,* vol. 95, no. 4, pp. 746-765, 2007.

[5] I. Boldea, L. N. Tutelea, L. Parsa and D. Dorrell, "Automotive electric propulsion systems with reduced or no permanent magnets: An overview," *IEEE Trans. Ind. Electron.,* vol. 61, no. 10, pp. 5696-5711, 2014.

[6] M. Yilmaz, "Limitations/capabilities of electric machine technologies and modeling approaches for electric motor design and analysis in plug-in electric vehicle applications," *Renew. Sustain. Energy Rev.,* vol. 52, pp. 80-99, 2015.

[7] D. G. Dorrell, A. M. Knight, M. Popescu, L. Evans and D. A. Staton, "Comparison of different motor design drives for hybrid electric vehicles," *Proc. IEEE Energy Convers. Congr. Expo. (ECCE),* pp. 3352-3359, 2010.

[8] M. Zeraoulia, M. E. H. Benbouzid and D. Diallo, "Electric motor drive selection issues for HEV propulsion systems: A comparative study," *IEEE Trans. Veh. Technol.,* vol. 55, no. 6, pp. 1756-1764, 2006.

[9] S. Ramarathnam, A. K. Mohammed, B. Bilgin, A. Sathyan, H. Dadkhah and A. Emadi, "A review of structural and thermal analysis of traction motors," *IEEE Trans. Transport. Electrific.,* vol. 1, no. 3, pp. 255-265, 2015.

[10] R. R. Fessler, "Final report on assessment of motor technologies for traction drives of hybrid and electric vehicles," 2011.

[11] J. d. Santiago and et.al, "Electrical motor drivelines in commercial all-electric vehicles: A review," *IEEE Trans. Veh. Technol.,* vol. 61, no. 2, pp. 475-484, 2012.

[12] M. Ehsani, K. M. Rahman and H. A. Toliyat, "Propulsion system design of electric and hybrid vehicles," *IEEE Trans. Ind. Electron.,* vol. 44, no. 1, pp. 19-27, 1997.

[13] M. Kamiya, "Development of traction drive motors for the Toyota hybrid system," *IEEJ Trans. Ind. Appl.,* vol. 126, no. 4, pp. 473-479, 2006.

[14] F. G. Capponi, *Lecture on Dynamic Analysis and Control of AC Machines,* Rome, 2015.

[15] S. J. Chapman, Electric Machinery Fundamentals, New York: Mc-Graw Hill, 2011.

[16] C. Mi, M. A. Masrur and D. W. Gao, Hybrid Electric Vehicles: Principles and Applications with Practical Perspectives, Sussex: John Wiley & Sons Ltd., 2011.

[17] D. Ronanki and S. S. Williamson, "Comparative analysis of DITC and DTFC of switched reluctance motor for EV applications," in *2017 IEEE International Conference on Industrial Technology (ICIT)*, Toronto, 2017.

[18] J. W. Jiang, B. Bilgin and A. Emadi, "Three-Phase 24/16 Switched Reluctance Machine for a Hybrid Electric Powertrain," *IEEE Transactions on Transportation Electrification,* vol. 3, no. 1, pp. 76-85, 2017.

[19] J. Larminie and J. Lowry, Electric Vehicle Technology Explained, Sussex: John Wiley & Sons Ltd., 2003.

[20] J. Zhu, K. W. E. Cheng, X. Xue and Y. Zou, "Design of a New High-Torque-Density In-Wheel Switched Reluctance Motor for Electric Vehicles," *IEEE Transactions on Magnetics,* vol. PP, no. 99, pp. 1-1, 2017.

[21] T. Miller, Switched Reluctance Motors And Their Control, Magna Physics Publishing, 1993.

[22] E. C. S. R. Machines, T.J.E. MIller, Newnes, 2001.

[23] I. Husain, "Minimization of torque ripple in SRM drives," *IEEE Transactions on Industrial Electronics,* vol. 49, no. 1, pp. 28-39, 2002.

[24] A. Sarr, I. Bahri, D. Diallo and E. Berthelot, "Sensorless control of Switched Reluctance Machine," in *IECON 2016 - 42nd Annual Conference of the IEEE Industrial Electronics Society*, Florence, 2016.

[25] J. Dang and R. G. Harley, "Sensorless control scheme for ultra high speed switched reluctance machine," in *2013 IEEE Energy Conversion Congress and Exposition*, Denver, 2013.

[26] I. Husain, *Lecture on Switched Reluctance Machine,* Gijon, 2016.

[27] P. Rafajdus, A. Peniak, D. Peter, P. Makyś and L. Szabó, "Optimization of switched reluctance motor design procedure for electrical vehicles," in *2014 International Conference on Optimization of Electrical and Electronic Equipment (OPTIM)*, Bran, 2014.

[28] S. R. Patel, N. Gandhi, N. Chaithanya, B. N. Chaudhari and A. Nirgude, "Design and development of Switched Reluctance Motor for electric vehicle application," in *2016 IEEE International Conference on Power Electronics, Drives and Energy Systems (PEDES)*, Trivandrum, 2016.

[29] B. Anderson, "Lumped Parameter Thermal Modelling of Electric Machines," 2013. [Online]. Available: http://publications.lib.chalmers.se/records/fulltext/185192/185192.pdf. [Accessed 10 September 2017].

[30] D. Staton, D. Hawkins and M. Popescu, "Motor-CAD Software for Thermal Analysis of Electrical Motors - Links to Electromagnetic and Drive Simulation Models," [Online]. Available: https://www.motor-design.com/wp-content/uploads/2016/12/cwieme_2010_paper_mdl.pdf. [Accessed 10 September 2017].

[31] The Association of Electrical & Mechanical Trades, “Classification of Insulation Systems,” 2014. [Online]. Available: http://www.theaemt.com/technical-info/general-engineering/classification-of-insulation-systems. [Accessed 22 August 2017].

Appendix A

A-1 Design Data

The design data of the three topologies after the improvement is tabulated below:

	3ph_6_4_final		**3ph_12_8_final**		**4Ph_8/6_final**	
General Settings						
Specifications						
Supply voltage	345.6	V	345.6	V	345.6	V
Rated current	282.84	A	282.84	A	282.84	A
Rated speed	2456	rpm	2456	rpm	2456	rpm
Global						
Outer diameter	270	mm	270	mm	270	mm
Air gap thickness	1	mm	1	mm	1	mm
Stack height	107	mm	107	mm	107	mm
Description						
Rotor						
Rotor location	Interior		Interior		Interior	
Rotor type	General		General		General	
Number of rotor poles	4		8		6	
Stator						
Stator type	General		General		General	
Number of phases	3		3		4	
Number of stator & rotor poles	6 stator poles - 4 rotor poles		12 stator poles - 8 rotor poles		8 stator poles - 6 rotor poles	
Number of stator poles	6		12		8	
Rotor (General)						
Diameters						
Inner diameter	50	mm	60	mm	60	mm
Outer diameter	160	mm	180	mm	160	mm
Core						
Core thickness	29.4	mm	25	mm	26	mm

Teeth						
Bifurcation radius	0	mm	0	mm	0	mm
Rotor pole angle	32	º	17	º	20	º
Tooth angle	87	º	90	º	93	º
Fillets						
Pole bottom radius	1	mm	1	mm	1	mm
Pole tip radius	0	mm	0	mm	0	mm
Stator (General)						
Diameters						
Inner diameter	162	mm	182	mm	162	mm
Outer diameter	270	mm	270	mm	270	mm
Coils						
Coil angle	75	º	75	º	80	º
Coil bottom width	28	mm	17	mm	18	mm
Coil length	25.8	mm	25	mm	29.4	mm
Teeth						
Bifurcation radius	0	mm	0	mm	0	mm
Slot depth	26	mm	26	mm	31	mm
Stator pole angle	30	º	16	º	19	º
Tooth angle	93	º	90	º	80	º
Fillets						
Bottom fillet radius	2	mm	2	mm	2	mm
Tooth tang radius	0	mm	0	mm	0	mm
Stator Windings						
Drive						
Number of parallel paths	1		1		1	
Wire						
Wire size method	Coil fill factor		Coil fill factor		Coil fill factor	
Coil fill factor	50		50		50	
Layout						
Layout method	Automatic		Automatic		Automatic	

Number of turns	23		15		24	
Stator End Windings						
End Effects						
Gap height	1	mm	1	mm	1	mm
Outer diameter	214	mm	234	mm	224	mm
Height	50.3144	mm	30.3954	mm	32.0853	mm
Fill factor	25.2		23.5		29.2	
Turn length	420	mm	339	mm	362	mm
Resistance	0.0121	Ω	0.011	Ω	0.0109	Ω
Inductance	0.0503	mH	0.0205	mH	0.0335	mH
Materials						
Rotor Materials						
Rotor back iron material	M300-35A		M300-35A		M300-35A	
Rotor tooth material	M300-35A		M300-35A		M300-35A	
Rotor stacking factor	1		1		1	
Rotor magnetization adjustment factor	1		1		1	
Rotor iron loss adjustment factor	1		1		1	
Stator Materials						
Stator back iron material	M300-35A		M300-35A		M300-35A	
Stator tooth material	M300-35A		M300-35A		M300-35A	
Stator coil material	Copper: 100% IACS		Copper: 100% IACS		Copper: 100% IACS	
Stator slot liner material	Epoxy resin		Epoxy resin		Epoxy resin	
Stator stacking factor	1		1		1	
Stator magnetization adjustment factor	1		1		1	
Stator iron loss adjustment factor	1		1		1	

A-2 Torque-Speed Profile Data

The torque-speed profile data obtained for the selected 3-phase 12/8 machine is provided here for the different current levels. The advancements in turn-on and turn-off angles (as required by Motor Solve) are also tabulated in electrical degrees.

Current = 100%							
Rotor speed (rpm)	**500**	**1000**	**1500**	**2000**	**2500**	**3000**	**3500**
Torque (N·m)	202	201	199	196	194	190	182
Input power (kW)	14.0	24.3	34.5	44.5	54.7	63.7	70.7
Output power (kW)	10.6	21.1	31.2	41.1	50.8	59.7	66.6
Efficiency (%)	75.6	86.7	90.4	92.4	92.9	93.7	94.2
Torque per unit volume (N·m/mm³)	7.4E-05	7.4E-05	7.3E-05	7.2E-05	7.1E-05	7.0E-05	6.7E-05
Loss - Total (kW)	3.4	3.2	3.3	3.4	3.9	4.0	4.1
Loss - Winding (kW)	3.3	2.9	2.9	2.8	3.1	3.1	3.0
Loss - Stator back iron hysteresis (W)	49.8	97.9	142.0	174.4	199.0	234.0	273.2
Loss - Stator back iron eddy current (W)	13.5	31.6	52.7	76.8	108.4	137.5	174.5
Loss - Stator teeth hysteresis (W)	24.2	49.3	75.8	99.2	120.9	144.3	172.5
Loss - Stator teeth eddy current (W)	6.4	15.1	25.6	36.5	46.2	59.1	76.8
Loss - Rotor back iron hysteresis (W)	15.4	27.8	39.2	48.0	64.5	76.9	97.1
Loss - Rotor back iron eddy current (W)	3.4	7.4	11.9	16.6	25.7	33.8	48.1
Loss - Rotor teeth hysteresis (W)	27.5	52.6	78.8	101.4	130.0	155.7	191.6
Loss - Rotor teeth eddy current (W)	6.3	15.0	26.2	38.5	57.4	77.1	109.3

Rotor speed (rpm)	**4000**	**4500**	**5000**	**5500**	**6000**	**6500**	**7000**
Torque (N·m)	166	144	109	98	89	78	71
Input power (kW)	73.2	71.4	59.8	59.1	58.4	55.3	54.1
Output power (kW)	69.4	68.1	57.1	56.6	55.9	52.9	51.9
Efficiency (%)	94.9	95.3	95.6	95.7	95.7	95.8	95.8
Torque per unit volume (N·m/mm³)	6.1E-05	5.3E-05	4.0E-05	3.6E-05	3.3E-05	2.9E-05	2.6E-05
Loss - Total (kW)	3.7	3.3	2.6	2.5	2.5	2.3	2.3
Loss - Winding (kW)	2.6	2.1	1.5	1.4	1.4	1.3	1.3
Loss - Stator back iron hysteresis (W)	268.5	267.0	245.0	227.5	213.7	200.7	189.8
Loss - Stator back iron eddy current (W)	182.2	189.2	184.2	179.8	176.3	172.5	168.6
Loss - Stator teeth hysteresis (W)	177.9	180.0	173.2	168.4	164.2	158.8	153.8
Loss - Stator teeth eddy current (W)	86.1	95.8	102.2	106.6	110.7	113.9	116.3
Loss - Rotor back iron hysteresis (W)	88.7	87.3	83.0	72.7	63.0	56.7	47.2
Loss - Rotor back iron eddy current (W)	47.1	50.5	51.4	47.5	43.3	40.8	35.2
Loss - Rotor teeth hysteresis (W)	185.7	185.3	178.8	166.8	156.3	149.0	137.2
Loss - Rotor teeth eddy current (W)	115.1	126.2	131.7	131.1	130.6	132.2	128.9

Speed (rpm)	On Angle Advance (° elect.)	Off Angle Advance (° elect.)
500	0	10
1000	0	25
1500	0	25
2000	10	35
2500	30	35
3000	35	40
3500	35	40
4000	50	55
4500	55	60
5000	55	60
5500	65	70
6000	75	80
6500	85	90
7000	90	95

Current = 77%							
Rotor speed (rpm)	**500**	**1000**	**1500**	**2000**	**2500**	**3000**	**3500**
Torque (N·m)	151	151	150	146	143	139	134
Input power (kW)	10.0	18.0	25.7	32.7	39.9	46.1	51.9
Output power (kW)	7.9	15.9	23.5	30.5	37.5	43.5	49.1
Efficiency (%)	79.1	88.3	91.5	93.4	94.1	94.4	94.5
Torque per unit volume (N·m/mm³)	5.5E-05	5.6E-05	5.5E-05	5.4E-05	5.3E-05	5.1E-05	4.9E-05
Loss - Total (kW)	2.1	2.1	2.2	2.2	2.4	2.6	2.8
Loss - Winding (kW)	1.9	1.8	1.8	1.6	1.6	1.7	1.8
Loss - Stator back iron hysteresis (W)	46.6	90.9	130.9	166.1	197.4	232.0	245.8
Loss - Stator back iron eddy current (W)	12.6	29.3	49.6	73.6	105.3	142.1	162.6
Loss - Stator teeth hysteresis (W)	22.4	45.9	70.5	93.2	115.9	140.8	161.6
Loss - Stator teeth eddy current (W)	5.9	13.9	23.9	35.3	47.9	62.5	76.6
Loss - Rotor back iron hysteresis (W)	14.5	27.0	37.9	47.2	60.7	79.0	88.2
Loss - Rotor back iron eddy current (W)	3.2	7.0	11.4	16.1	23.9	35.1	43.2
Loss - Rotor teeth hysteresis (W)	25.4	49.8	74.7	97.7	123.8	155.0	177.3
Loss - Rotor teeth eddy current (W)	6.0	14.2	24.8	36.9	54.1	77.6	99.9

Rotor speed (rpm)	**4000**	**4500**	**5000**	**5500**	**6000**	**6500**	**7000**
Torque (N·m)	118	103	93	81	77	72	66
Input power (kW)	52.0	51.0	51.1	49.0	50.6	50.8	50.3
Output power (kW)	49.5	48.6	48.8	46.8	48.5	48.7	48.2
Efficiency (%)	95.1	95.3	95.5	95.5	95.7	95.8	95.9
Torque per unit volume (N·m/mm³)	4.3E-05	3.8E-05	3.4E-05	3.0E-05	2.8E-05	2.6E-05	2.4E-05
Loss - Total (kW)	2.6	2.4	2.3	2.2	2.2	2.1	2.1

Loss - Winding (kW)	1.5	1.4	1.3	1.3	1.2	1.1	1.1
Loss - Stator back iron hysteresis (W)	229.8	211.0	209.5	189.3	196.3	193.9	187.9
Loss - Stator back iron eddy current (W)	161.4	157.6	163.8	154.7	164.9	168.4	168.0
Loss - Stator teeth hysteresis (W)	159.7	155.2	158.2	148.6	154.5	154.6	152.2
Loss - Stator teeth eddy current (W)	82.5	87.3	95.5	96.6	105.7	111.8	116.0
Loss - Rotor back iron hysteresis (W)	79.4	69.7	68.9	56.4	60.8	58.2	53.3
Loss - Rotor back iron eddy current (W)	41.3	38.4	41.1	35.2	40.9	41.5	40.0
Loss - Rotor teeth hysteresis (W)	167.9	155.8	157.5	141.5	150.2	148.8	144.0
Loss - Rotor teeth eddy current (W)	103.1	103.3	113.4	108.7	124.1	131.2	134.5

Speed (rpm)	On Angle Advance (° elect.)	Off Angle Advance (° elect.)
500	0	10
1000	0	20
1500	0	25
2000	0	35
2500	5	35
3000	10	35
3500	30	40
4000	45	50
4500	55	60
5000	60	65
5500	70	75
6000	70	75
6500	75	80
7000	80	85

Current = 50%							
Rotor speed (rpm)	**500**	**1000**	**1500**	**2000**	**2500**	**3000**	**3500**
Torque (N·m)	86	86	85	84	82	80	74
Input power (kW)	5.4	10.1	14.6	18.8	23.1	26.8	28.9
Output power (kW)	4.5	9.0	13.4	17.5	21.6	25.3	27.2
Efficiency (%)	82.4	89.0	91.9	93.2	93.6	94.2	94.1
Torque per unit volume (N·m/mm³)	3.1E-05	3.1E-05	3.1E-05	3.1E-05	3.0E-05	3.0E-05	2.7E-05
Loss - Total (kW)	1.0	1.1	1.2	1.3	1.5	1.6	1.7
Loss - Winding (W)	836.1	851.2	798.9	769.5	804.9	773.2	806.3
Loss - Stator back iron hysteresis (W)	41.0	81.1	114.4	143.6	172.4	197.7	204.8
Loss - Stator back iron eddy current (W)	11.3	27.3	44.9	65.3	95.3	121.4	139.7
Loss - Stator teeth hysteresis (W)	19.5	41.5	61.9	82.5	103.6	121.6	137.5
Loss - Stator teeth eddy current (W)	5.2	12.9	21.7	32.4	44.6	57.5	70.8

Loss - Rotor back iron hysteresis (W)	13.1	26.0	35.4	43.9	57.1	65.9	72.3
Loss - Rotor back iron eddy current (W)	3.0	6.9	10.7	15.1	22.7	29.2	34.9
Loss - Rotor teeth hysteresis (W)	22.2	46.6	67.8	89.5	113.9	133.2	151.3
Loss - Rotor teeth eddy current (W)	5.4	13.6	23.0	34.4	50.7	66.5	83.7

Rotor speed (rpm)	**4000**	**4500**	**5000**	**5500**	**6000**	**6500**	**7000**
Torque (N·m)	63	56	50	46	43	40	38
Input power (kW)	28.1	27.7	27.7	27.8	28.4	28.9	29.0
Output power (kW)	26.5	26.2	26.2	26.2	27.0	27.5	27.6
Efficiency (%)	94.2	94.5	94.6	94.3	94.9	94.9	95.2
Torque per unit volume (N·m/mm³)	2.3E-05	2.0E-05	1.8E-05	1.7E-05	1.6E-05	1.5E-05	1.4E-05
Loss - Total (kW)	1.6	1.5	1.5	1.6	1.5	1.5	1.4
Loss - Winding (W)	696.5	650.1	606.3	544.3	529.6	497.7	500.8
Loss - Stator back iron hysteresis (W)	203.6	185.6	174.4	198.8	174.6	178.8	157.8
Loss - Stator back iron eddy current (W)	148.9	144.4	143.9	164.3	153.4	161.3	149.9
Loss - Stator teeth hysteresis (W)	143.0	136.8	133.6	146.7	136.4	139.1	129.1
Loss - Stator teeth eddy current (W)	79.3	81.9	85.6	97.5	96.5	103.2	101.8
Loss - Rotor back iron hysteresis (W)	76.0	68.9	64.5	79.2	66.5	69.2	56.6
Loss - Rotor back iron eddy current (W)	39.7	38.4	38.1	51.2	44.2	48.9	40.6
Loss - Rotor teeth hysteresis (W)	157.1	146.8	141.2	160.9	144.5	148.6	132.9
Loss - Rotor teeth eddy current (W)	96.1	96.9	100.4	126.7	119.0	130.9	123.0

Speed (rpm)	On Angle Advance (° elect.)	Off Angle Advance (° elect.)
500	0	10
1000	0	10
1500	0	20
2000	0	25
2500	10	30
3000	10	35
3500	30	40
4000	30	40
4500	40	45
5000	45	50
5500	35	40
6000	45	50
6500	45	50
7000	55	60

Current = 20%							
Rotor speed (rpm)	**500**	**1000**	**1500**	**2000**	**2500**	**3000**	**3500**
Torque (N·m)	17	17	17	16	16	16	16
Input power (kW)	1.1	2.0	2.9	3.8	4.7	5.4	6.2
Output power (kW)	0.9	1.8	2.6	3.4	4.2	5.0	5.7
Efficiency (%)	81.9	87.3	89.2	89.9	91.0	91.6	91.7
Torque per unit volume (N·m/mm³)	6.2E-06	6.2E-06	6.1E-06	6.0E-06	5.9E-06	5.8E-06	5.7E-06
Loss - Total (W)	197.1	255.6	317.8	383.1	418.6	451.8	515.7
Loss - Winding (W)	140.4	139.0	141.2	142.6	135.2	128.5	129.8
Loss - Stator back iron hysteresis (W)	18.1	35.2	51.7	67.7	77.1	84.7	96.2
Loss - Stator back iron eddy current (W)	5.8	13.5	21.8	31.7	40.0	48.2	60.3
Loss - Stator teeth hysteresis (W)	8.9	18.0	26.9	36.1	42.1	47.6	56.4
Loss - Stator teeth eddy current (W)	2.8	6.6	10.8	15.8	20.2	24.9	31.3
Loss - Rotor back iron hysteresis (W)	6.3	12.2	17.7	23.1	25.4	27.5	31.6
Loss - Rotor back iron eddy current (W)	1.7	3.9	6.0	8.5	10.4	12.2	15.1
Loss - Rotor teeth hysteresis (W)	10.0	20.2	30.2	40.6	46.6	51.9	61.7
Loss - Rotor teeth eddy current (W)	3.0	7.1	11.5	17.0	21.6	26.3	33.3

Rotor speed (rpm)	**4000**	**4500**	**5000**	**5500**	**6000**	**6500**	**7000**
Torque (N·m)	15	15	15	15	13	12	10
Input power (kW)	7.0	7.8	8.4	9.1	9.2	9.0	8.3
Output power (kW)	6.5	7.2	7.7	8.4	8.5	8.3	7.7
Efficiency (%)	91.7	91.8	91.8	91.8	91.9	92.1	92.3
Torque per unit volume (N·m/mm³)	5.7E-06	5.6E-06	5.4E-06	5.3E-06	4.9E-06	4.5E-06	3.8E-06
Loss - Total (W)	583.1	637.9	699.0	762.3	749.8	716.7	640.2
Loss - Winding (W)	131.7	135.5	150.7	151.8	144.5	135.8	128.3
Loss - Stator back iron hysteresis (W)	107.2	114.8	120.6	128.4	124.0	116.6	101.3
Loss - Stator back iron eddy current (W)	73.8	86.5	97.5	111.9	113.9	111.7	100.3
Loss - Stator teeth hysteresis (W)	65.3	70.3	75.0	82.7	81.0	76.9	67.6
Loss - Stator teeth eddy current (W)	38.3	44.0	50.4	58.1	60.4	60.8	57.7
Loss - Rotor back iron hysteresis (W)	35.8	39.1	40.7	43.9	41.3	37.7	30.4
Loss - Rotor back iron eddy current (W)	18.2	21.6	24.4	27.9	27.9	26.7	22.7
Loss - Rotor teeth hysteresis (W)	71.7	77.2	82.8	91.6	88.5	82.7	69.7
Loss - Rotor teeth eddy current (W)	41.1	48.9	56.8	66.2	68.3	67.7	62.1

Speed (rpm)	On Angle Advance (° elect.)	Off Angle Advance (° elect.)
500	0	5
1000	0	10
1500	0	10
2000	0	10
2500	0	20
3000	0	30
3500	0	30
4000	0	30
4500	10	35
5000	35	40
5500	35	40
6000	40	45
6500	45	50
7000	55	60